NBSIR 74-543

OCR-14-32-0001-1230

High Temperature MHD Materials

S. J. Schneider, W. Capps, H. P. R. Frederikse, W. R. Hosler
D. A. Kauffman, E. M. Levin, C. L. McDaniel, T. Negas and
E. R. Plante

Institute for Materials Research
National Bureau of Standards
Washington, D. C. 20234

August 1974

Interim Report for Period
July 1, 1972 – June 30, 1974

Prepared for

Office of Coal Research
Department of the Interior
Washington, D. C. 20240

NBSIR 74-543

OCR - 14-32-0001-1230

HIGH TEMPERATURE MHD MATERIALS

S. J. Schneider, W. Capps, H. P. R. Frederikse, W. R. Hosler,
D. A. Kauffman, E. M. Levin, C. L. McDaniel, T. Negas and
E. R. Plante

Institute for Materials Research
National Bureau of Standards
Washington, D. C. 20234

August 1974

Interim Report for Period
July 1, 1972 - June 30, 1974

Prepared for
Office of Coal Research
Department of the Interior
Washington, D. C. 20240

U. S. DEPARTMENT OF COMMERCE, Frederick B. Dent, Secretary

NATIONAL BUREAU OF STANDARDS, Richard W. Roberts, Director

PREFACE

For the past several years the Inorganic Materials Division, Institute for Materials Research, National Bureau of Standards, has been engaged in materials research appropriate to open cycle coal fired magnetohydrodynamic (MHD) systems. Since July 1972 a portion of the work has been sponsored by the Office of Coal Research under Contract No. 14-32-0001-1230. The purpose of this report is to present a summary of the technical activities of the combined NBS-OCR program on High Temperature MHD Materials.

TABLE OF CONTENTS

LIST OF FIGURES

LIST OF TABLES

1. Introduction

The successful development and eventual commercialization of open cycle, coal fired MHD systems requires an accelerated effort to develop and optimize materials which can withstand the rigors of the severe MHD environment. Materials must resist not only erosion through vaporization and corrosion by alkali and slag attack, but also must possess the requisite physical properties necessary for system operation. Under the auspices of the Office of Coal Research, the National Bureau of Standards has underway a program of materials research appropriate to MHD. The overall objective of the work is to provide materials property information necessary for the design, construction and operation of a coal fired MHD facility. The program consists of several interrelated projects in the following areas:

Phase Equilibria

Condensed and noncondensed systems, melting behavior, compound formation, phase assemblages, phase transformations.

Electrical Conductivity

Electrical properties as a function of temperature, composition and atmosphere.

Vaporization

Mass loss and vapor species under reactive and non-reactive conditions.

Viscosity

Behavior of liquid slags as a function of composition, atmosphere and temperature.

Materials Testing

Durability, reliability, and operating characteristics of materials tested under real MHD conditions.

Initial work has centered around the behavior of coal slag since there is a definite lack of basic data in this area. The program also encompasses investigations on other MHD process contaminants, particularly alkali seeds, and on important structural and operating components such as insulators and electrodes. The following sections summarize the important technical results achieved thus far in the NBS-OCR program.

2. Coal Slag Characterization

Coal always contains inorganic materials which vary both in amount and constitution depending on the type and locale of the coal bed. Major elemental components consist of Si, Al, and Fe present as silica, aluminosilicates and iron pyrite. Smaller quantities of Mg, Ca, K and S in various compound forms make up the balance of constituents. It is the behavior of these inorganic materials, the residue of coal combustion (commonly termed coal ash), which will ultimately determine the success or failure of MHD. Proper manipulation of the ash is crucial.

MHD coal combustion techniques are designed to remove a large percentage of coal ash as a liquid (slag). A certain fraction of ash however will be vaporized during combustion only to condense again downstream at cooler sections. Additionally, another fraction of ash will be mechanically carried throughout the system as solid or liquid (flyash). Consequently different components of the MHD system can "see" different types and forms of coal ash, all dependent upon local conditions of gas pressures (partial and total) and temperatures as well as the initial combustion parameters. The condensed layers, which may be partly liquid or solid, can have detrimental as well as beneficial effects. It may, for instance, chemically tie up an unacceptable portion of the alkali seed in the form of an insoluble compound or it may inhibit or short circuit the electrical current between channel electrodes. On the other hand, it may protect the walls from degradative processes and still enhance current passage. Consequently, it is important to determine the physical and chemical properties of the coal ash (slag).

Extensive information is available on the inorganic content for a wide variety of coals [1]. These analytical data however only provide a guide to the starting or limiting chemical compositions. The extent to which these limiting or maximum chemical compositions are modified as the ash moves through the MHD system is unknown. Thermodynamic calculations of course give some insight as to possible gas, liquid and solid phase compositions. Direct information however may be obtained through the characterization of materials selectively sampled from different segments of a MHD system. The combination of data obtained from thermodynamic predictions and that from a characterization of real materials allow the formulation of synthetic materials or model systems appropriate to a wide range of environmental conditions of MHD.

In an effort to characterize coal ash behavior under real MHD conditions several samples of slag and flyash were obtained from the Bureau of Mines combustor facility at Bruceton, Pennsylvania and from the University of Tennessee Space Institute, Tullahoma, Tennessee. These slag specimens were selectively sampled from different parts of the respective systems and generally represent combustor slag, channel slag and condensed gas phase constituents at the exit of the channel (probe deposit). All samples were subjected to a variety of analytical techniques: chemical analysis, microscopic examinations, x-ray diffraction, differential thermal analysis and Mossbauer spectroscopy. From these data several general conclusions can be drawn:

a. There is a significant difference in slag types found in different parts of the MHD system. However, all deposits regardless of location are composed of largely Al_2O_3-FeO-Fe_2O_3-SiO_2 mixtures. The portions of each vary depending on location as does the relative amounts of glassy (liquid) and crystalline material.

b. Combustor slags contain a significant amount of alkali (up to 2%), indicating that at least a portion of the alkali content of the coal is not vaporized during combustion. In addition, there is little evidence of crystalline material and all samples were largely glassy (including immiscible liquids).

c. Condensed gas phase constituents collected by a cold copper probe contain large amounts of alkali (under seeding conditions). The alkali content is probably present as both salts (K_2SO_4-K_2CO_3 solid or liquid solutions) and as aluminosilicate-rich liquids. These liquids are immiscible.

d. The presence of large concentrations of alkali on copper surfaces (e.g. electrodes) promotes diffusion of Cu to the slag layer. This is evidenced by the presence of Cu (or CuO) in slag samples collected by the probe and from the electrodes. In contrast, the probe samples did not contain any Cu when seed was not present during combustion. It would appear that long time operation with seeding would cause degradation of copper surfaces.

e. The slag deposited on cold Cu electrode surfaces contained both glassy and crystalline material. It would appear that the condensed phase first deposited as a liquid(s) and then cooled to a

glass phase(s) which slowly crystallized. The predominant crystalline material is $KAlSiO_4$ ($K_2O \cdot Al_2O_3 \cdot 2SiO_2$) with little or no K_2CO_3 or K_2SO_4 being present. This is significant since most of the alkali is tied up as a high temperature oxide phase (mp $KAlSiO_4$ ~1700°C) rather than as water soluble salt.

f. The base oxide composition (excluding alkali) suggested by the chemical analysis of the electrode deposits (channel slag) for the UTSI channel are tabulated in Table 1. For comparative purposes the base oxide composition for the Bureau of Mines probe deposit is included. The main differences between the two nominal compositions are higher Al_2O_3 contents and lower Fe_3O_4 amounts for the UTSI electrode slags. A more important difference, however, is that in the UTSI channel the alkali when combining with the base oxide slag forms a crystalline phase $KAlSiO_4$ + excess SiO_2 containing iron oxide. In the Bu Mines samples, the alkali combines at least initially to form two immiscible liquids (K_2SO_4-K_2CO_3 liquid + base oxide liquid).

g. The data and conclusions stated above represent only a first attempt at establishing slag behavior. It is evident that all such data are very general and cannot be applied as of yet to all MHD situations, because of the many variables. In effect, however the data implies that slag behavior can be determined and possibly controlled by appropriate modification of the system parameters and coal types.

3. Phase Equilibria

In order to increase gas phase conductivity in magnetohydrodynamics (MHD), certain salts such as K_2CO_3 and K_2SO_4 are added to the gas stream passing through the channel. However, these salts with relatively low melting points (<1100°C) can react with the refractory oxides (mp >2000°C) to form low temperature eutectics, which have a deleterious effect on structural stability of the insulators and electrodes and on their electrical conductivities. A knowledge of the phase relations between seed materials and the possible oxide components of the MHD channel are important in understanding the reactions taking place in a channel under various conditions and could provide a basis for developing better performing materials.

Investigations of possible seed (e.g. K_2CO_3, K_2SO_4)-coal slag reactions (silicates, aluminates, aluminosilicates) are of fundamental importance in seed recovery technology and could provide additional data which would aid in the evaluation of refractories (e.g. Al_2O_3) in air preheaters and duct insulators. Phase equilibrium studies of condensed phase reactions (liquids-solids) and vapor phase - condensed phase reactions can provide invaluable information for the design and operation of MHD combustors.

3.1. Materials and Methods

ACS reagent grade materials were used. Homogeneous mixtures in the binary systems were prepared by several cycles of grinding, pressing into pellets, and heating below the solidus. Liquidus and/or solidus data were determined with a commercially available DTA instrument,

using 10-20 mg samples in Pt microholders, with Al_2O_3 as a reference material, and at a heating rate of 10°C/min. The instrument was calibrated against one or more standard reference materials [2]. Subsolidus phase relations and unit cell dimensions were deduced from x-ray powder diffraction patterns (using CuKα radiation) obtained by heating thin specimens of the pure salts or mixtures in air in an x-ray diffractometer furnace equipped with an improved sample holder [3].

The binary systems were also studied by conventional quenching techniques using open Pt tubes for specimen containers. In some cases sealed Pt tubes were used to avoid volatilization. Volatility of a component such as K_2O was also minimized by preparing materials at elevated temperatures using a buffering method. Data were also combined with thermodynamic calculations of activities to estimate phase relations under (1) different total pressures of dissociated K_2CO_3 or K_2SO_4 gaseous species and (2) in the presence of additional gases. Phase relations and vaporization rates in systems containing K_2O were investigated using a commercially available, high precision, DTGA apparatus. The TGA portion of the unit was used in combination with a Knudsen cell to obtain phase equilibrium and vapor pressure data.

3.2. Polymorphism of Seed Materials

3.2.a. K_2CO_3

Although a number of phase transformations have been reported in K_2CO_3 [4], later work [5,6] by DTA indicated only one transformation in a CO_2 atm, at 422°C. Other thermal effects in air were ascribed to impurities, such as H_2O, KOH and KCℓ. Schneider and Levin [7]

studied the system both by DTA and by high-temperature x-ray diffractometry. Figure 1 shows a plot of the unit cell dimensions of K_2CO_3 vs temperature obtained in air with the high temperature x-ray furnace. It is seen that K_2CO_3 indeed shows only two polymorphs, a low temperature monoclinic and a high temperature hexagonal form, with a transformation temperature of 420±5°C, in good agreement with Reisman's value [5,6] of 422°C. Cell dimensions of the monoclinic form were determined by x-ray patterns indexed by comparison with room temperature data reported by deWolff [8]. Indexing of the hexagonal form was accomplished by inspection.

It is to be noted that no discontinuity exists in the cell dimensions or in the density at the transformation temperature and that the β angle reduces continuously to 90°. The DTA traces for K_2CO_3 showed a small, almost imperceptible, but reproducible endothermal effect in both CO_2 and air at the transformation temperature. These findings strongly suggested that the transformation occurs with no discontinuity in enthalpy or volume but with a discontinuity in the first derivative of the enthalpy, i.e., in C_p. Figure 2, a plot of C_p vs temperature obtained with a differential scanning calorimeter shows a second order transition at 420±5°C. No peak is evident, but an abrupt shift in base line was observed, corresponding to a change in C_p and not in enthalpy.

3.2.b. K_2SO_4

Majumdar and Roy [9] in agreement with Bernard and Jaffray [10], on the basis of thermal anomalies in DTA traces and high temperature x-ray results, proposed several new low-temperature, possibly second order,

transitions in K_2SO_4, e.g., one at 300±10°C. Pistorius and Rapoport [11] did not observe any second order phase changes by means of high pressure DTA, but by indirect calculation of the volume change at the transition conclude that K_2SO_4 at ∿580°C differs crystallographically from the phase stable at room temperature.

Figure 3 shows unit cell dimensions and density data obtained by use of the high temperature x-ray furnace. The orthorhombic and hexagonal forms were indexed by referral to data, respectively, of Swanson, et al [12] and Pannetier and Gaultier [13]. From the discontinuity at 588°C in the c dimension and in the density plots, it is apparent that the transition is first order. Also, within the limits of accuracy of the x-ray measurements, there are no other transitions. The transition temperature of 588±5°C is in agreement with previous values: 582±1°C [14], 583°C [9], 584°C [11], and 586±2°C [13].

3.2.c. Cs_2SO_4

As a seed material Cs_2SO_4 has a greater electronic conductivity and might even be superior to K_2SO_4, but its cost is also greater. Unit cell dimensions and density as a function of temperature are shown in Figure 4. The transition temperature both by DTA and high temperature x-ray diffraction methods was located at 718±5°C. The value is in reasonable agreement with previous ones of: 710°C [15], 712°C [16], and 713±2°C [17]; but it is almost 60° higher than the earlier reported value of 660°C [18], which is the one listed in the Standard Reference Data Series [19]. Rao and Rao [20] report a value of 698°C, corresponding

to the peak temperature in a DTA heating curve; and as late as 1970, Denielou, et al [14] in a calorimetric study reported the transition at ∿667°C. Detailed data were not given so it is not possible to re-examine their two enthalpy equations for a better fit of the data at a higher transition temperature. To account for the very low values, other than on an impurity basis, Plyushchev and Markovskaya [18b] suggested that Cs_2SO_4 might be trimorphic. The figure shows, however, that Cs_2SO_4 is dimorphic, similar to K_2SO_4, possessing orthorhombic [17,21] and hexagonal [17] forms.

Unlike K_2SO_4, however, which undergoes a first order transition and shows a definite discontinuity in the specific volume (1/d) at the transition, Cs_2SO_4 resembles the K_2CO_3 transition, in that the cell dimensions and density appear to be continuous curves. Also, the heat effect at the transformation is small, estimated by Rao and Rao [20] at 150 cal/mol or at ∿1/14 of the heat of transformation of K_2SO_4. In the present study, the ratio was approximated, from DTA data, at ∿1/30. Thus the data for Cs_2SO_4 suggest a second order transition. Rao and Rao [20], in fact, postulate that the transformation has considerable second order contributions and that the measured heat effect (by DTA) is small due to the occurrence of the transformation over a wide temperature range.

3.3. Alkali Seed Equilibria

3.3.a. The System K_2SO_4-Cs_2SO_4

A knowledge of the K_2SO_4-Cs_2SO_4 phase diagram could be helpful in selecting a suitable seed mixture for MHD. The diagram reported by

Dombrovskaya [22] in 1933 (figure 5) does not include the polymorphism of the components, and the indicated melting point of Cs_2SO_4 at 846°C is over 150° below the value of 1004±5°C reported in the National Standard Reference Data Series [19] and confirmed in the present study [23]. Also an unresolved inconsistency exists in the literature. Diogenov and Ermachkov [24] in relation to the ternary system Cs_2SO_4-K_2SO_4-Na_2SO_4 show the boundary Cs_2SO_4-K_2SO_4 system as a complete solid solution extending from 1069°, the melting point of K_2SO_4 to 1013°C, the melting point of Cs_2SO_4, with a minimum at 930°C and 50 mol % K_2SO_4. The diagram of Dombrovskaya (figure 5), however, is cited as the reference.

Figure 6 shows the phase diagram for the system as obtained from DTA and high temperature x-ray studies of the components and intermediate compositions. The solidus and liquidus curves have been drawn close to each other, as the DTA peaks were relatively sharp with no apparent differentiation. This region of the diagram is in agreement with that referenced by Diogenov and Ermachkov [22]. The subsolidus shows a eutectoid with slight mutual solid solubility of the components in the low temperature orthorhombic forms and complete solid solubility in the hexagonal phase. The hexagonal phase could not be quenched, and as the DTA results were inconsistent and not interpretable, the high temperature x-ray proved the decisive method of study. From the standpoint of seeding a MHD channel, the 50:50 mol % composition with a minimum liquidus at 940°C would be a most likely choice.

A plot of the unit cell dimensions vs composition for the hexagonal solid solution phase is shown in Figure 7. Whereas the a parameter shows a small negative deviation from linearity, the c parameter shows a large positive deviation. It can be seen that the substitution of a K^+ (I.R., 1.33A) for a much larger Cs^+ (I.R., 1.67A) on the Cs_2SO_4-rich side has a relatively small effect on the c parameter. However, the substitution of a larger Cs^+ for K^+ on the K_2SO_4-rich side has a pronounced effect. It is unusual for complete solid solution to exist between two isostructural molecules with such widely different cationic radii, and Vegard's law is not obeyed for the c parameter.

These results can be rationalized by consideration of the general crystal structure for the high temperature sulfates. Figure 8 shows a schematic [110] view of Cs_2SO_4, based on the structure of $KNaSO_4$, as reported by Wyckoff [25]. The structure contains two essentially different types of Cs atoms: Cs(1) and Cs(2) forming columns through the structure in the c direction, and Cs(3) forming parallel strings of alternating Cs atoms and SO_4 tetrahedra. The effect of the gradual addition of K atoms may be considered. If the K atoms first substitute mainly for Cs(3) atoms, the smaller atoms replacing the central larger ones within the rigid framework will have relatively little effect, except for a slight contraction of the structure in the a dimension. After about 50 mol % addition of K_2SO_4, however, the Cs(3) atoms will have been mostly replaced and further addition of K_2SO_4 will result in substitution of Cs(1) and Cs(2) atoms. Replacement of columnar Cs atoms will have a large effect on the reduction in c dimension but even less effect on the a dimension

than for the Cs(3) substitution. If Cs^+ and K^+ were randomly substituted over all of the sites in the structure, a much closer adherence to Vegard's law would be expected. In Figure 7, deviation from linearity occurs at about 50 mol % Cs_2SO_4. Thus this mechanism explains the curvature for the a and c parameters. From the fan-shaped nature of the curves for the c parameter, it is apparent that the thermal expansion increases with increased Cs_2SO_4 content.

A plot of x-ray density vs composition at 500°C, 600°C, and 700°C is shown in Figure 9. The plot shows a positive deviation from linearity but not nearly so pronounced as for the parameter plot, because in the density formula, $0.865a^2c$, the a dimension has a much greater contribution to the density than does c.

3.3.b. The System K_2CO_3-K_2SO_4

When a dirty fuel such as sulfur-containing coal is used in MHD, K_2CO_3 seed acts in pollution abatement, as the volatilized seed provides free K to form K_2SO_4 on condensation of the vapor. Therefore, a knowledge of the K_2CO_3-K_2SO_4 system might be useful in formulating seed mixtures and in interpreting their behavior. Le Chatelier [26] and Amadori [27] studied the liquidus by visual observation in thermal analysis. They observed a continuous solid solution between the end members. The liquidus was found to be relatively flat on the K_2CO_3 side and relatively steep on the K_2SO_4 side.

In the present study (figure 10), the liquidus was determined from the DTA results of eleven intermediate compositions. In approximate agreement with earlier work it is almost horizontal (slight rise) up

to about 25 mol % K_2SO_4. Similar to the K_2SO_4-Cs_2SO_4 system, it was not possible to differentiate the solidus from the liquidus. Subsolidus phase relations were deduced with the use of the high temperature x-ray diffraction furnace for a number of intermediate compositions. The low temperature orthorhombic solid solution phase extends from pure K_2SO_4 to about 90 mol % K_2CO_3 and shows a maximum along the hexagonal solid solution boundary at 635°C. Thermal expansion data for the various solid solution phases as a function of composition and temperature will be reported separately.

3.4. The System K_2SO_4-MgO

3.4.a. Condensed Phase Equilibria Diagram

The condensed state phase diagram for the K_2SO_4-MgO system is given in Figure 11. Experiments conducted in open and sealed Pt tubes gave the same results except the K_2SO_4 had a tendency to vaporize during prolonged heating in open tubes. No intermediate phases were detected in the system at temperatures up to 1700°C. Data obtained by DTA in this study indicated no change in the K_2SO_4 orthorhombic to hexagonal transformation at 588°C using the various K_2SO_4-MgO mixtures. The system is a simple eutectic type with the eutectic located at 1067°C and ∿2 mol % MgO. The liquidus was determined up to 1700°C, the maximum temperature attainable in the quenching furnace. This work illustrates the harmful effect the seed material K_2SO_4 would have on the refractory insulator MgO. Under equilibrium conditions, MgO dissolution (liquid formation) will occur at any temperature above 1067°C in situations where condensed K_2SO_4 is in contact with MgO.

3.4.b. Vaporization Equilibria

The condensed state phase diagram shown in Figure 11 does not take into account the possibility that the K_2SO_4 (soln) in the system may become part of the vapor phase. Although the cold wall concept in an MHD channel has had some success, the problems of corrosion and electrode and insulator characterization appear less formidable if wall temperatures are maintained at some value below that imposed by vaporization restraints but above that at which condensation can take place. The basis for this contention is that corrosion of the electrode or insulator of the MHD duct leading to formation of a liquid solution can only take place if the activity of the vapor phase component in the liquid solution is significantly less than the activity of that component in the vapor. This would happen only if the vapor could form a stable condensed state compound with the insulator or electrode. On the other hand, if the vapor is allowed to exceed its saturation pressure, the pure condensed phase may form which can then interact with and corrode the wall, even though the activity of the vapor component in the corrosion product is only slightly less than that in the vapor.

An example of this can be illustrated through use of the activity diagram shown in Figure 12. This shows the activity of K_2SO_4 in the pseudo two component system K_2SO_4-MgO at 1700°C. The dotted line running from an activity of 1 to 0.85 represents the activity of K_2SO_4 in the K_2SO_4 rich single phase region of the condensed state phase diagram and shows the gradual decrease in activity of K_2SO_4 as MgO is dissolved in it. This line need not be linear but its true shape

is not known. When the mole fraction of MgO in the melt exceeds a mole fraction of 0.15, MgO containing an unknown amount of dissolved K_2SO_4 precipitates as a solid solution. The extent of solid solution is not known and is not detectable by x-ray methods. A constant K_2SO_4 activity of 0.85, assuming its activity is equal to its mole fraction, is then found all the way across the two phase region until at some composition close to pure MgO, the activity of K_2SO_4 drops quickly to 0 over a narrow composition range. It follows therefore that if the pressure is reduced, a vapor phase will form at some appropriate pressure, and if the pressure is reduced to a sufficiently low value, the composition will become richer in MgO as the K_2SO_4 evaporates and eventually the liquid phase will entirely disappear.

These concepts are applied to the phase diagram shown in Figure 13 in which three isobars have been introduced. This diagram was constructed by assuming that total pressures of 0.01, 0.1, and 1 atm consisting entirely of $K_2SO_4(g)$ and its decomposition products are present in the vapor phase.

All data for this calculation were from JANAF [28] except for the thermodynamic data for $K_2SO_4(g)$. Several studies have indicated that $K_2SO_4(g)$ is an important vaporization product of $K_2SO_4(s,\ell)$ [29,30]. Data for $K_2SO_4(g)$ was therefore based on JANAF data for $K_2SO_4(s)$, the heat of sublimation of $K_2SO_4(s)$ reported by Halstead [30] and molecular constant data modeled after that reported by Cubicciotti [31] for $Cs_2SO_4(g)$ and $Rb_2SO_4(g)$. For $K_2SO_4(g)$, a number of vibrational frequencies were adjusted so that the entropy of sublimation calculated from the thermal functions agreed with that reported by Halstead

at 1300K. Taking the case for a total pressure of 0.1 atm as an example we can note that at 1697°C pure $K_2SO_4(\ell)$ would exert a pressure of 0.1 atm. If it existed in contact with pure MgO at this temperature, it could react to form a solution consisting of slightly less than 15 mol % of MgO and the pressure would fall by somewhat less than 15%. If the temperature were gradually raised to 1709°C however, the pressure would gradually increase to 0.1 atm and at a temperature slightly above 1709°C, the liquid solution phase would disappear. The same arguments apply to the other isobars at 0.01 and 1 atm.

3.5. The System K_2CO_3-MgO

3.5.a. Condensed Phase Equilibria Diagram

One system of obvious interest is that between K_2CO_3 and MgO, seed and insulator materials, respectively. Preliminary experiments revealed that pure K_2CO_3 was very reactive with moisture in the air, forming $K_2CO_3 \cdot 1.5H_2O$, as identified by x-ray powder diffractometry [32]. Likewise, the K_2CO_3 in the heated and quenched MgO:K_2CO_3 mixtures reacted at room temperature to form the hydrate, during the exposure time of grinding the sample for specimen preparation and taking the x-ray powder pattern. In one experiment, a sample of K_2CO_3 was dissolved in H_2O and allowed to dry in air at ∿50°C for five weeks. The x-ray pattern showed only $K_2CO_3 \cdot 1.5H_2O$. Ignition loss at 130° for 18h was 16.19% (vs 16.34%, theoretical).

The melting point of K_2CO_3 was found to be sensitive to the environmental conditions. Using the quenching technique for material sealed in Pt tubes, the melting point was 902±1°C. By DTA in a stream of flowing CO_2, at a heating rate of 10°C/min, the melting point was 901±5°C. These

melting points are in good agreement with 901±1°C, reported by Reisman [5], and obtained also in a CO_2 atmosphere. Using an open Pt tube with the quenching technique the melting point was found to be 888±5°C; and by DTA (air atm), 889±5°C. The depression of the melting point in an air atmosphere of about 13° is consistent with a depression of the freezing point of 5-10° reported by Reisman [5].

Figure 14 shows the phase diagram for the system K_2CO_3-MgO, as determined by the quenching technique using sealed Pt tubes. The liquidus was traced only up to 1656°C (and 33 mol % MgO), the maximum temperature reached by the quenching furnace. The system is a simple eutectic one, with the eutectic located at 895.5±5°C and ∿2 mol % MgO. This diagram illustrates dramatically the deleterious effect of the seed material on the refractory MgO insulator. Anywhere in the MHD channel that condensed K_2CO_3 exists in contact with MgO, melting will start at ∿896°C.

3.5.b. Vaporization Equilibria

Figure 15 shows the vaporization equilibrium diagram for the K_2CO_3-MgO system. It is similar to the K_2SO_4-MgO system, the most notable difference is the lower temperatures at which liquid formation occurs in the K_2CO_3-MgO system.

3.6. The System K_2SO_4-$LaCrO_3$

3.6.a. System Under Its Own Vapor Pressure

Considerable research has been focused on SrO doped $LaCrO_3$ as a possible material for use as electrodes in MHD-generators. The system K_2SO_4-$LaCrO_3$ has been studied to obtain knowledge of the chemistry and phase relations of the pure end members. This study will give insight to the behavior of the doped material ($SrO \cdot LaCrO_3$). Single phase $LaCrO_3$

specimens were prepared from $La(OH)_3$ and Cr_2O_3. Due to the fact that La_2O_3 readily hydrates when exposed to air, $La(OH)_3$ of high purity was used. However, this study did not detect any hydrolysis (temperatures up to 150°C) of the $LaCrO_3$ compound when in contact with water or exposed to air for periods up to one month. Pavlikov et al [33] reports the $LaCrO_3$ compound melts congruently at ∿2430°C. Ruiz et al [34] reports an orthorhombic to rhombohedral transition in $LaCrO_3$ at 277°C, Geller et al [35] reports the transition at 260°C. The present work based on DTA data agrees with the latter. Several investigators [34,35] report a rhombohedral to cubic transition in $LaCrO_3$ (perovskite type structure) at some temperature between 1200 and 2000°C. This study did not resolve the temperature of the rhombohedral to cubic transformation.

Single crystal x-ray diffraction data from $LaCrO_3$ was collected in an attempt to determine the space-group symmetry. Data obtained from x-ray precession photographs were not conclusive. Various sizes and shapes of single crystals were studied and all indicated twinning which perhaps occurred during the rhombohedral to orthorhombic transition on cooling.

The equilibrium relationships between the condensed phases in the K_2SO_4-$LaCrO_3$ system under its own vapor pressure (in sealed containers) are given in Figure 16. Homogeneous mixtures (K_2SO_4, $LaCrO_3$) were heated at 900 and 1000°C (in open Pt containers) for 18 to 21 hours. Portions of the previously calcined material were then heated in sealed Pt tubes at various temperatures for different periods of time (up to 9 days) and quenched. At temperatures above 1000°C, sealed Pt tubes were used as specimen containers. The K_2SO_4-$LaCrO_3$ system is a simple eutectic type, with the eutectic located at 1063°C and ∿2 mol % $LaCrO_3$. No intermediate

phases were detected in the system at temperatures up to 1700°C. Under equilibrium conditions, $LaCrO_3$ dissolution will occur at any temperature above 1063°C in situations where condensed K_2SO_4 is in contact with the $LaCrO_3$ electrodes.

3.6.b. System in Air

The system K_2SO_4-$LaCrO_3$ under its own vapor pressure is given in Figure 16. The equilibrium relationships between the condensed phases in this system (in sealed specimen containers) indicate a simple eutectic type system with no intermediate compound formation. However, specimens heated at the higher temperatures in an air environment gave results indicating $LaCrO_3$ is not stable in contact with condensed K_2SO_4. Table 2 shows experimental data for the compositions studied in the K_2SO_4-$LaCrO_3$ system in air. Limited experiments were performed on these mixtures due to the fact that compound formation indicates the phases are represented by the more complex quaternary-type system K_2O-La_2O_3-Cr_2O_3-O_2. The data in Table 2 indicate that liquid K_2SO_4 reacts with $LaCrO_3$ at temperatures of 1100°C and above. The electrode material decomposes leaving La_2O_3 as a condensed phase. Compositions rich in K_2SO_4 indicate the presence of a phase or phases, as yet unidentified, over the temperature range of 1100 to 1200°C. The unknown phase is a compound that appears to contain K, La, Pt, and O. It is somewhat similar to such compounds detected in the K_2CO_3-La_2O_3 system at approximately the same temperature range. These phases contain Pt and form only when the specimens are heated in Pt containers. It should be noted the K_2SO_4 tends to volatilize at the higher temperatures thus reducing the amount of reaction with the $LaCrO_3$.

Neither La_2O_3 nor K_2SO_3 react with Pt to any great extent. However, when both are present there is obvious degradation of the Pt. It seems possible that it is this type of K-metal oxide-Pt reaction which causes degradation of Pt electrodes in the MHD environment.

3.7. The System K_2CO_3-$LaCrO_3$ in Air

The K_2CO_3-$LaCrO_3$ system is similar to the K_2SO_4-$LaCrO_3$ system in as much as both cannot be represented by a binary-type system. Compound formation indicates phases that exist in the ternary-type system K_2O-La_2O_3-Cr_2O_3. Table 3 shows experimental data for the compositions studied in the K_2CO_3-$LaCrO_3$ system in air. All specimens were placed in open containers due to the decomposition of K_2CO_3 and release of CO_2 gas. No attempt was made to contain the CO_2 in a closed container. It was found in earlier work that mixtures containing K_2CO_3 heated in sealed specimen containers resulted in essentially no reaction. The CO_2 gas would reach an equilibrium pressure until such temperatures were reached where the sealed containers would rupture. The data in Table 3 indicates that serious corrosion problems might occur when condensed K_2CO_3 is in contact with the electrode material. For example, at the 50:50 mixture K_2CO_3:$LaCrO_3$, the electrode material decomposes completely at 700°C. However, the decomposition products combine to reform the $LaCrO_3$ at 1200°C. Various phases, as yet unidentified, occur in the system. Some of the phases are thought to contain Pt, similar to those discussed in the K_2SO_4-$LaCrO_3$ system.

It may be concluded that $LaCrO_3$ may exist in equilibrium with K vapor at high temperatures and may be used in the MHD channel, but only if protection is supplied to the $LaCrO_3$ when subjected to K at temperatures below ∿1200°C.

3.8. The System "K_2O"-Al_2O_3

This system was investigated using two sources of potash, K_2SO_4 and K_2CO_3.

3.8.a. K_2SO_4-Al_2O_3 System

The following conclusions can be made from a study of the K_2SO_4-Al_2O_3 system:

1. At temperatures below about 1400°C, the system is a simple eutectic one, with the start of melting (solidus) occurring at 1055°C. Thus below 1055°C, there is no reaction between K_2SO_4 and Al_2O_3, which means in a practical sense that Al_2O_3 will be unaffected by K_2SO_4 at low temperatures.

2. The eutectic composition between K_2SO_4 and Al_2O_3 lies very near pure K_2SO_4 (>99% K_2SO_4), and the liquidus curve rises very steeply, i.e., almost parallel to the K_2SO_4 component. Thus, even between 1055° and 1400°C, in this two component system, less than 2% Al_2O_3, and possibly much less, is dissolved in the predominantly K_2SO_4 liquid. In this temperature range, therefore, even though K_2SO_4 liquid is present, its effect on the dissolution and degradation of Al_2O_3 should be minimal.

3. The orthorhombic to hexagonal transition of K_2SO_4 at 588°C is unchanged in the two phase region. The transition is accompanied by about a 3% volume increase, as determined from the thermal expansion data for K_2SO_4.

4. Above about 1400°C, however, the system is no longer binary as βAl_2O_3 is formed in an open system, according to the reaction:

$$K_2SO_4 + 11Al_2O_3 = K_2O \cdot 11Al_2O_3 + SO_2 + 1/2O_2$$

A composition $30K_2SO_4:70Al_2O_3$ when heated at 1300°C for 20h consisted of K_2SO_4 and Al_2O_3 and gave a weight loss of 0.61%, probably mostly water. When heated at 1400°C for 20h, however, the total weight loss was 4.8% and x-ray analysis showed the sample to consist mostly of βAl_2O_3 and K_2SO_4, with a trace of Al_2O_3. In support of this conclusion, the composition $50K_2SO_4:50Al_2O_3$ when heated at 1500° for 1.5h showed only K_2SO_4 and βAl_2O_3.

5. In a sealed Pt tube the formation of βAl_2O_3 occurs between 1500 and 1650°C, as the increased vapor pressure of SO_3 raises the temperature of reaction.

6. One interesting conclusion is that K_2SO_4 and βAl_2O_3 are non-reactive up to at least 1650°C, the upper temperature limit studied, and, therefore, βAl_2O_3 has potential use in MHD systems, as for example, a preheater material. Potassium - βAl_2O_3, however, is probably not suitable as a MHD electrode or insulator material because of the ionic conductivity. The vapor pressure of potash over β-alumina also may be too high at high temperature.

3.8.b. K_2CO_3-Al_2O_3 System

K_2CO_3 reacts readily (800°-1000°C) with Al_2O_3 to produce $KAlO_2$. Compounds richer in K_2O than $KAlO_2$ have not been found and, hence, the system can be described as the $KAlO_2$-Al_2O_3 join. $KAlO_2$ shows a reversible endothermic peak near 535°. High temperature x-ray diffraction confirmed this transition. The high temperature form has cubic symmetry with $\underline{a}$=7.78A (600°C). The low temperature form appears to be a distorted variant, possibly having tetragonal symmetry. $KAlO_2$ is extremely reactive with atmospheric moisture and care must be taken in handling the material.

When $KAlO_2$ or compositions containing $KAlO_2$ are heated in air above 1225°C, vaporization of potash occurs and this tends to drive the initial bulk composition toward progressively higher Al_2O_3 contents. This precludes the preparation of accurate starting compositions by normal calcining methods for a study of the $KAlO_2$-Al_2O_3 join. It was found, however, that if K_2CO_3-Al_2O_3 compositions were pelletized, wrapped in Pt foil, then completely covered with a powder of like composition, potash losses can be minimized at temperatures up to 1350°C and compositional integrity could be maintained. Starting materials in the $KAlO_2$-Al_2O_3 system were prepared by this method and are now being used for high temperature equilibration studies using sealed Pt containers.

During the course of the work above a new DTGA apparatus was obtained, assembled and calibrated. It became apparent that advantage could be taken of the vaporization of potash from $KAlO_2$ such that phase relations and vaporization data for the entire $KAlO_2$-Al_2O_3 join could be derived. Using a Knudsen cell in the apparatus, the 1350°C isotherm in the system was defined. These results are preliminary and will be reported later in detail. Briefly, at 1350°C, potash vaporizes from $KAlO_2$ and the bulk composition enters the two phase $KAlO_2$-β-alumina field. With continued vaporization (linear rate) all $KAlO_2$ is lost as the bulk composition enters a single phase β-alumina solid solution region. The rate of vaporization decreases curvilinearly until the bulk composition enters the β-alumina plus Al_2O_3 two phase region (vaporization rate linear). This method, used for a number of isotherms, should define condensed phase relations and vapor pressures for the entire $KAlO_2$-Al_2O_3 join. Additionally, this

technique permits a determination of the composition of β-alumina independent of quenching studies.

It is apparent from the TGA data that potash is mobile from potassium aluminum oxides even at moderate temperatures. Although complete vapor pressure data will be obtained for additional isotherms, the preliminary data suggest that alumina will not be subject to degradation effects of potash vapors, certainly above 1500°C.

3.9. K_2O-SiO_2 System

Condensed phase relations in this system were determined by Kracek et al [36]. Vaporization data for this system, however, are not available. As silica is one of the major constituents of slag it becomes important to determine experimentally its affinity for potash. Such a study has been initiated using the DTGA-Knudsen cell method.

4. Electrical Conductivity and Related Properties

4.1 Introduction

The objective of this project is to provide engineering data on the electrical properties of MHD materials and to develop an understanding of the parameters that determine the conductivity in such solids. Attention is focussed on the electrical behavior of promising solids for electrodes and insulators in MHD ducts and on the characteristics of coal slag at high temperatures.

The amount of electrical data on these materials available in the literature appears to be very limited and needs drastic augmentation. The selection of materials to be measured and studied, and the setting of priorities has been done in cooperation with the investigators of other properties of MHD materials. Close contact has been maintained with the technical and engineering staff of MHD-facilities in this country. The collaborative effort with scientists of the USSR, aimed at the testing of materials in the U-02 MHD channel in Moscow, is very helpful in focussing attention on some of the major materials problems.

During the last 2 years our research work has emphasized the characterization of coal slag. Electrical (and other) measurements were made on a variety of slag and slag-seed samples.

The choice of electrode material is not yet fully decided. Ca-stabilized ZrO_2 has been used in a number of MHD-channels. However, its conduction is ionic and deterioration is inevitable. Hence,

various other materials are being considered; we have made measurements on a number of these compounds.

Several MHD-facilities have experimented with channel-coatings to prevent arcing and/or to keep the wall temperature reasonably low. The electrical conductivity of one of these materials (ZrO_2:MgO used in the AVCO channel) has been investigated.

Another crucial parameter of MHD-duct components is their thermionic emission. During the last 8 months we have assembled equipment to measure this high temperature property and have performed initial experiments.

Besides the characterization of MHD-materials in laboratory experiments it is important to determine how they stand up in actual operation. For this purpose we have started a testing program in cooperation with the University of Tennessee Space Institute (see section 7). Thus far, 4 different specimens have been exposed to two runs in the channel of the UTSI MHD-facility. These specimens have been subjected to a number of analytical tests.

4.2 Coal Slag

Coal contains about 10 percent in weight of inert material (slag), which is not burned in the combustion process. Consequently, the water-cooled walls of an MHD-channel will be covered with a thin layer (1-5 mm) of slag. The surface temperature of this layer facing the gas flow will depend on the degree of cooling of the walls. In general, this temperature will be higher than 1500 °C, and hence, the top layer will be in a vitreous state with low viscosity. It then follows that some of the liquid slag will be "sheared-off" by the gas stream and that a steady-state slag layer of certain thickness

will be established. This slag layer must have sufficient conductivity to permit passage of the MHD current perpendicular to the wall. On the other hand, the conductivity should be low enough not to cause a short circuit between adjacent electrodes. (see Figure 17). It is important therefore to know the electrical conductivity of different coal slags.

Experiments were performed on a "natural" slag sample obtained from the U. S. Bureau of Mines (MHD-12) and also on a few synthetic specimens. The "natural" slag specimen contained the following amounts of oxides (in wt. %): 50 SiO_2, 21 Al_2O_3 14 ($FeO + Fe_2O_3$), 5 MgO, 1 CaO, 1 K_2O and 2 SO_3. Electrical measurements were made on bar-shaped compacted samples using the 4-probe technique. Results are shown in Figure 18. The conductivity is rather high ($\sim 10^{-2}$ ohm^{-1} cm^{-1} at 1700 K) and is attributed to the transfer of electrons between ferric and ferrous ions. Anomalies in the range 1450 - 1610 K are the result of devitrification; below about 1610 K one or more crystalline phases begin to appear. The electrical conductivity of these phases is rather high and is determined by the ratio Fe^{2+}/Fe^{3+}. In turn this ratio depends on the degree of oxidation or reduction of the environment, on the presence of other ions, and on the solubility of ferric and ferrous ions in the different crystalline phases.

Similar experiments were performed on several synthetic slags (4 component system). Results of measurements on one of these samples (K 216), which contained a large amount of iron (36 wt. % Fe_2O_3), is shown in Figure 19. The conductivity is about 10 times higher than that of sample MHD-12 and both the temperature and pressure dependence are small.

Originally these measurements were made up to 1700 K (1427 °C). Later, this range was extended to 2050 K (1777 °C). At the higher temperatures the conductivity was determined using a 2 probe technique: one electrode was a cylindrical Pt "bucket" containing the liquid slag, while the other electrode was a Pt-wire dipping into the center of the liquid. The resistivity was "normalized" to the highest temperature result of the 4 probe method.

One important question is how the conductivity of slag will be affected by the presence of seed (e.g., K_2SO_4). In order to investigate this problem a base oxide (K 257) was prepared consisting of 43 SiO_2, 19 Al_2O_3, 30 Fe_3O_4 and 8 MgO (in wt. %). The conductivity of this synthetic slag specimen is shown in Figure 20.

The base oxide was mixed with K_2SO_4 seed at 1550 °C. Three melts were prepared: (A) 1 slag-4 seed, (B) 1 slag-1 seed, and (C) 4 slag-1 seed (weight ratios). Melts A and B showed strong separation while C appeared to be homogeneous to the eye. Chemical analysis showed that melt C contained 12.38 wt. % K_2O and no SO_2 or SO_3 was detected. The conductivity of the slag-seed mixture (melt C) is shown in the lower curve of Figure 20. The presence of potassium apparently inhibits the conduction rather than contributing to it.

4.3 Electrode Materials

One of the most interesting candidate materials for MHD electrodes is $LaCrO_3$ (doped with Sr or Ca) because of its high <u>electronic</u> conductivity. This compound was first introduced by Meadowcroft [37] who found that $LaCrO_3$ containing 16 mole % Sr was extremely corrosion resistant and had a nearly temperature-independent resistivity of $\sim$0.1 ohm^{-1} cm^{-1}. (Electrical resistivities of several promising electrode materials are plotted in Figure 21.)

Electrical and optical measurements were made on a number of doped and undoped La-chromites aimed at clarifying the conduction process in this compound. Single crystal growth of this material appeared to be very difficult. W. S. Brower (NBS) succeeded in growing one small crystalline sample of the undoped material. The electrical conductivity of this specimen appeared to be about 3 orders of magnitude higher than that reported by Meadowcroft [37]; other samples were produced by pressing the powdered material and firing at high temperatures (1500 °C and 1800 °C). Figure 22 shows the conductivities of a crystalline undoped sample, a Sr-doped sample and a Ca-doped specimen. The temperature dependence is surprisingly similar. Below 500 K the activation energy is between 0.10 and 0.20 eV; exhaustion is reached at about 1000 K. The activation energies of the heavily doped samples consistently appear to be the smallest.

It was impossible, unfortunately, to obtain Hall data. If the molar concentration of Sr or Ca is an indication of the number of carriers (in the exhaustion range) one calculates a mobility of 0.04 cm^2/volt sec. Such a value is entirely reasonable for electrons in oxides and explains the difficulties in measuring the Hall coefficient. A rough measurement of the sign of the thermo-electric power showed the carriers to be holes. It is possible that these holes can be thought of as residing on Cr^{4+} ions at low temperatures and producing an electric current, when the temperature increases, by transfer of the hole between Cr^{4+} and Cr^{3+} ions. Another interpretation is that the holes are localized at vacancies or near Sr- or Ca-ions and that transport occurs by excitation of the hole into the (oxygen ?) valence band.

Other attempts to produce an electronically conducting high temperature material were made by doping the very stable compound $SrZrO_3$. In contrast with ZrO_2 this material is not subject to so many phase transitions (as a function of temperature and pressure). We have prepared one sample consisting of 86 $SrZrO_3$ and 14 CeO_2 (mole %) and another with the composition 89.7 $SrZrO_3$, 5.9 $SrTiO_3$, 1.5 Ta_2O_5 and 2.9 $SrCO_3$ (mole %). It was hoped to produce Ce^{3+} and Ce^{4+} in the former case and Ti^{3+} plus Ti^{4+} in the latter.

Results of d.c. conductivity experiments on these two samples are presented in Figures 23 and 24. A.C. measurements performed at 100 Hz duplicate the d.c. results within the margin of error. In both cases the conductivity rises steeply with temperature; for the Ce-doped sample the activation energy is 4.0 eV and for the Ti-Ta-doped specimen E = 3.6 eV. The fact that the conductivity is nearly independent of frequency and of the surrounding oxygen pressure suggests that the conduction is electronic in nature. Considering the size of the activation energies it is possible that we are dealing with intrinsic excitation across the energy gap.

The magnitude of σ at 1700 °C is 0.1 ohm^{-1} cm^{-1}, an acceptable value for an MHD-material at that temperature. However, the conductivity drops off very rapidly towards lower temperature, posing severe problems with respect to the current carrying capacity in the neighborhood of the ceramic-metal contact.

4.4 Channel Coating

The conductivity of a sample of channel coating from the AVCO-Mark VI MHD-channel was measured over the temperature range 900 to 2000 K. This material consists primarily of ZrO_2 with additions of MgO (10-20 %).

Results of this experiment are shown in Figure 25. Little or no polarization effects were observed. The slope indicates an activation energy of ∿1.4 - 1.45 eV which is equal to that of ZrO_2-20% CaO reported by Strickler and Carlson [38]. This is taken as proof that the conduction mechanism in the MgO-doped material is the same as in the Ca-stabilized ZrO_2:diffusion of oxygen.

4.5 Thermionic Emission

The emissivity of the electrodes is of great importance for the transfer of electrons from the cathode to the plasma and from the plasma to the anode. Hence, it is useful to obtain some data concerning the thermionic emission of MHD-wall materials. We have started to construct an apparatus to investigate the emission from slag. It was decided to use an external heat source, rather than a heating wire. A 60 W CO_2-laser was used to heat the slag, which was deposited as a liquid drop on a small Pt-bead and then solidified by cooling. The temperature of the slag surface was measured by means of an optical pyrometer. The current from this emitter was collected on a thin semi-spherical Pt cup at a distance of 4 or 5 mm from the sample. The collector could be biased with respect to the emitter (+ or - 50 Volt). Measurements were performed in 1 atm. of air, 1 atm. of oxygen and 0.01 atm. of oxygen in nitrogen. It appeared that sizable currents - negative as well as positive carriers - were emitted even at relatively low temperatures (1200 - 1300 °C). The difference with common thermionic emission experiments on metals is that the slag material is much more volatile than solids like W or Pt. Hence, the measured currents are not pure electrons, but are mixed with all kinds of ions. (e.g., K^+, Fe^{++}, etc.). It is to be expected that at higher temperatures the electron emission will take over.

Unfortunately, the reflectivity of the spherical samples is very large and the power of the laser beam is not sufficient to heat the slag sample to temperatures much above 1300 °C. Consequently, further thermionic emission measurements will have to wait until a higher powered CO_2 laser will be available.

5. VAPORIZATION

The vaporization program is concerned with the transport of material to or from the walls of an MHD device. Efforts to study this problem fall into two categories.

The first consists of theoretical modeling of a) condensation of seed material, b) evaporation of structural materials, and c) reaction of structural materials with gaseous constituents of an MHD plasma to form stable gaseous species. Such modeling utilizes existing thermodynamic data and assumes that thermodynamic equilibrium is attained as the temperature and pressure change in the device.

The second category involves the experimental study of evaporation properties of coal slag under non-reactive conditions and the interaction of potential MHD construction materials with water vapor, which is present in relatively large concentrations in the MHD plasma. The latter process could lead to the formation of gaseous hydroxide vapor species which can become important transporters of material. In the following sections of the report, some of the results previously reported during the term of this project will be discussed.

5.1 Condensation of Seed Material

A significant problem in development of MHD devices has resulted from interaction of seed materials with the ceramic walls. Since the stability of K_2O-metal oxide compounds appears minimal with respect to decomposition to the metal oxide and gaseous K and O_2 in the temperature region of interest, it would appear that the observed interaction could be avoided if the device were operated with a sufficiently

high wall temperature. Two approaches to this problem were made. The lowest temperature at which interaction of seed would take place would be that at which pure seed material condenses on the ceramic in question and this is followed by solution of the ceramic in the liquid seed. Secondly, the activity of the seed in the melt in equilibrium with the ceramic in question can be estimated from the phase diagram by assuming ideal solution behavior. This will predict somewhat higher interaction temperatures because the activity of the seed in the gas phase will be less than unity when interaction takes place.

Two limiting cases have been considered. First, if clean "coal" having nominal composition $CH_{0.7}$ is burned with a stoichiometric amount of "air" consisting of N_2/O_2 in the molar ratio of 4, and seeded with K_2CO_3 so that the K content of the combustion products is 1% by weight, the condensation temperature of the $K_2CO_{3(\ell)}$ can be estimated. Secondly, if the same combustion process is carried out using K_2SO_4 as seed, $K_2SO_{4(\ell)}$ condensation will occur.

Figure 26 shows the variation in pressure as a function of temperature for CO_2, K, O_2, KOH, KO, and K^+ for a total pressure of 1 atm, the activity of K_2CO_3 in the melt assuming the activity is equal to the mole fraction in the K_2CO_3-MgO phase diagram, and the activity of K_2CO_3 in a hypothetical liquid phase for total pressures of 1 and 10 atm. The formation temperature of a stable liquid phase consisting of MgO dissolved in K_2CO_3, occurs at the point of intersection of the activity curve for the hypothetical liquid and the curve representing the activity of K_2CO_3 in solution (about 1385 K at 1 atm. total pressure). In the absence of this interaction, pure K_2CO_3 would

condense at the point where the activity of the hypothetical liquid phase equals 1 (about 1380 K). All of the pressure curves have been drawn below the condensation temperature as though condensation did not take place at 1380 K. At a total pressure of 10 atm condensation of K_2CO_3 will occur at 1580 K as indicated by the intersection of the line representing the activity of K_2CO_3 at 10 atm and the line representing the activity of solution. If no interaction took place, condensation would occur at about 1565 K. No pressure curves are shown in Figure 26 for the 10 atm case. Vapor species assumed to be present at equilibrium were CO_2, N_2, KOH, CO, OH, E^-, H_2O, H_2, O_2, K, KO, O NO, H, K^+, and OH^-. These results were obtained using a multicomponent equilibrium program based on the method described by Kandiner and Brinkley [39] and using thermodynamic data from JANAF [40].

Figure 27 shows results for the case where stoichiometric combustion takes place but the combustion products are seeded with K_2SO_4. The interpretation is similar to that of Figure 26. The activity of K_2SO_4 in the hypothetical condensed state equals that in the MgO saturated K_2SO_4 phase (derived from the MgO-K_2SO_4 phase diagram) at temperatures of about 1575 and 1775 K for total pressures of 1 atm and 10 atm respectively. Curves showing pressures of additional K bearing species, K_2SO_4(g), and KOH(s) have been shown. The pressure curves are for the 1 atm case. Below the condensation temperature, all of the pressure curves have been drawn to indicate that K_2SO_4 is being removed from the vapor phase. The sharp peak in the curve depicting the pressure of K_2SO_4 is due to the onset of condensation or exhaustion of $K_2SO_4(\ell)$ from the condensed phase.

Figure 28 shows essentially the same information as Figure 27, but in addition shows pressures of all those vapor species whose pressures are in excess of 10^{-6} atm under equilibrium conditions and shows the mole fraction of $K_2SO_4(s,\ell)$ in the solid or liquid form. Not shown are the activities of K_2SO_4 in the hypothetical condensed state nor the activities of K_2SO_4 in equilibrium with MgO. Since the total pressure is 1 atm, the mole fraction equals the partial pressure. In this calculation 57 additional vapor species were considered but were found to have pressures of less than 10^{-7} atm for the conditions and composition specified. The computations shown in Figure 28 were made using a program by Gordon and McBride [41].

All data for this computation were from JANAF with the exception of data for $K_2SO_4(g)$. Several studies have indicated that $K_2SO_4(g)$ is an important vaporization product of $K_2SO_4(s,\ell)$ [42,43] Data for $K_2SO_4(g)$ was therefore based on JANAF data for $K_2SO_4(s)$, the heat of sublimation of $K_2SO_4(s)$ reported by Halstead[43] and molecular constant data modeled after that reported by Cubicciotti [44] for $C_2SO_4(g)$ and $Rb_2SO_4(g)$. For $K_2SO_4(g)$, a number of vibrational frequencies were adjusted so that the entropy of sublimation calculated from the thermal functions agreed with those reported by Halstead at 1300 K. Additional details on this work can be found in the papers by Levin et al.,[45] and McDaniel and Plante [46].

These calculations show that in the case of MgO, wall temperatures in excess of 1800 K will be sufficient to eliminate condensed state seed interaction. Most ceramics which are considered potential condidates for MHD application can readily withstand such temperatures. The

problem of seed loss to coal slag and interaction of seed materials with other potential MHD materials is an important one and is being further studied in conjunction with the phase-equilibrium group at NBS. Of special importance is loss of seed to SiO_2.

5.2 Evaporation and Reaction of Structural Materials

The maximum temperature at which an MHD device can operate is dictated by the vaporization rate or vapor pressure of a material. Although the rate of loss of material through vaporization cannot be accurately predicted because of the high gas flow rate and boundary layers in an MHD device, experience seems to indicate that pressures in the range 10^{-5}-10^{-6} atm may be sufficiently low so that continuous operation for hundreds of hours could be achieved. The relatively high oxygen pressure in open cycle MHD will lead to enhanced stability of oxide ceramics which primarily vaporize by decomposition, will have no effect on those which vaporize to yield gaseous molecules having the same composition as the solid phase, and will lead to enhanced volatility of oxides which can form oxide vapor species having a higher oxidation state than the condensed phase. In addition, because of the relatively large hydrogen content of most coals, conditions will be favorable for formation of gaseous hydroxide species. Some of these principles are illustrated in the following discussion.

In Figure 29, saturation pressures of Mg bearing species that would be present in an MHD environment at 1 atmosphere total pressure are shown as a function of temperature.

In this calculation, it is assumed that coal ($CH_{0.7}$) is burned with a

stoichiometric amount of dry air (80/20 molar ratio N_2/O_2) and that the combustion products contain 1 wgt% K added as K_2CO_3. Gaseous species considered in this calculation are CO_2, N_2, KOH, O_2, H_2O, OH, CO, H_2, K, KO, O, NO, H and other gaseous atoms or molecules that can be formed by interaction of a metal oxide with H_2O or O_2 as indicated.

All data used for this calculation were from JANAF [40]. In addition, some MgO(g) data were taken from Brewer and Rosenblatt [47]. Two curves shown for MgO(g) represent the pressure based on the JANAF [40] tabulation and the pressure based on Brewer and Rosenblatt's [47] assessment of existing thermodynamic data. Although we believe that the assessment of Brewer and Rosenblatt probably predicts the MgO(g) pressure more reliably than the JANAF tabulation, this is not of particular importance for the point being made here. The major point here is that in the temperature range where the walls of a hot wall device would be expected to operate, say 1800-2200 K, the importance of hydroxide species appears to be about as great as other species responsible for transport and probably would become more important as the pressure is increased because of the increase in the partial pressure of water and the decrease in importance of reduced species such as Mg(g). (Figure 30).

Additional calculations have been made for other potential MHD materials. Figures 31 and 32 show partial pressures of Cr bearing species under MHD conditions and at total pressures of 1 and 5 atm. In this case pressures of Cr bearing species have been calculated as though pure Cr_2O_3 is the material undergoing interaction in the MHD environment. $LaCrO_3$, a potential MHD electrode material has a heat of formation from the pure oxides of about -10 kcal, and each of the gaseous species has

a single Cr atom so that the partial pressures of the Cr bearing species over $LaCrO_3$ will be reduced by about a factor of 4 at 1800 K below those shown i.e., $\Delta \log P = -5000/4.576\ (1800)$. This calculation shows therefore that the losses of material due to vaporization from $LaCrO_3$ will be much greater than losses from MgO due largely to formation of the gaseous species CrO_2OH. The oxidized species CrO_2 and CrO_3 will also be transporters of significant amounts of Cr and the utilization of $LaCrO_3$ as an electrode material at temperatures as high as 1800 K appears doubtful. For calculations of the partial pressures of the chromium bearing species heats of formation and free energy functions for CrO(g), CrO_2(g), and CrO_3(g) were from Schick [48], the heat of formation for Cr_2O_3(s) was from Brewer and Rosenblatt [47] while free energy functions for Cr_2O_3 were derived from the table given by Kelley [47]. The heat of formation and free energy functions for CrOH were from Jackson [50] while the data for Cr(g) were from JANAF [40]. The standard heat formation of CrO_2OH(g) was derived from an equation given by Graham and Davis [51] and was attributed to measurements of Belton and Kim [52]. Free energy functions for CrO_2OH(g) were derived at NBS from a molecular model adjusted to give the observed entropy change at 1500 K. Another value for the heat of formation of CrO_2OH has been reported by Bulewicz and Padley [53] from flame studies and is about 30 kcal more negative than that based on the equation given by Graham and Davis [51]. If the heat of formation based on the work of Bulewicz and Padley [53] is the more nearly correct value, use of $LaCrO_3$ as an MHD electrode material would be extremely doubtful.

Other calculations carried out show that ZrO_2 will not undergo significant transport because of formation of species such as ZrOH or $Zr(OH)_2$, but that calcia stabilized zirconia will tend to lose Ca because of formation of CaOH(g) and $Ca(OH)_2$(g) molecules in addition to vaporization of Ca(g) or (CaO(g).

5.3 Vaporization of a Model Slag

Studies on the evaporation of synthetic slag have involved the mass analysis of vapor effusing from an Ir Knudsen cell with a modulated beam mass spectrometer. Beam modulation makes it possible to distinguish between vapor molecules which come from the Knudsen cell and those which are due to residual gases in the vacuum chamber. Use of the mass spectrometric method to study evaporation processes is well known and several excellent reviews are available [54,55]. Vaporization pressures can be determined from the relationship

$$P_i = k_i I_i^+ T$$

where P_i is the pressure, k_i is a constant, I_i^+ is the ion current, i refers to a particular vapor species, and T is the absolute temperature. The value of k_i depends on geometrical constants, the cross section for ionization of the molecular species by electrons and multiplier gain factors. It must be evaluated by calibration experiments. However, even if the value of k_i is not known, some conclusions can be reached by using ratios of the product $I_i^+ T$ where the factor k_i cancels.

Four experiments have been run during this study. These have involved the vaporization of a 500 mg sample of slag as a function of temperature, the evaporation of a pure SiO_2 sample as a function of

temperature, the total evaporation of a 10 mg sample of SiO_2 at constant temperature and the evaporation of a 50 mg slag sample at 2000 and 2130 K. The latter two experiments serve the purpose of calibrating the spectrometer for its sensitivity to each of the major evaporation products.

The synthetic slag initially had a composition consisting of 0.582 mole fraction SiO_2, 0.152 Al_2O_3, 0.105 Fe_3O_4, and 0.161 MgO. Attention has been focussed mainly on the vaporization of the iron oxide and silicon dioxide from the slag. Ion currents due to their major vaporization products, namely, SiO(g), Fe(g), and O_2(g) have been measured. The analysis of these results is not completely unambiguous because changes in the concentration of the solution undergoing evaporation take place, the pressures of the species have different temperature coefficients, and phase separation may occur. Nonetheless, an attempt to understand the results in terms of ideal solution theory and presently available thermochemical data [40] can be made.

In principle, the oxygen pressure would be controlled by the vaporization of the more volatile component. From thermodynamic data, and assuming that the slag forms an ideal solution, we can expect that the oxygen pressure would be governed sequentially by the following reactions at temperatures up to about 2200 K,

$$Fe_3O_4(Soln) = 3FeO(Soln) + 1/2\ O_2(g)$$

$$FeO(Soln) = Fe(g) + 1/2\ O_2(g)$$

$$SiO_2(Soln) = SiO(g) + 1/2\ O_2(g)$$

The decomposition of Fe_3O_4(Soln) to FeO(Soln) and O_2(g) would give rise to an oxygen pressure orders of magnitude greater than the other decomposition processes until essentially all the Fe_3O_4(Soln) had decomposed. The oxygen pressure over the solution would next be controlled by the decomposition of FeO(Soln) and finally by SiO_2(Soln).

Figure 33 represents ion current data as a function of time obtained during an isothermal evaporation experiment. An initial vaporization period at 2000 K shows a decrease in the ion intensity of O_2^+ and corresponding increases in the Fe^+ and SiO^+ intensities, all intensities apparently becoming constant after about 20 minutes. The decrease in O_2 intensity and increase in SiO^+ and Fe^+ intensities are likely due to the gradual decomposition of Fe_3O_4. The following flat portions represent the interval during which FeO in solution controls the oxygen pressure.

After this period, the temperature was increased to 2130 K. The increase in intensity of the SiO^+ peak with decreasing oxygen pressure represents that concentration region in which the oxygen pressure is falling below the value controlled by FeO in the solution. The portion of the SiO^+ curve having essentially zero slope corresponds to the region of concentration where the SiO_2 in solution is controlling the O_2 pressure. The flat in the O_2^+ ion intensity curve at the same time interval confirms this, while the continual decrease in the Fe^+ curve during this interval indicates that no equilibrium with respect to an FeO species in the solution is being obtained, or the concentration of such a species is rapidly changing.

Figure 34 shows I^+T data for Fe(g), O_2(g), and SiO(g) above evaporating slag and some SiO(g) and O_2(g) data above pure SiO_2(s). The I^+T data for slag were obtained in order of increasing temperature after some initial heating to temperatures of 1930 K had been made. During the initial heating, O_2^+ signals slightly higher than those shown at the lower temperatures were observed. The most notable feature of the slag data is the high I^+T for O_2 at the lower temperatures as compared with the I^+T of O_2^+ over pure SiO_2. In addition, it can be seen that the ratio of ion currents of O_2^+ to SiO^+ are very much higher at the lower temperature than those shown in Figure 33 at 2000 K or 2130 K. This again is evidence that decomposition of Fe_3O_4 is controlling the oxygen pressure at these temperatures and at this particular time.

The I^+T data for SiO(g) and O_2(g) over pure SiO_2(s) can be used with the I^+T data for SiO(g) and O_2(g) over slag to show that the activity of SiO_2 in the slag solution must be close to unity. This follows from the stoichiometry involving evaporation of SiO_2 and the equilibrium constant for the process applied to both pure SiO_2 and the slag. Thus, at 1850 K it can be seen that the I^+T of SiO^+ for the slag is about 1/2 that for pure SiO_2 while the I^+T of O_2^+ for the slag is about 4 times that for SiO_2. This can only happen if the activity of SiO_2 in the solution is near unity. At the highest temperature, about 2060 K, the I^+T data points noted as 1 and 2 were taken in that order, and show changes in the SiO, Fe and O_2 pressures as the oxygen pressure over the slag begins to be governed by the SiO_2 decomposition rather than the FeO decomposition.

A preliminary conclusion reached from this study is that the decomposition of Fe_3O_4(Soln) is slower than it would be if thermodynamic

equilibrium were achieved. Equilibrium appears to be achieved, however, with respect to evaporation of SiO_2 from the slag solution with the activity of the SiO_2(Soln) near unity. The behavior of FeO in the slag remains to be determined. The possibility that the Ir cell can extract Fe from the FeO in the slag needs to be examined.

6. VISCOSITY OF COAL SLAGS

6.1 Introduction

The goal of this study is the development of viscosity data on coal slags over a temperature range that will be useful in the design and operation of coal-fired MHD systems.

The reason for this study is that the flow properties of the slags formed from the combustion of coal and from the reaction between these slags and the seeding material will affect the removal rate of the slags and they will affect the thickness of the slag layer which adheres to the electrodes and insulating walls of the channel.

Because of the great compositional variations that exist in American coals, it is considered paramount that equations should be developed for the prediction of the viscosity from compositional data rather than relying on making viscosity measurements on the slags from each batch of coal reaching a generating plant.

Coal slags are, for the most part, oxides in various proportions. The main impurities in the coal and therefore the main ingredients in the slags are the oxides of silicon, aluminum, iron, calcium and magnesium. The other impurities are minor and can be ignored for the present. The most useful viscosity data then would be that for the system which includes these five oxides. There is some viscosity-temperature data in the literature on parts of the compositional system involved. The detailed experimental study of a five component system over a broad compositional range appeared to be too complicated. Initial work, therefore, was designed to fill in the gaps in the literature in the several four-component systems

that make up this five-component system. In order to put the experimental work in perspective a brief mention of some pertinent literature follows:

Selvig and Gibson [56] reported the compositions of ashes of literally hundreds of U.S. coals along with temperatures at which samples of their slags or ashes either deformed, softened or became fluid. These three points for each slag, although roughly related to viscosity, are rather subjective and not useful in equations for determining flow rates.

Machin and co-workers [57,58,59] published a series of papers dealing with the viscosity of melts in the $CaO-MgO-Al_2O_3-SiO_2$ system.

Heywood and Womack [60] show the effect on viscosity-temperature relationships of one five-component slag when 15% K_2O is added. This gives an idea of the effect to be expected when coal slags are exposed to seeding materials. The authors also show the effect of alkali additions on the viscosity of the composition $3SiO_2 \cdot Al_2O_3 \cdot CaO$.

Elliott, Gleiser and Ramakrishna [61] review the viscosity literature pertinent to steelmaking and include material from Machin and others that also pertain to coal slags.

Other studies could be referenced here but the complete data needed for predicting the viscosity of coal slags is not available. For this reason laboratory studies were deemed necessary.

6.2 Model Slag Studies

The logical approach to the development of equations that would permit the calculation of viscosity from composition was to make a model slag study. By melting a series of relatively simple compositions differing from each other in some systematic way, it was believed that rules for flow behavior

could be formulated. Two systems not found in the literature were chosen for the initial study. These were the silica-alumina-iron oxide-lime and silica-alumina-iron oxide-magnesia systems. Preliminary melts were made in the former system to determine melting characteristics while awaiting some changes in viscometer instrumentation. Attention was drawn to the magnesia containing system, and most of the four-component studies dealt with this system.

Viscosity values were determined over a temperature range which was limited partly by the instrumentation and partly by the nature of the melts. The upper temperature limit was approximately 1550° C in some of the earlier melts; this was increased to about 1600° C by rebuilding the viscosity furnace. The lower temperature limit for each melt usually depended on the liquidus temperature of that particular composition. Most of the melts encountered in this study crystallized rapidly as soon as the temperature got below the liquidus. As crystals began to grow on the spindle or on the surface of the melt, the viscosity would start to increase with no change in temperature. Once viscosity determinations became time-dependent they were considered useless and were discontinued. In these studies the liquidus temperatures usually fell between 1250° and 1400° C. Figure 35 illustrates the singular nature of the viscosity datum points above the liquidus temperature and the multiplicity of values possible below the liquidus temperature.

Figure 36 shows typical viscosity data for the four-component synthetic slags. Although the viscosities of these melts differ from each other at

any given temperature, the remarkable feature is the similarity of the temperature coefficients of viscosity for the different compositions.

During the course of the investigation of these simple melts, each containing four oxides, attention was focused on a British publication that offered the type of equations for calculating the viscosity that was the goal of this study. If the equations should prove satisfactory for predicting viscosities of slags from American coals then further model studies would not be necessary. The four-component study, therefore, was at least temporarily terminated in order to test the validity of the new equations with synthetic or model five-component melts. This new task is described in the following paragraphs.

6.3 Model Studies to Test Watt-Fereday Equations

Watt and Fereday [62] measured the viscosity-temperature relationships of the ashes of more than one-hundred different coals from Great Britain. From this data they generated equations for the purpose of calculating the viscosity at any temperature and composition within their specified limits. The authors claim that the important constituents in coal slags with respect to viscosity determinations are the oxides of silicon, aluminum, iron, calcium and magnesium. They ignore all others as individual oxides and lump them together with magnesium.

The Watt-Fereday equations are as follows:

$$\log_{10} \eta = \frac{10^7 M}{(T-150)^2} + C$$

where η is viscosity in poises*

$M = 0.00835\ (SiO_2) + 0.00601\ (Al_2O_3) - 0.0109$

$C = 0.0415\ (SiO_2) + 0.0192\ (Al_2O_3) + 0.0276$

$(\text{equivalent } Fe_2O_3) + 0.0160\ (CaO) - 3.92$

T is temperature in degrees Celsius.

The oxides in parentheses are the concentrations of these oxides in the melt expressed in weight percents.

* To convert poises to pascal seconds, multiply by 10^{-1}. Therefore, to express $\log_{10}$ viscosity in SI units, subtract 1 from $\log_{10}$ above.

If these equations satisfactorily describe the viscosity-temperature relationships for slags from American coals there will be no need for further model studies.

When these equations came to light a series of five-component melts was made and viscosities were determined. The experimental data were compared with viscosities calculated with the Watt-Fereday equations. Table 4 lists the compositions of the melts whose specific purpose is to test out the usefulness of the Watt-Fereday equations over the range of slag compositions which might be expected from different U.S. coals. Figures 37 through 42 allow the comparison of the viscosity data of these melts obtained in the laboratory with the calculated values using the Watt-Fereday equations. The data points at 1700° C in Figures 37, 38 and 39 are

mathematical extrapolations of data at lower temperatures. In Figures 40, 41, and 42 the extrapolations are graphical. The mathematical method is described in detail in the next section of this report.

In almost all of these comparisons of calculated viscosities with measured viscosities the ability of the equations to predict the slope of the curves (the temperature coefficient of viscosity) is remarkably good. It is also noteworthy that the equations are satisfactory for predicting the viscosity of a majority of the melts, but they are very poor in some cases. Those melts where the agreement between measured and calculated viscosities is poorest are K391 in Figure 39, K388 in Figure 40, K396 in Figure 41 and K394, K398 and K390 in Figure 42. In these cases, there appears to be a pattern that would indicate that the equations are not suited for melts containing unusually large amounts of either iron oxide or the oxides of calcium and magnesium. This discussion does not lead to any positive conclusions except that the Watt-Fereday equations are not entirely satisfactory over the desired compositional range but they seem to predict satisfactorily the change of viscosity with temperature.

The measured data on all of these melts will be used to redetermine the factors associated with each of the four oxides determined by Watt and Fereday, in an attempt to achieve a better overall prediction of viscosity over the desired temperature and composition ranges. The form of the equation will be changed to include a factor for MgO as well. Perhaps an extra term will extend the capability of the equations.

Two other articles have been published recently by geologists that are of great interest. Bottinga and Weill [63] analyzed viscosity data from the literature on glasses, slags, lavas and magmatic silicate melts. They formulated equations for calculating the viscosity of a melt from its composition and temperature. Unfortunately, these authors are primarily interested in magmatic melts in which they assume the Al_2O_3 to be associated in stoichiometric proportions with the alkali and alkaline earth oxides. They make no provision for Al_2O_3 in excess of the amount required to combine with CaO and MgO in a 1:1 ratio. The excess alumina present in many coal slags cannot be accounted for by their technique, yet this material influences the viscosity very strongly.

Shaw [64] refined the method of Bottinga and Weill but his method is still restricted to alumina compounds of the alkalis and alkaline earths. It is possible that their techniques may be useful if a separate factor is provided for Al_2O_3 by itself.

6.4 Extrapolation of Viscosity to 1700° C

Interest has been shown in obtaining viscosity information on slags at 1700° C for purposes of estimating slag layer thickness in the channel at this temperature. 1700° C is being considered as an optimum operating temperature for the gas flow through an MHD channel. There will be a temperature gradient across the slag layer from gas temperature on the inside to electrode temperature on the outside of the slag layer.

1600° C is the upper limit of the present furnace and viscometer and, therefore, some sort of calculation or extrapolation of known viscosities will be necessary over an interval of at least 100 degrees.

The Watt-Fereday equations described above make a direct calculation from composition at any temperature. The data from which these authors derived the constants for their equations were determined by actual viscosity measurements at temperatures up to 1800° C and should therefore be valid at 1700° C.

One method for extrapolating data on actual compositions being measured is to assume some type of equation form to describe the known behavior of the liquids, use that data in the equation to determine the constants and then to apply the equation to solve for viscosities at new temperatures.

This has been done by Napolitano and Hawkins [65] for glasses including some used as standard reference materials for calibrating viscometers. They used the Fulcher equation having the form:

$$\log_{10} \text{viscosity} = B + \frac{C}{T-T_o}$$

where viscosity is expressed in poises, T and T_o are temperatures in Celsius degrees. They used the equation together with a large amount of carefully gathered data to determine via a least squares solution the constants B, C and T_o. The constants then were published and are furnished with a sample of the material when it is purchased for calibration purposes. Its intended use is for interpolation to any temperature within the range of the data upon which the constants were determined. Extrapolation was not intended but should be satisfactory over a short interval with increasing temperature and decreasing viscosity.

Figures 37, 38 and 39 not only show the viscosity over the measured range for the model slags, but they show extrapolation of each melt to 1700° C using the Fulcher equation based on data not exceeding 1600° C. These figures show that in many cases there is a very close agreement between the Fulcher extrapolation to 1700° C of real data with the Watt-Fereday calculation using composition and temperature values only.

Mathematically the Watt-Fereday expression for viscosity, in terms of temperature, is only slightly different from the Fulcher expression. In the former the $(T-T_o)$ term is squared, whereas the same term in the latter case is a first power term. The influence of this difference is to give the Watt-Fereday log viscosity-temperature relationship a smaller temperature dependence than the Fulcher expression. This effect is quite noticeable when comparing the measured with the calculated curves, especially with MHD-11 and K384 in Figure 37, K257 in Figure 38 and K363, K385 and even K391 in Figure 39.

6.5 Phase Separation in Seeded Melts

The composition of coal slags which enter an MHD channel will be different from the composition of slags tapped from the combustor and therefore their viscosities and other properties will be different. The seeding material, which is necessary for gas conduction, will affect the viscosity of the channel slag and must be assessed along with the other constituents.

In order to get some idea of the composition to be expected of a seeded channel slag, a cold probe was inserted in the exhaust gases of a Bu Mines

coal combustor into which a K_2CO_3 solution was being sprayed. The material which condensed on this probe was not necessarily a perfect representation of everything in the exhaust stream of this unit but it should be somewhat representative of that which would condense on a cold channel wall. This material is identified as MHD-12F. An analysis showed that the material was a mixture of oxides, and a K_2SO_4-K_2CO_3 solid solution. Potassium sulfate is used in melting operations in commercial silicate glass manufacture and is known to form an immiscible layer on the surface of the melt. It could exhibit this type of behavior with coal slags and its viscosity behavior should be understood. Consequently, a series of melts were made in which the composition of the oxide portion was kept constant and approximately the same as in MHD-12F. This oxide portion contains 43% SiO_2 by weight, 19% Al_2O_3, 30% Fe_3O_4 and 8% MgO. This is identified as melt K257 in Table 4 and Figure 38. The proportions of K_2SO_4 and the oxide mixture were varied, in order to determine the extent of the immiscibility.

Melts were stirred for an hour at 1550° C and then held at 1500° C without stirring for another hour. In some cases, the melts separated into two layers. The upper layer was fluid, much less dense, and, when decanted from the remaining liquid, cooled to a tan crystalline mass. The lower layer was viscous by comparison, heavy, and cooled to a black crystalline mass.

Mixtures were melted in the following proportions: 80% K_2SO_4-20% oxides, 50% K_2SO_4-50% oxides, 30% K_2SO_4-70% oxides and 20% K_2SO_4-80% oxides. Table 5 gives the analyses of the upper and lower layers. Very little K_2SO_4 was found dissolved in the oxide layers (lower), but amounts of K_2O were found in these lower layers. This indicates that the K_2SO_4 decomposed upon reaction with the slag oxides releasing "SO_3". The almost pure K_2SO_4 dissolved very little of the oxides.

The boundary between the one-liquid and two-liquid regions at 1500° C is very close to the 30% K_2SO_4-70% oxides because the melt of this composition contained but very little of the upper or sulfate layer. The 20% K_2SO_4-80% oxide mixture remained a single liquid; no separation was observed at all. There is undoubtedly some temperature above 1500° C at which the materials are completely miscible and on quenching no phase separation could be seen.

This phenomenon of phase separation in the liquid state in these slags can be important in designing and operating real-life MHD systems. From a point of view of maximum seed recovery it might be desirable to operate on a schedule that would permit phase separation. For other reasons, it might be desirable to operate at higher temperatures where phase separation might not occur. By understanding this phenomenon in relation to the slag compositions, it will be possible to control the slag behavior by means of seed-slag proportioning and by temperature control.

6.6 Viscosity of K_2SO_4 Layer

In further exploration of the oxide-sulfate system representing seeded channel slags, it was desirable to determine the viscosity of the fluid K_2SO_4 liquid and the effect on this viscosity of a small amount of dissolved oxide slag. Two melts were prepared; one was pure K_2SO_4 (K330) and the other was 95% K_2SO_4 and 5% of the oxide slag described in the section above on immiscibility (K348). Both melts had such low viscosities that accurate values can not be reported. They are both estimated to be between 0.1 and 0.3 poises. No change in viscosity could be observed between 1318 and 1080° C for the pure K_2SO_4 and between 1518 and 1080° C for the melt containing the oxides. The lower temperature is only a few degrees above the freezing temperature of the K_2SO_4. The presence of the dissolved oxide had no observable effect on the viscosity of the K_2SO_4.

6.7 Viscosity of Oxide Layer

The viscosity of the synthetic oxide slag used throughout the phase studies (K257) is shown in Figure 35 and Figure 38. This represents the pure oxide starting material. After melting this with K_2SO_4 it has been noted that there is considerable K_2O present but no appreciable "SO_3" in this layer. The K_2O will have a considerable effect on the viscosity of the oxide slag. Heywood and Womack [60] showed the effect of 15% K_2O on a five-component oxide slag. The effect of K_2O additions to this oxide slag used in the present studies (K257) will be reported in the future.

6.8 Instrumentation

Viscosity measurements were made throughout this study with a high-temperature adaptation of a Brookfield "Synchrolectric" viscometer unit. Essentially, the unit rotates a cylindrical spindle or "bob" at a constant rate and measures the torque required to maintain this rotation against the opposing viscous drag of the test liquid into which the spindle is immersed. See Figure 43. The torque-rpm relationship is uniquely related to the viscosity of a Newtonian liquid (one whose viscosity is not affected by the shear rate). This is not an absolute measurement method; it is calibrated with a National Bureau of Standards standard reference glass intended for this exact purpose. The particular glass used was SRM 710, although there are others. This was chosen because its temperature-viscosity relationships are similar to the silicate melts in these coal slag studies.

The high temperatures encountered require that the cylindrical spindle as well as the containing vessel are made of a refractory and inert material. A rhodium alloy of platinum was chosen for both. The furnaces used for melting the batch materials and for viscosity determinations are heated electrically, using silicon carbide resistance heating elements, in an open or oxidizing atmosphere. The torque unit was mounted on special ways for maintaining proper centering of the spindle with respect to the melt, while allowing for coarse and fine vertical adjustment. The fine adjustment is an important feature to insure controlled immersion depth of the spindle in the melt. Figure 44 is a schematic diagram of this furnace-viscometer arrangement.

During the course of adapting the viscometer unit for high-temperature use it was determined that the long platinum alloy spindle was too heavy for the bearings in the torque unit. An air-bearing was constructed which supports the weight of the spindle on a cushion of air which escapes in a radial direction from the axis of the system. This provides support while introducing no torque or drag to influence the viscosity determination. The air pressure is from a 15 psi line through a reducing regulator to provide low pressure and fine control. A schematic of this air-bearing is shown in Figure 45.

The temperature limitation of the viscometer is that of both the electric furnace and the platinum alloy vessel and spindle. 1600° C is considered the maximum regular operating temperature of the system. The temperature is determined and controlled by thermocouples, each having one leg of a 30% Rh-70% Pt alloy and the other of a 6% RH-94% Pt alloy.

6.9 Viscosity-Composition-Temperature Calculations

The Watt-Fereday equations for calculating viscosities from composition and temperature data are found to be inadequate for certain compositions. Additional model slag data are needed to compute new coefficients to be used with the general equations of Watt and Fereday. At present there is no coefficient to be applied to the MgO concentration. An extra term needs to be added to the W-F equations to include MgO directly rather than by difference.

Shaw's method should be analyzed to determine if an Al_2O_3 factor can be added to his equations for viscosity prediction.

7. Materials Testing

7.1. NBS-UTSI Program

Since Dec. 1973, NBS has engaged in a cooperative materials testing program with the University of Tennessee Space Institute. The MHD-facility at UTSI is relatively small; however, it has the distinction of being the only coal-fired MHD-generator in the world. The walls of the channel consist of segmented copper electrodes that are water-cooled; the entrance of the duct has a cross section of 2" x 4". Copper sample holders were fabricated that could be inserted in cut-out sections of the electrodes. Samples of test materials can be fitted into these sample holders; a thin coat of plasma sprayed alumina was applied between the holder and the specimens. Holes were drilled in some of the samples and thermocouples fitted into these holes (1 mm from top surface) (see Figures 46 and 47).

Four different materials were tested in 2 runs. In the first test (March 1974) clean fuel (kerosene) was used and in the second coal (April 1974); both tests lasted 12 minutes. During the March run the thermocouples indicated temperatures of 900 - 1000°C; in the April test the temperature was much lower (∿300 - 700°C), due to the coal-slag layer.

The four materials were:

1. Mo-metal - UTSI, m.pt. 2610°C.
2. $La_{1-x}Ca_xCrO_3$ (x = 1%) - Nippon Kagaku Togyo Co., Osaka, Japan, m.p. 2500°C.
3. ZrB_2 (+ 20% SiC) - ("Boride V") - Manlabs - m.pt. >2664°C.
4. SiC (hot pressed) - ("Noralide") - Norton Co. - m.pt. 2450°C.

Data on these materials were assembled (before the test) from the literature and from some additional measurements. After the test runs the samples were examined by means of visual observation under the microscope and by x-ray diffraction. The results of these examinations can be summarized as follows:

1. Mo metal Run #1: strong oxidation (MoO_3?)
   Run #2: Mo-metal plus K_2SO_4.

2. $La_{1-x}Ca_xCrO_3$ (x=1%) Run #1: essentially unchanged
   Run #2: drastic change, none of the original material left, no K_2SO_4.

3. ZrB_2 Run #1: strong oxidation to ZrO_2.
   Run #2: little change, K_2SO_4 present, no ZrO_2.

4. SiC Run #1: no change
   Run #2: little change, K_2SO_4 present.

A chunk of the coal slag layer was examined also. The top half millimeter was entirely glassy and hence the surface temperature must have been as high as 1300°C and possibly 1500°C (depending on the K content). Deeper into the slag layer the materials appeared to be strongly crystalline; the stronger x-ray diffraction lines correspond to orthorhombic $KAlSiO_4$.

Near the coal wall of the channel the K-concentration was very high. It seems that the seed condenses first before the slag layer is formed. Delayed seed injection can probably reverse this sequence.

7.2. US-USSR Program

As part of its regular work on MHD materials NBS has been participating in the planning and related activites connected with the materials testing program now being set up under the joint US-USSR Cooperative Program on

MHD. The materials testing effort involves reciprocal tests in both the USSR and the United States MHD facilities. These tests are designed to provide information relative to the durability and reliability of high temperature MHD components, particularly electrodes and insulators, under controlled MHD conditions. Emphasis will be placed on the effect the design of the component has on the materials performance. Further advanced in planning is the sub-program utilizing the USSR U-02 MHD unit. Phase 1 of this effort consists of a 100h test of a series of ZrO_2 base (with CeO_2 or Y_2O_3 additions) solid electrodes under clean fuel and hot wall conditions. Actual testing is scheduled for the first quarter of 1975 (CY).

NBS will continue to aid in the planning and coordination of this joint program and in addition, participate in the conduction of various tests and in the characterization of pre-test and post-test materials.

8. Publications and Talks

The information and data summarized in the preceeding sections are given in greater detail in quarterly reports regularly submitted to the Office of Coal Research. In addition to these, however, significant aspects of the work are often published in professional journals and presented orally at various technical meetings. These are tabulated in the following list:

1. H.P.R. Frederikse* and W.R. Hosler, "Electrical Conductivity of Coal Slag", Proceedings of 13th Symposium on Engineering Aspects of Magnetohydrodynamics, Stanford University, March 26-28, 1973.

2. E.M. Levin*, S.J. Schneider and E.R. Plante, "Phase Equilibria Involving Seed Materials in MHD", Proceedings of 13th Symposium on Engineering Aspects of Magnetohydrodynamics, Stanford University, March 26-28, 1973.

3. S.J. Schneider and E.M. Levin, "Polymorphism of K_2CO_3", J. Am. Ceram. Soc. 56 [4] 218-219 (1973).

4. E.M. Levin, "The System K_2SO_4-Cs_2SO_4", J. Am. Ceram. Soc. 56 [8] 427-430 (1973).

5. J.B. Wachtman and S.J. Schneider, "Measurements and Standards of High Temperature Materials in Energy Conversion and Clean Fuel Production", Standardization News, STDNA 1 [8] 16-23 (1973).

6. H.P.R. Frederikse*, "Materials for MHD Power Generation", Wayne State University, Detroit, Michigan, May 16, 1973.

7. S.J. Schneider*, W. Capps, H.P.R. Frederikse, W.R. Hosler, C.L. McDaniel, and E.R. Plante, "High Temperature MHD Materials", US-USSR Colloqium on MHD Powder Generation, Moscow, Russia, Feb. 25-27, 1974.

8. C.L. McDaniel* and E.R. Plante, "Phase Relations Involving Seed-Electrode-Insulator Materials in MHD", 14th Symposium on Engineering Aspects of Magnetohydrodynamics, Univ. Tennessee Space Institute, April 8-10, 1974.

9. W.R. Hosler, W. Capps and E.R. Plante*, "Some Physical and Chemical Properties of Coal Slags", 14th Symposium on Engineering Aspects of Magnetohydrodynamics, Univ. Tennessee Space Institute, April 8-10, 1974.

10. H.P.R. Frederikse* and W.R. Hosler, "Electrical Conductivity of MHD" 14th Symposium on Engeering Aspects of Magnetohydrodynamics, Univ. Tennessee Space Institute, April 8-10, 1974.

11. L.H. Grabner*, W.R. Hosler and H.P.R. Frederikse, "Some Optical and Electrical Properties of Undoped and Sr-Doped $LaCrO_3$", 14th Symposium on Engineering Aspects of Magnetohydrodynamics, Univ. Tennessee Space Institute, April 8-10, 1974.

12. G.A. Candela*, R.A. Forman, A.H. Kahn, D.B. Meadowcroft, and J. Wimmer, "Magnetic Susceptibility of Lanthanum Chromite Doped with Strontium", 14th Symposium on Engineering Aspects of Magnetohydrodynamics, Univ. Tennessee Space Institute, April 8-10, 1974.

13. S.J. Schneider*, "Energy Conservation Through Improved Energy Conversion", Annual meeting-American Ceramic Society, Chicago, Illinois, April 28 - May 1, 1974.

14. W. Capps*, "Viscosity of Some Molten Coal Slags", Annual Meeting - American Ceramic Society, Chicago, Illinois, April 28 - May 1, 1974.

15. H.P.R. Frederikse*, "Materials Requirements for MHD", ASM Forum on on Materials for Power Generation, Seven Springs, Pa., June 17-19, 1974.

* Denotes talk by indicated author.

9. References

1. W. A. Selvig and F. H. Gibson, Bull. 567, Bureau Mines 33 pp (1456).

2. NBS-ICTA Standard Reference Material 759, DTA Temperature Standards (295-675 °C); Ibid, 760 (570-940°C).

3. E. M. Levin and F. A. Mauer, J. Am. Ceram. Soc. 46 [1] 59-60 (1963).

4. S. Makarov and M. P. Shugina, Bull. Acad. Sci. USSR 5, 691-700 (1940).

5. A. Reisman, J. Am. Chem. Soc. 80, 3558-61 (1958).

6. A. Reisman, J. Am. Chem. Soc. 81, 807-811 (1959).

7. S. J. Schneider and E. M. Levin, J. Am. Ceram. Soc. 56, 218-219 (1973).

8. P. M. de Wolff, Techn. Phys. Dienst, Delft, Holland. PDF Card No. 16-820, Powder Data File Issued by Joint Committee on Powder Diffraction Standards, Swarthmore, Pa. 19081.

9. A. J. Majumdar and R. Roy, J. Phys. Chem. 69, 1684-86 (1965).

10. M. Bernard and J. Jaffray, Compt. Rend. 240, 1078 (1955).

11. C.W.F.T. Pistorius and E. Rapoport, J. Phys. Chem. Solids 30, 195-201 (1969).

12. H. E. Swanson, R. K. Fuyat, and G. M. Ugrinic, NBS Circular 539, 3, 63 (1954); PDF Card No. 5-613.

13. G. Pannetier and M. Gaultier, Bull. Soc. Chim. Fr. 1966, 188-194 (1966); PDF Card No. 18-1060.

14. L. Denielou, Y. Fournier, J.-P. Petitet, and C. Tequi, C. R. Acad. Sci., Paris 270 [8] 1854-56 (1970).

15. L. Erdey, G. Liptay, and G. Sol, Talanta 12 [3] 256-67 (1965).

16. V. E. Plyushchev, R. G. Samuseva, and I. F. Poletaev, Zhur. Neorg. Khim. 7 [4] 860 (1962); Russ. J. Inorg. Chem. (English Transl.) 445 (1962); Also, Fig. 2886 in Phase Diagrams for Ceramists, E. M. Levin, C. R. Robbins, and H. F. McMurdie, The American Ceramic Soc. Inc., Columbus, Ohio (1969).

17. D. Tabrizi, M. Gaultier, and G. Pannetier, Bull. Soc. Chim. Fr. 1968 [3] 935-39 (1968).

18. (a) H. Muller, Kristallografiya 53, 511 (1914).

    (b) V. E. Plyushchev and N. F. Markovskaya, Dokl. Akad. Nauk USSR 95, 555 (1954).

19. K. H. Stern and E. L. Weise, High Temperature Properties and Decomposition of Inorganic Salts, Part I. Sulfates, National Standard Reference Data Series - National Bureau of Standards 7, 39 pp (1966).

20. K. J. Rao and C. N. R. Rao, J. Matls. Sci. 1, 238-48 (1966).

21. H. E. Swanson, N. T. Gilfrich and M. I. Cook, NBS Circular 539, Vol. 7, p. 17 (1957); PDF Card No. 8-462.

22. O. S. Dombrovskaya, Zhur. Obschchei Khim., 3 [8] 1017 (1933); Also Fig. 2884 in Phase Diagrams for Ceramists, E. M. Levin, C. R. Robbins, and H. F. McMurdie, The American Ceramic Soc. Inc., Columbus, Ohio (1969).

23. E. M. Levin, J. T. Benedict, J. P. Sciarello, and S. Monsour, J. Am. Ceram. Soc. 56 [8] 427-430 (1973).

24. G. G. Diogenov and V. I. Ermachkov, Zhur. Neorg. Khim. 11 [12] 2825 (1966); Russ. J. Inorg. Chem. (English Transl.) 1519-21 (1966).

25. R. W. G. Wyckoff, Crystal Structures, Vol. 3, 2nd ed; p. 113, John Wiley & Sons, Inc., New York (1965).

26. H. LeChatlier, Compt. Rendu 118, 350 (1894).

27. M. Amadori, Atti della Reale Accad. Dei Lincei [5] 21, II 65 (1912).

28. JANAF Thermochemical Tables, the Dow Chemical Co., Midland, Michigan updated through June 30, 1973.

29. P. J. Ficalora, O. M. Uy, D. W. Muenow and J. L. Margrave, J. Am. Ceram. Soc. 51, 574 (1968).

30. W. D. Halstead, Trans. Farad. Soc. 66, 1966 (1970).

31. D. Cubicciotti, High Temp. Sci. 3, 349 (1971).

32. P. M. de Wolff, Techn. Phys. Dienst, Delft, Holland, PDF Card No. 11-655, Powder Data File issued by Joint Committee on Powder Diffraction Standards, Swarthmore, Pa. 19081.

33. V. N. Pavlikov, A. V. Shevchenko, L. M. Lopato, and S. G. Trevyatskii, Chem. of High Temperature Materials, 57 (1969).

34. J. S. Ruiz, A. M. Anthony, and M. Foex, C. R. Acad. Sc. Paris 264, 1271-4 (1967).

35. S. Geller and P. M. Raccah, Phys. Rev. B2, 1167-71 (1970).

36. F. C. Kracek, N. L. Bown, and G. W. Morey, J. Phys. Chem. 41 [9] 1183 (1937).

37. D. B. Meadowcroft in "Open-Cycle MHD-Power Generation, Ed. by J. B. Heywood and G. J. Womack, Publ. by Pergamon Press, Oxford, England 1969, Chapter 7.

38. D. W. Strickler and W. G. Carlson, J. Am. Ceram. Soc., 47, 122 (1964).

39. H. J. Kandiner and S. R. Brinkley, Jr., Ind. and Eng. Chem., 42, 850 (1950).

40. JANAF Thermochemical Tables, The Dow Chemical Company, Midland, Michigan.

41. S. Gordon and B. McBride, NASA SP-273 (1971).

42. P. J. Ficalora, O. M. Uy, D. W. Muenow, and J. L. Margrave, J. Am. Ceram. Soc., 51, 574 (1968).

43. W. D. Halstead, Trans. Farad. Soc., 66, 1966 (1970).

44. D. Cubicciotti, High Temp. Sci., 3, 349 (1971).

45. E. M. Levin, S. J. Schneider, and E. R. Plante, 13th Symp. on Eng. Aspects of MHD, Stanford Univ., IV 5, March (1973).

46. C. L. McDaniel and E. R. Plante 14th Symp. on Eng. Aspects of MHD, Tullahoma, Tenn., April (1974).

47. L. Brewer and G. M. Rosenblatt, in "Advances in High Temperature Chemistry," Ed., L. Eyring, Vol. 2, Academic Press, New York (1969).

48. J. L. Schick, Ed., "Thermodynamics of Certain Refractory Compounds," Vol. II, Academic Press, New York (1966).

49. K. K. Kelley, U. S. Bur. Mines Bull. 584 (1960).

50. D. D. Jackson, UCRL-51137 (1971).

51. H. C. Graham and H. H. Davis, J. Am. Ceram. Soc., 54, 89 (1971).

52. G. R. Belton and Y. W. Kim, Quoted by [51].

53. E. M. Bulewicz and P. J. Padley, Proc. Roy. Soc., London, A323, 337 (1971).

54. J. Drowart, A. Pattoret, and S. Smoes, Proc. Brit. Cer. Soc., No. 8, 67 (1967).

55. R. T. Grimley, Mass Spectrometry, in "The Characterization of High Temperature Vapors," J. L. Margrave, Ed., John Wiley & Sons, Inc., New York (1967).

56. W. A. Selvig and F. H. Gibson, U.S. Bur. Mines Bull. 567 (1956).

57. J. S. Machin and D. L. Hanna, J. Am. Ceram. Soc., 28, 310 (1945).

58. J. S. Machin and T. B. Yee, J. Am. Ceram. Soc., 31, 200 (1948).

59. J. S. Machin, T. B. Yee and D. L. Hanna, J. Am. Ceram. Soc., 35, 322 (1952).

60. J. B. Heywood and G. J. Womack, "Open-Cycle MHD Power Generation," Pergamon Press (1969).

61. J. F. Elliott, M. Gleiser and V. Ramakrishna, "Thermochemistry for Steelmaking, Thermodynamic and Transport Properties," Vol. II, Addison-Wesley Publishing Co. (1963).

62. J. D. Watt and F. Fereday, J. Inst. of Fuel, 338, 99 (1969).

63. Y. Bottinga and D. F. Weill, Amer. J. of Sci, 272, 438 (1972).

64. H. R. Shaw, Amer. J. of Sci., 272, 870 (1972).

65. A. Napolitano and E. G. Hawkins, J. Res. NBS, 68A (Phys. and Chem.), No. 5, 439 (1964).

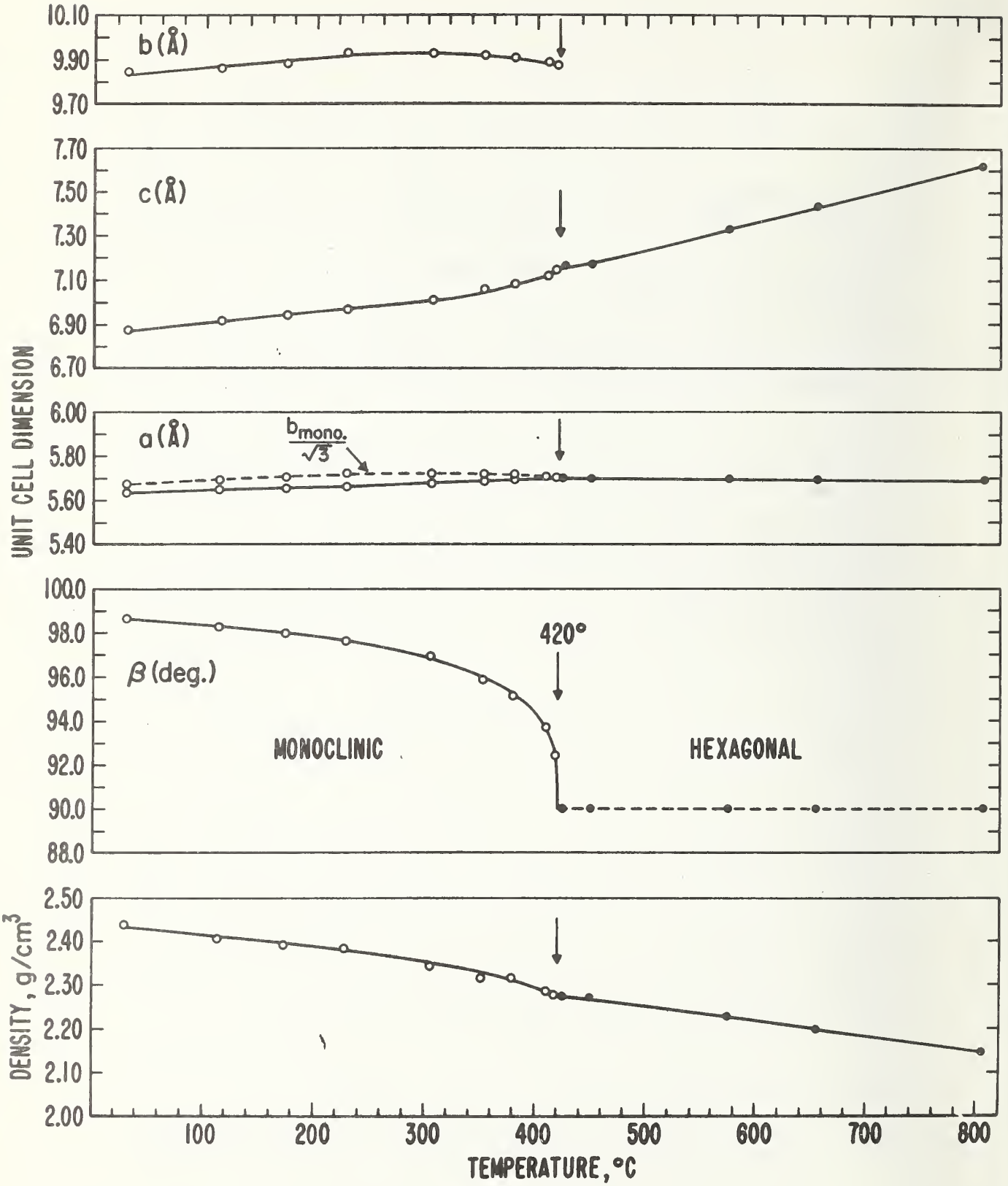

Figure 1. Unit cell dimensions and densities of monoclinic and hexagonal K_2CO_3.

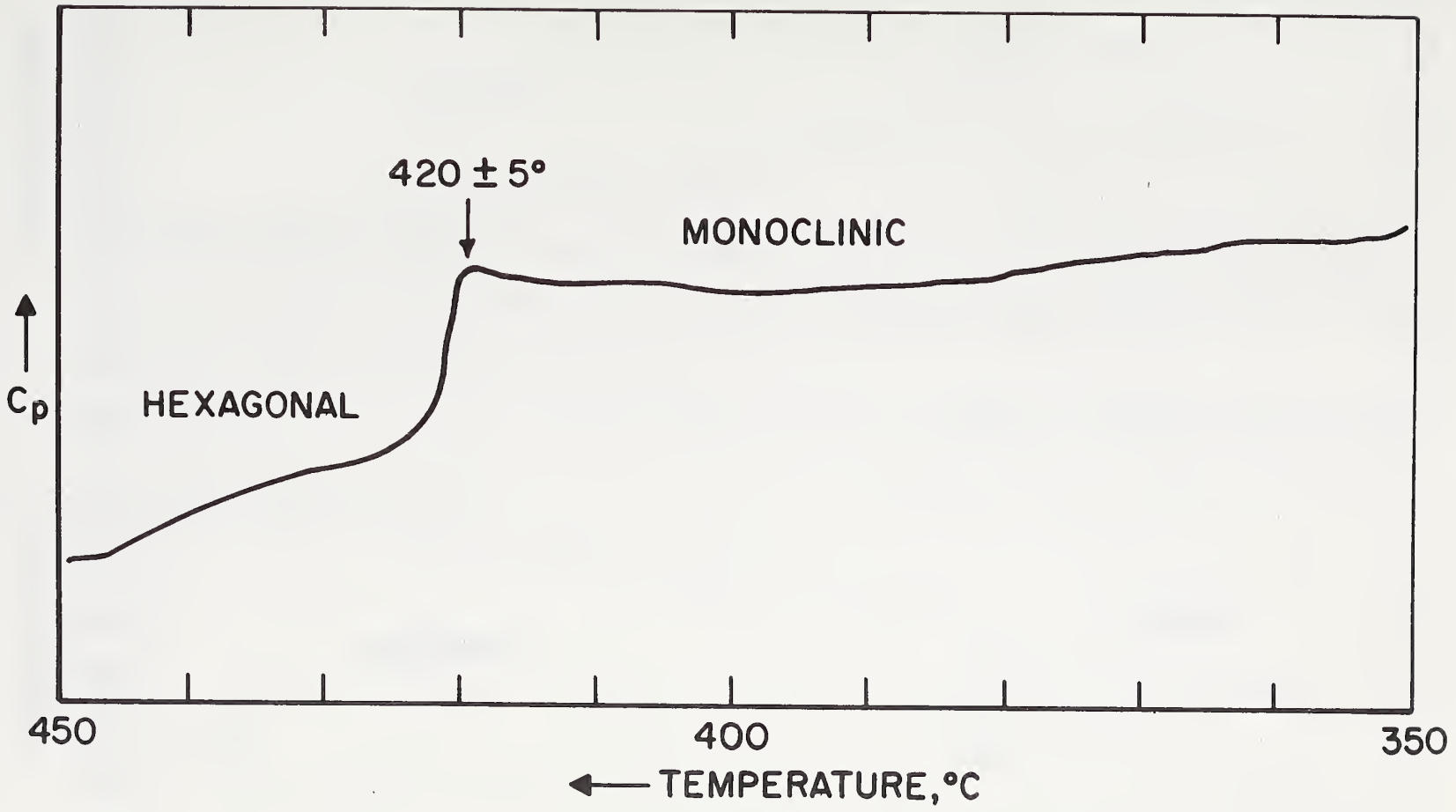

Figure 2. Scan of the monoclinic-hexagonal transformation (2nd order) of K_2CO_3 obtained by differential scanning calorimetry. C_p has not been calibrated for quantitative measurement.

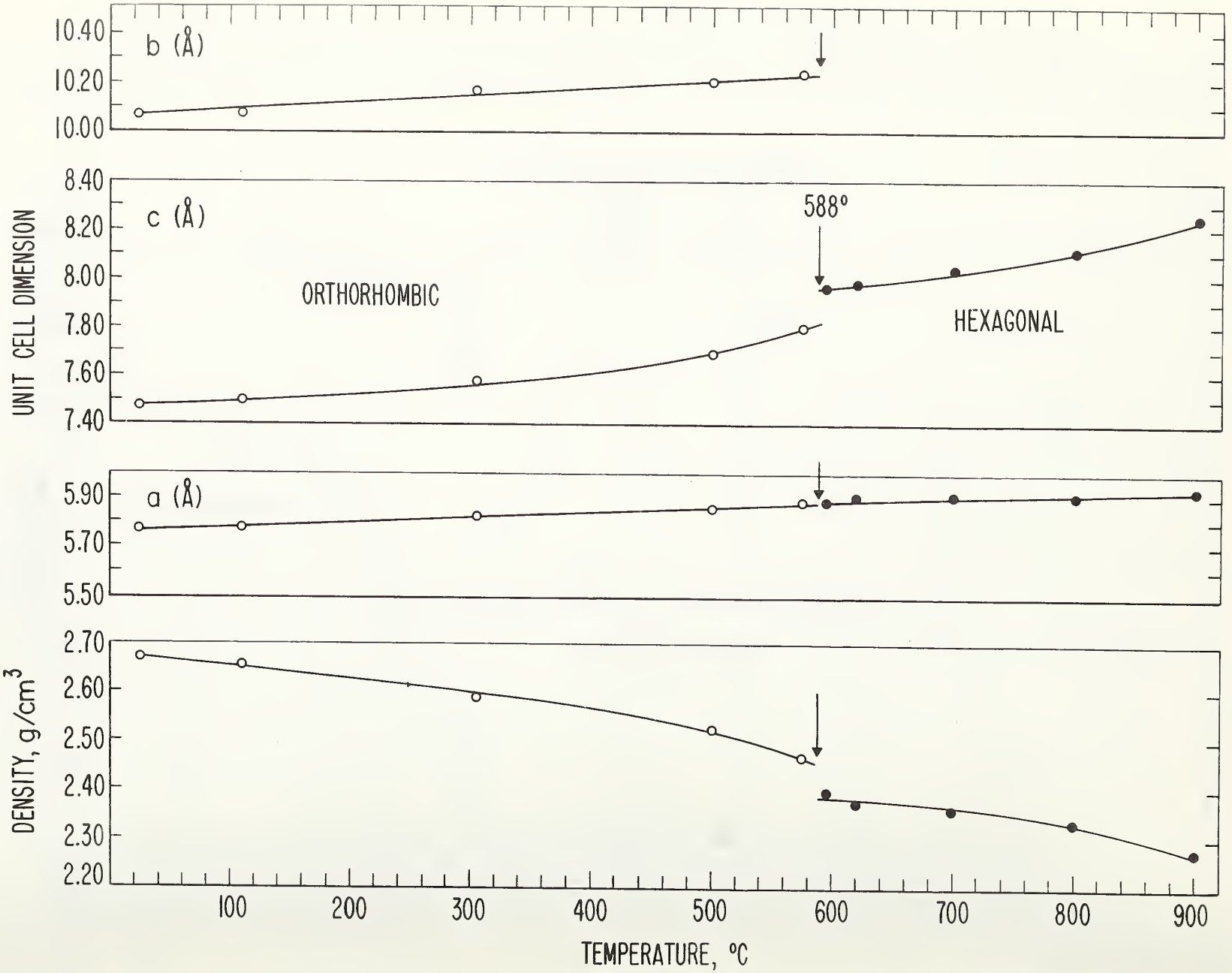

Figure 3. Unit cell dimensions and densities of orthorhombic and hexagonal K_2SO_4.

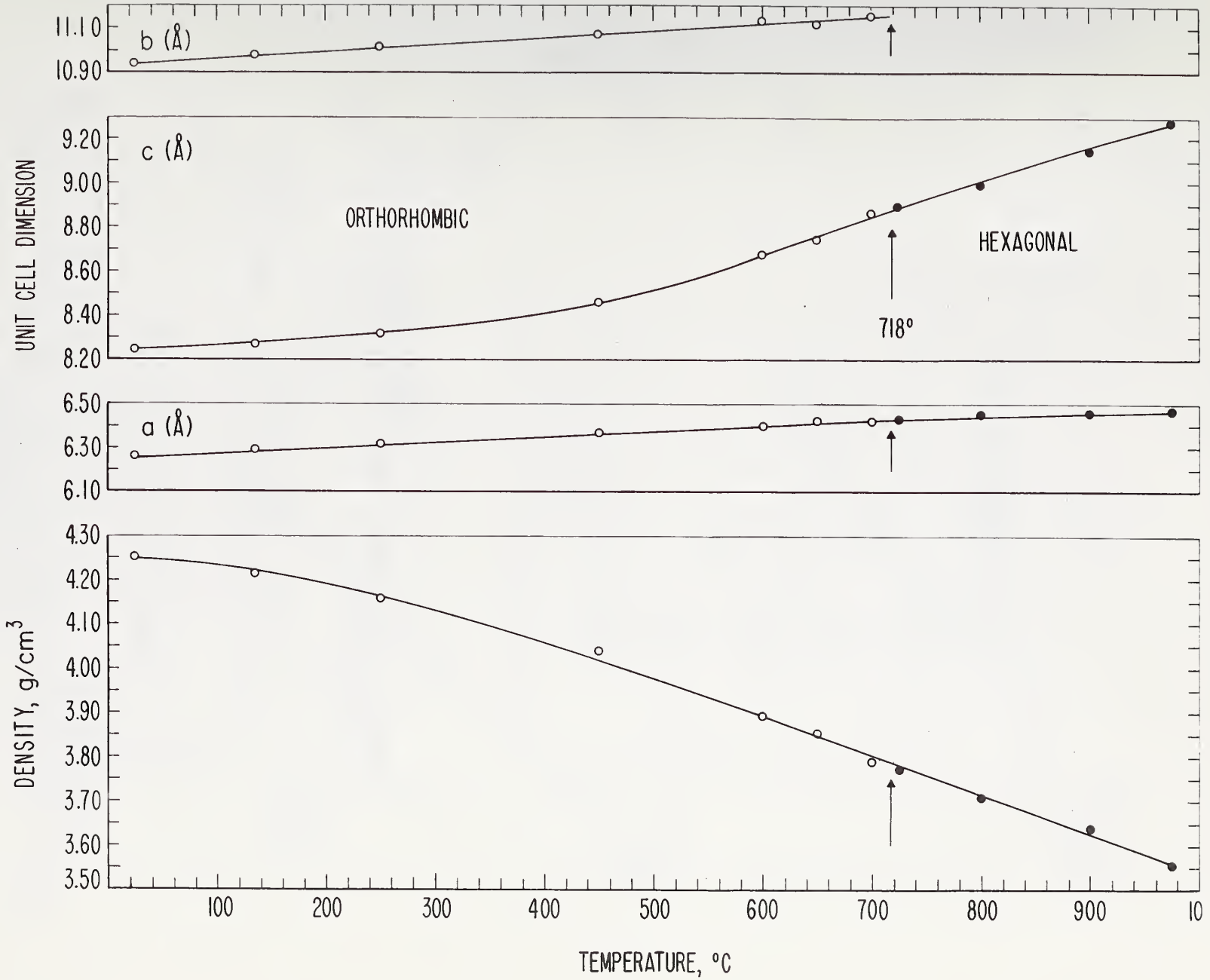

Figure 4. Unit cell dimensions and densities of orthorhombic and hexagonal Cs_2SO_4.

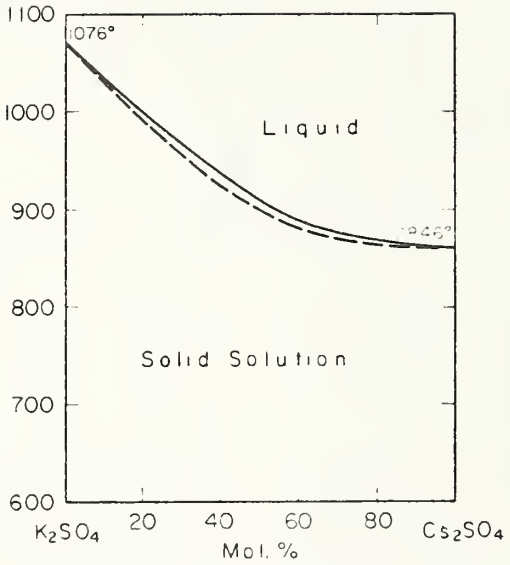

System Cs_2SO_4-K_2SO_4.

O. S. Dombrovskaya, *Zh. Obshch. Khim.* 3 [8] 1019 (1933).

Figure 5. System K_2SO_4-Cs_2SO_4 after Dombrovskaya [22].

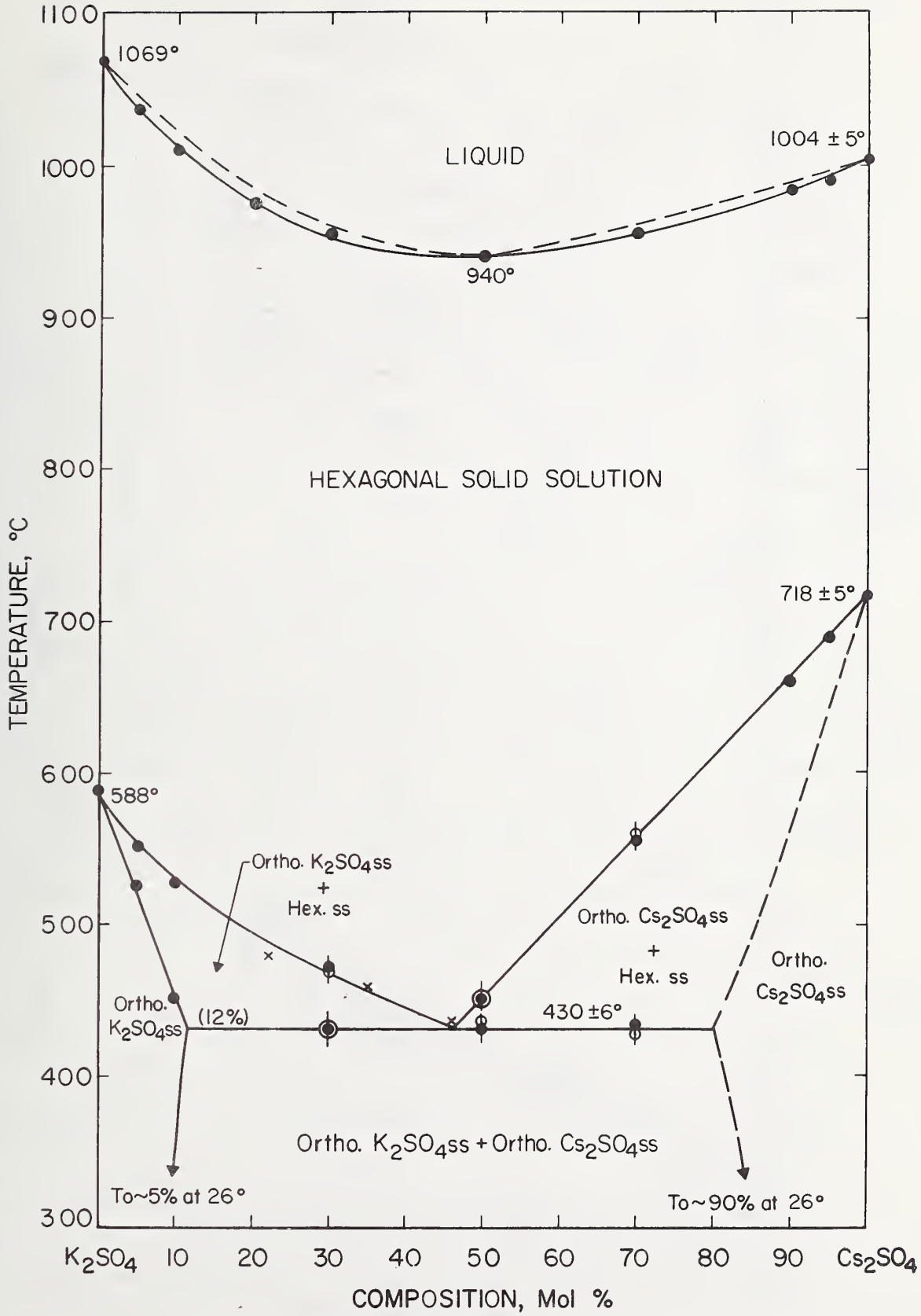

Figure 6. System K_2SO_4-Cs_2SO_4 after Levin, et al [23].

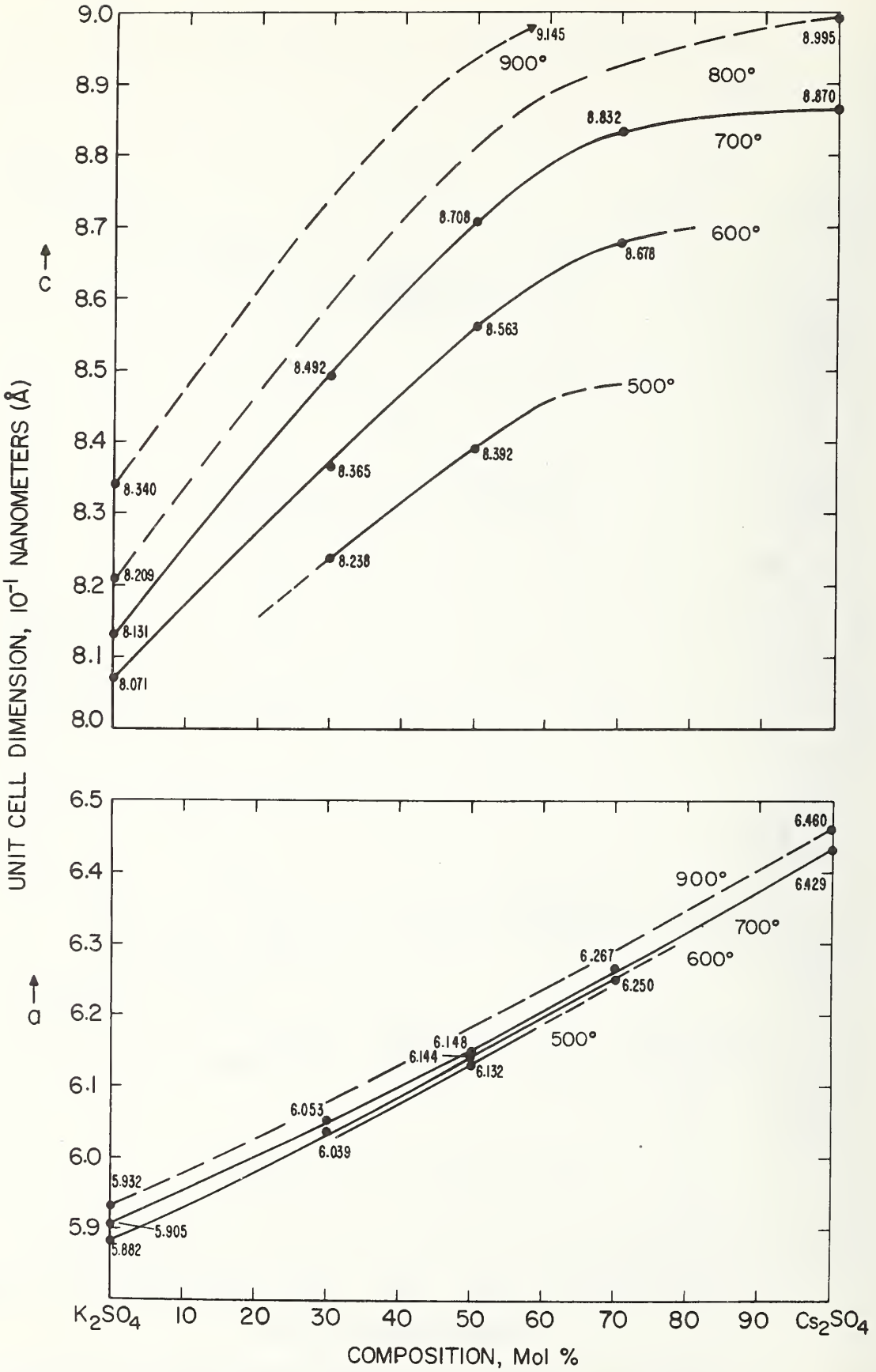

Figure 7. a and c unit cell dimensions of the hexagonal solid solution phase vs composition in the system K_2SO_4-Cs_2SO_4.

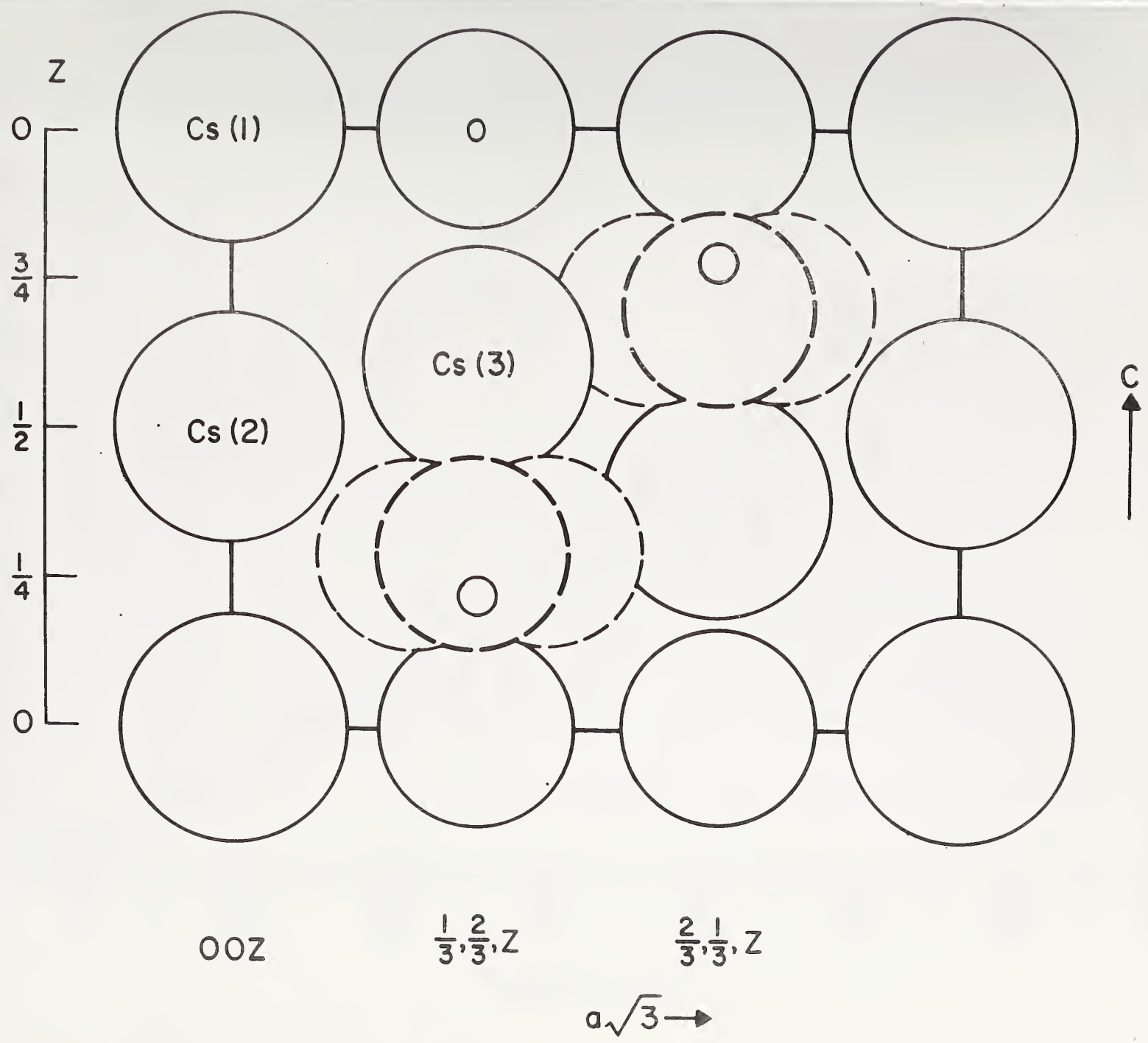

Figure 8. 110 plane of Cs_2SO_4 based on the $KNaSO_4$ (aphthitalite) structure, $P\bar{3}ma$.

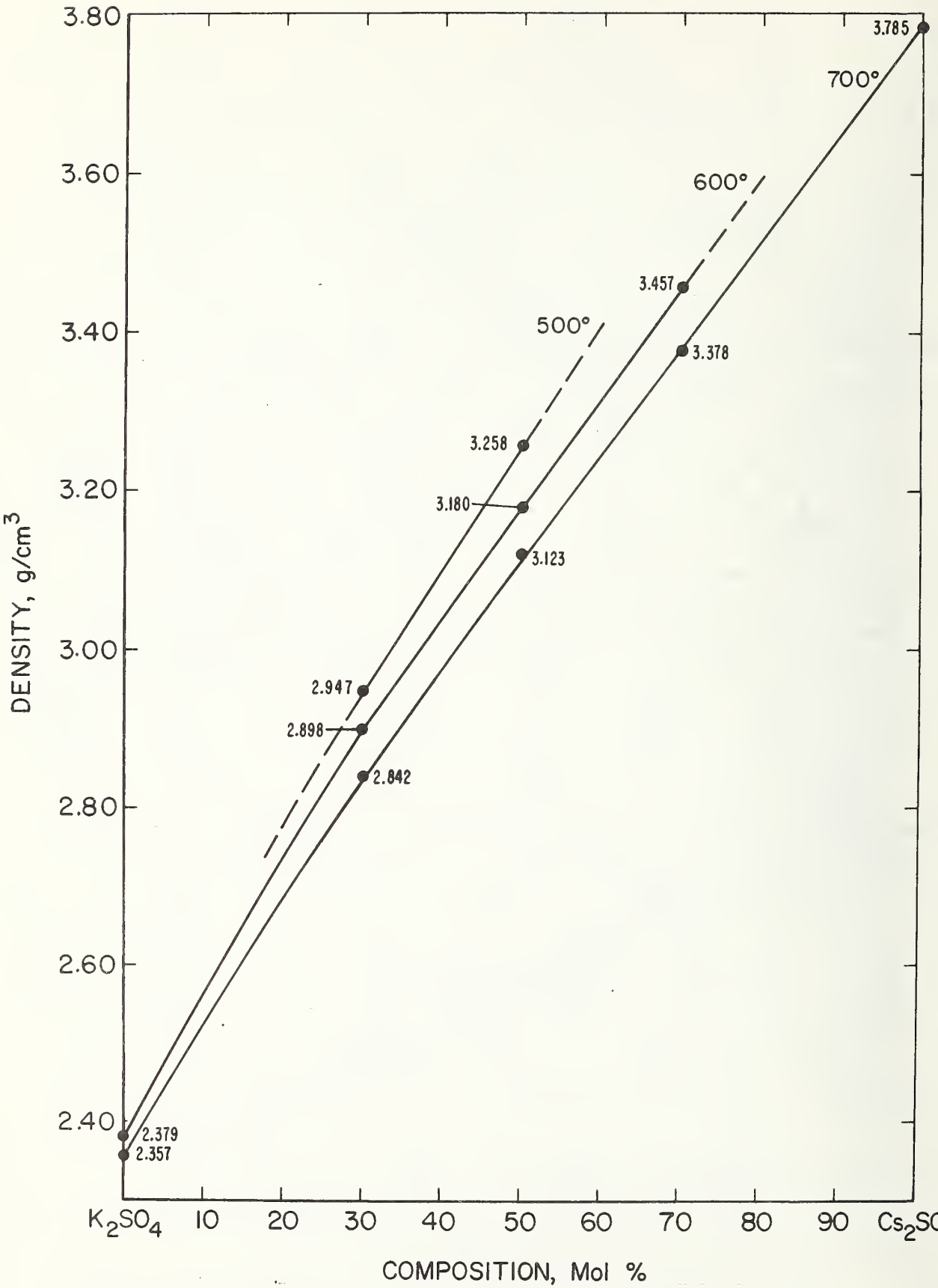

Figure 9. X-ray density vs composition for the hexagonal solid solution phase in the system K_2SO_4-Cs_2SO_4.

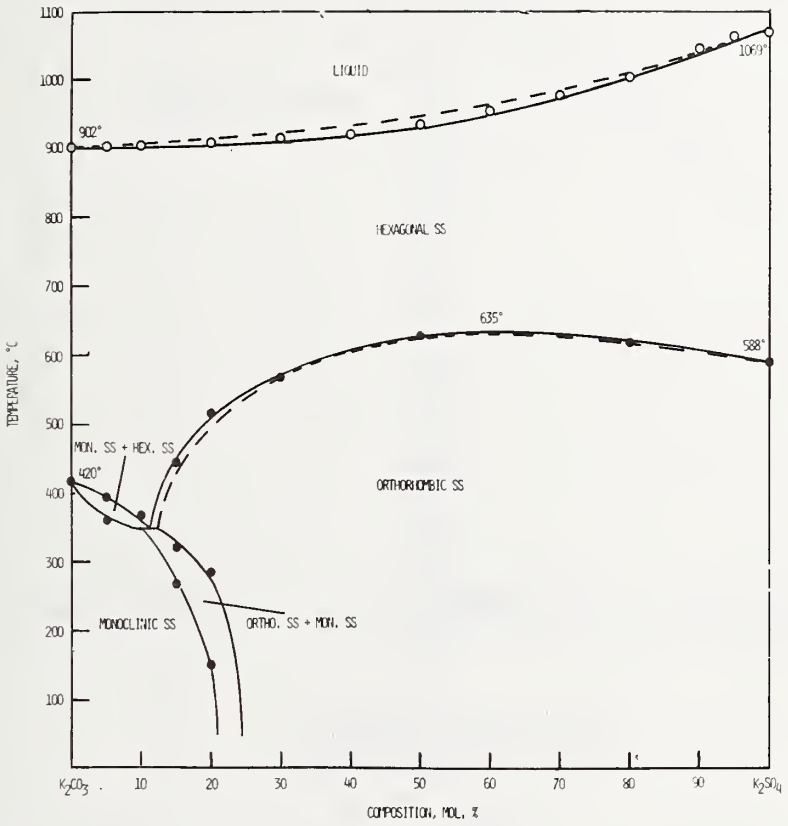

Figure 10. Phase diagram of the system K_2CO_3-K_2SO_4.

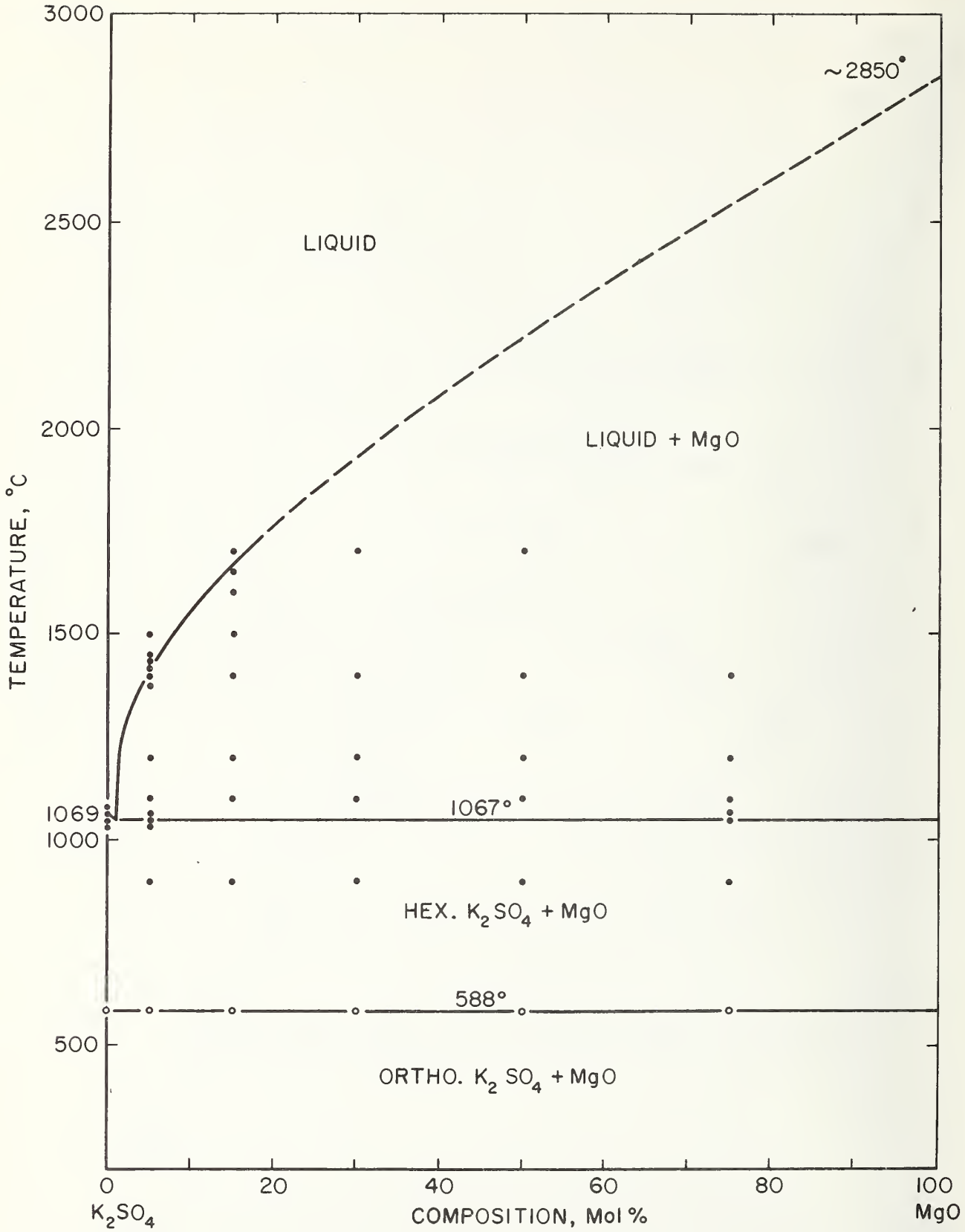

Figure 11. Condensed state phase diagram of the K_2SO_4-MgO system.
● - quenching o - DTA

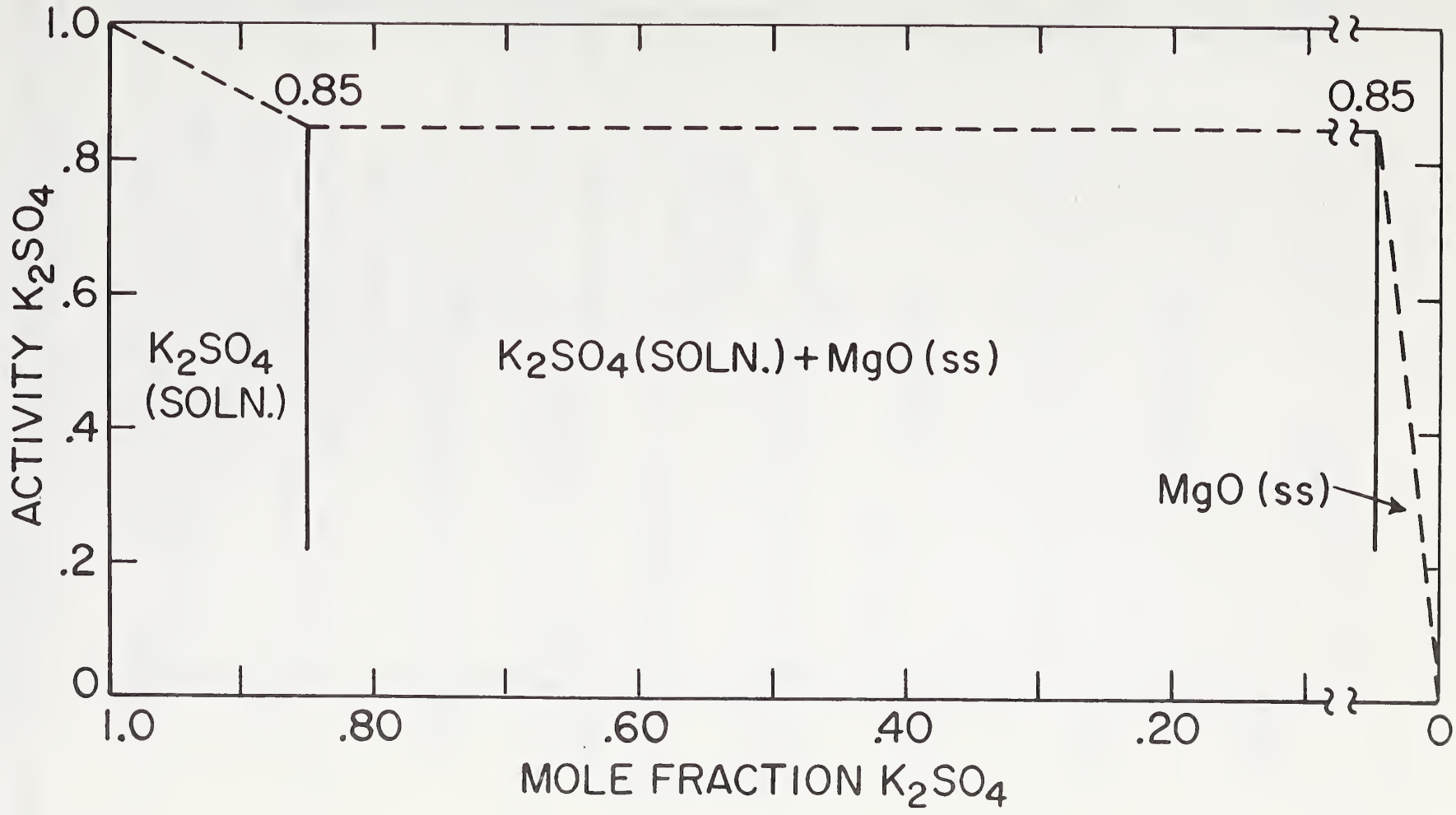

Figure 12. Schematic activity plot of the K_2SO_4-MgO system at 1700°C.

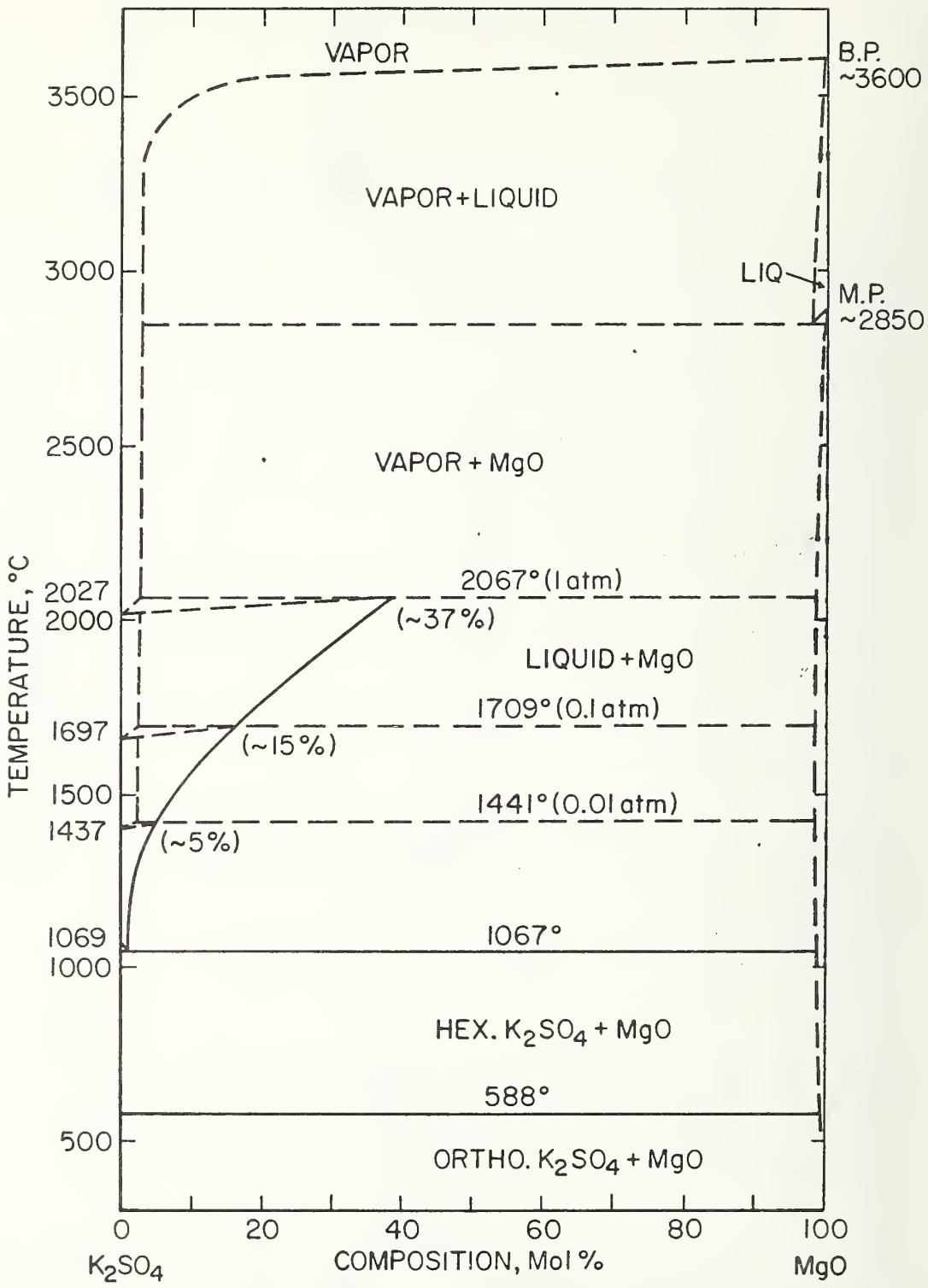

Figure 13. Phase diagram of the system K_2SO_4-MgO for 0.01, 0.1, and 1 atm total pressure K_2SO_4 species. (1 atm = 101,325 N/m^2, N/m^2 = 1 pascal)

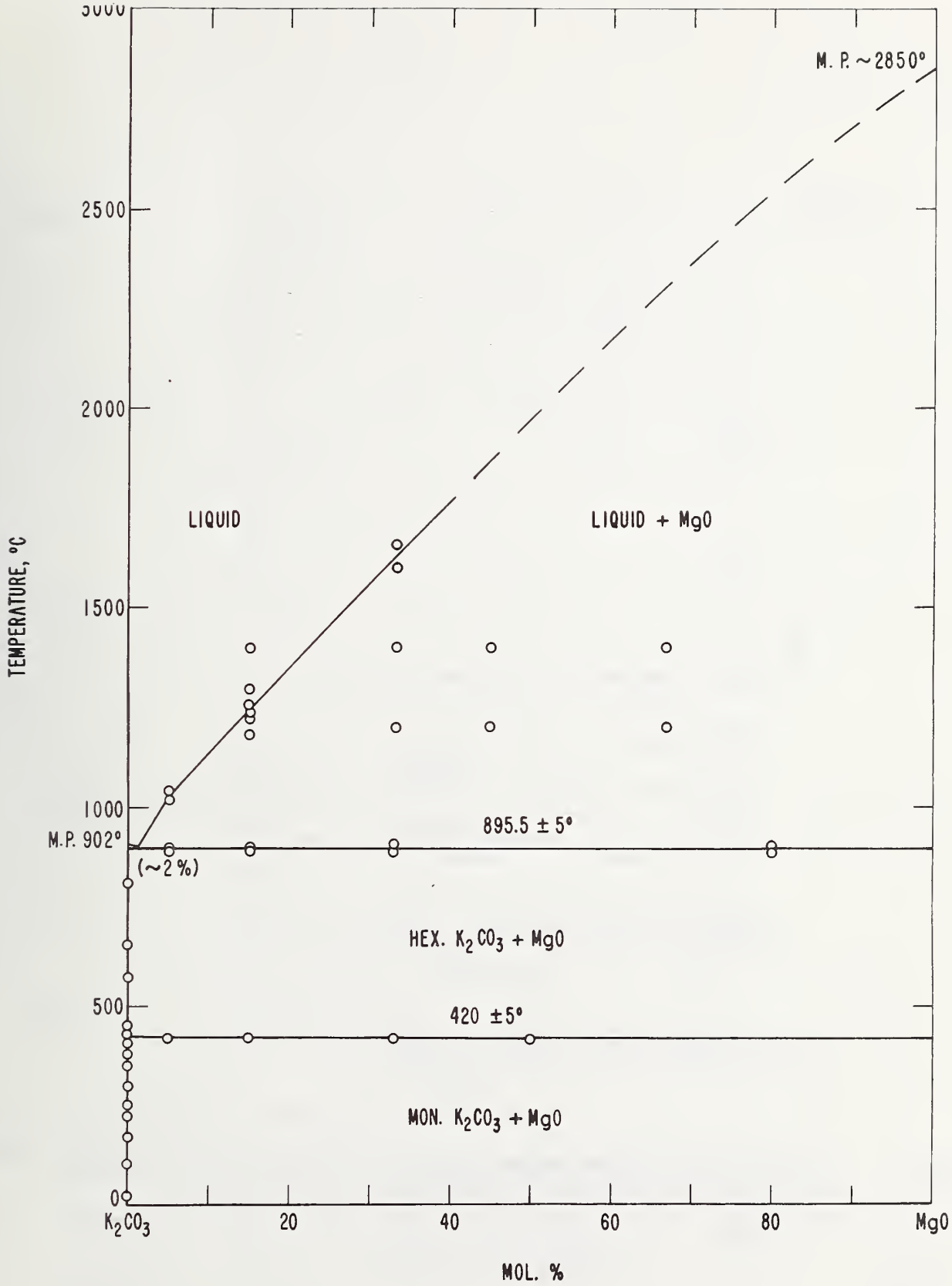

Figure 14. Phase diagram of the system K_2CO_3-MgO in a closed system.

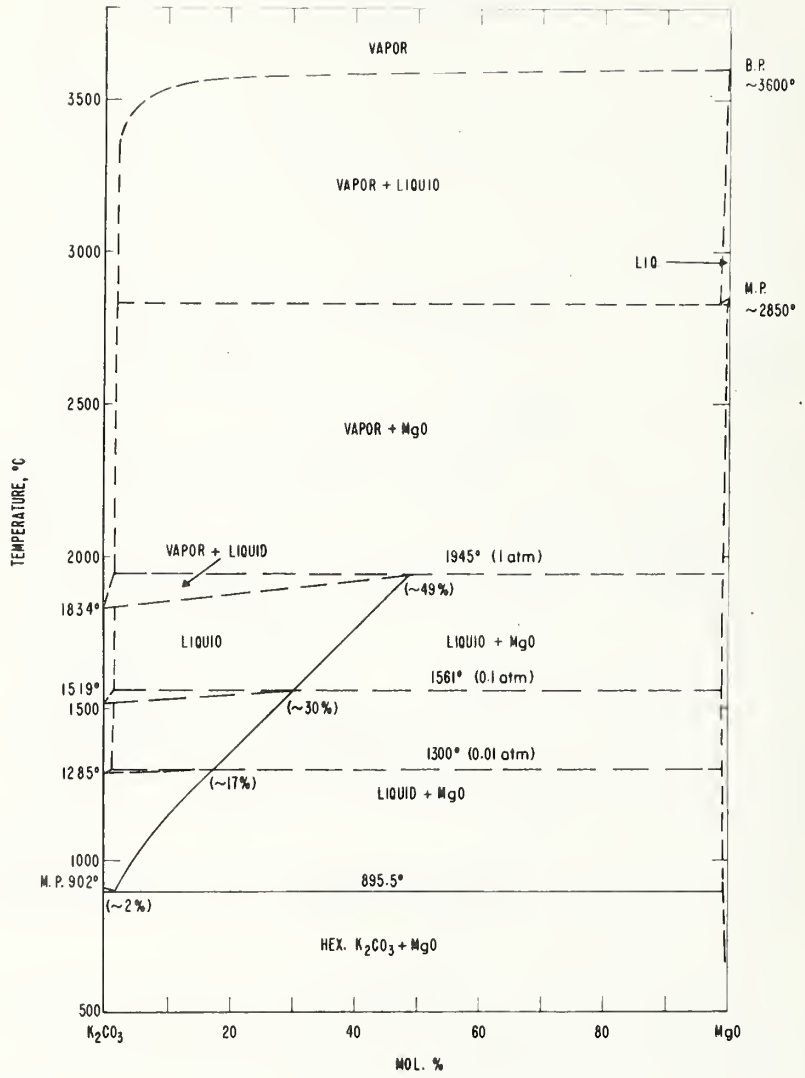

Figure 15. Phase diagram of the system K_2CO_3-MgO for 0.01, 0.1, and 1 atm total pressure K_2CO_3 species. (1 atm = 101,325 N/m2, N/m^2 = 1 pascal

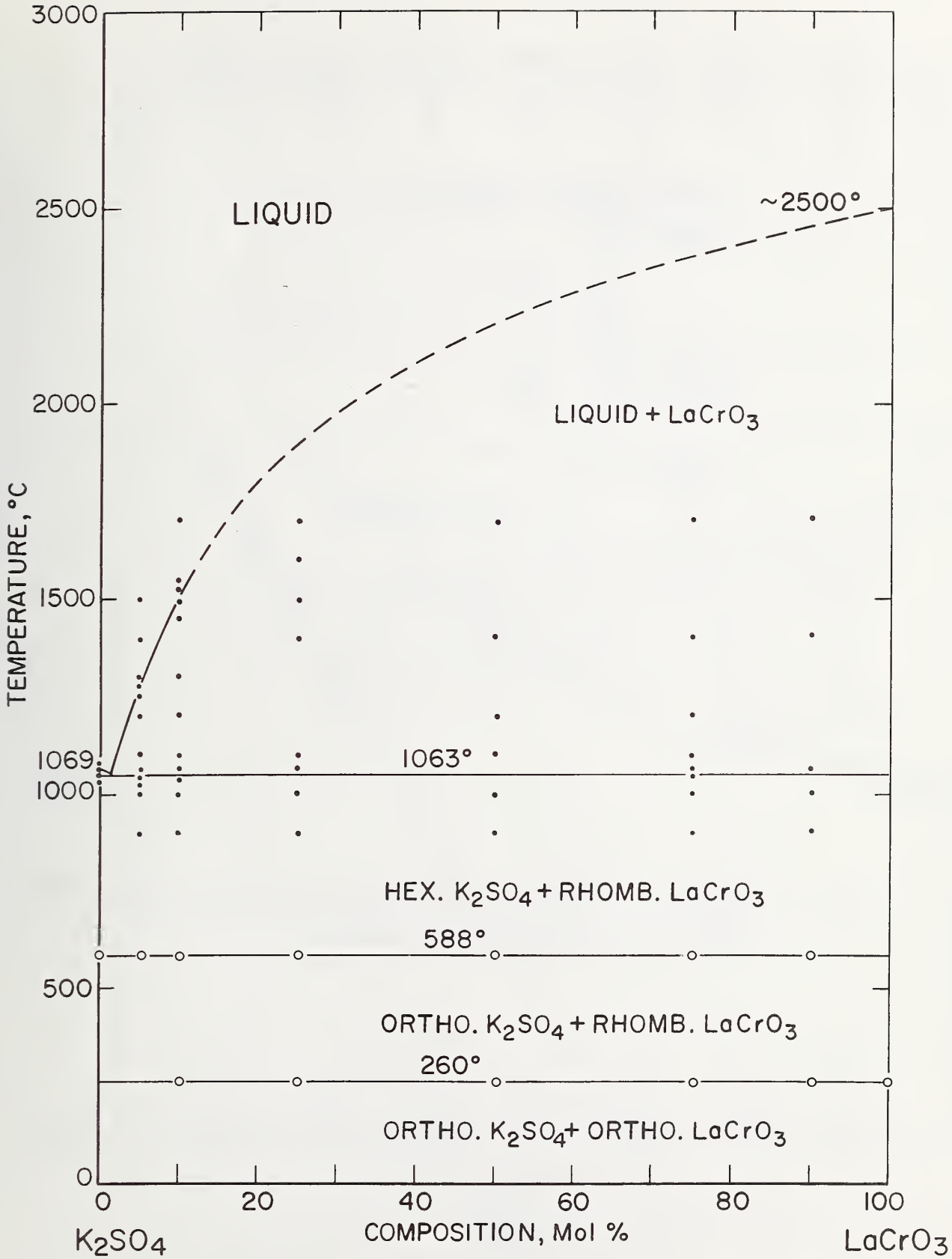

Figure 16. Phase diagram of the system K_2SO_4-$LaCrO_3$ in a closed system.
closed system - specimen containers were sealed Pt tubes
● - quenching o - DTA

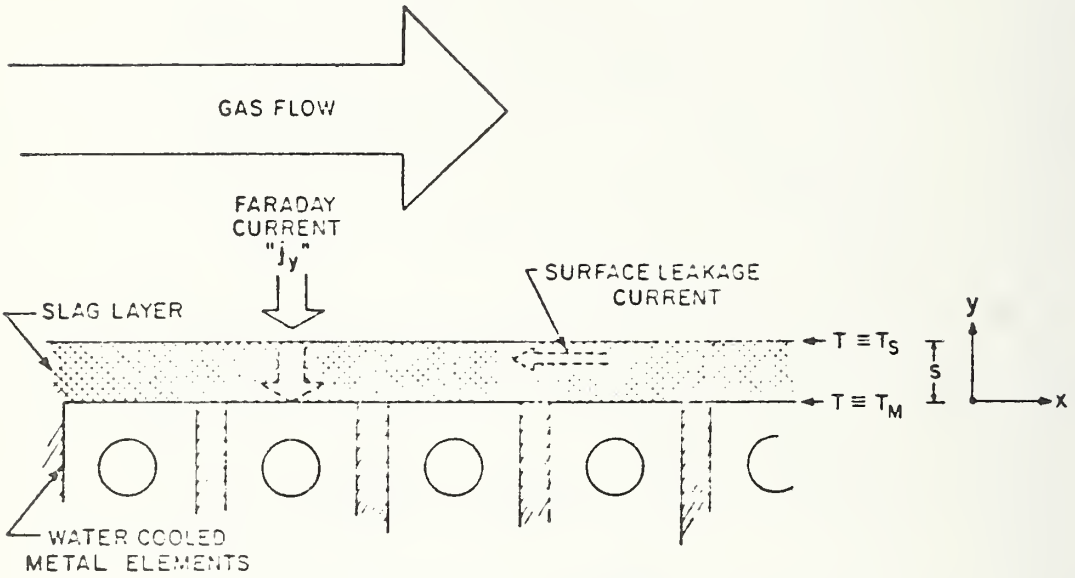

Figure 17. Schematic of MHD-duct wall. (from: R. J. Rosa, 5th International Conference on MHD-Power Generation, Munich, 1971, Vol. I. - Public. de l'O.C.D.E., Paris, France.)

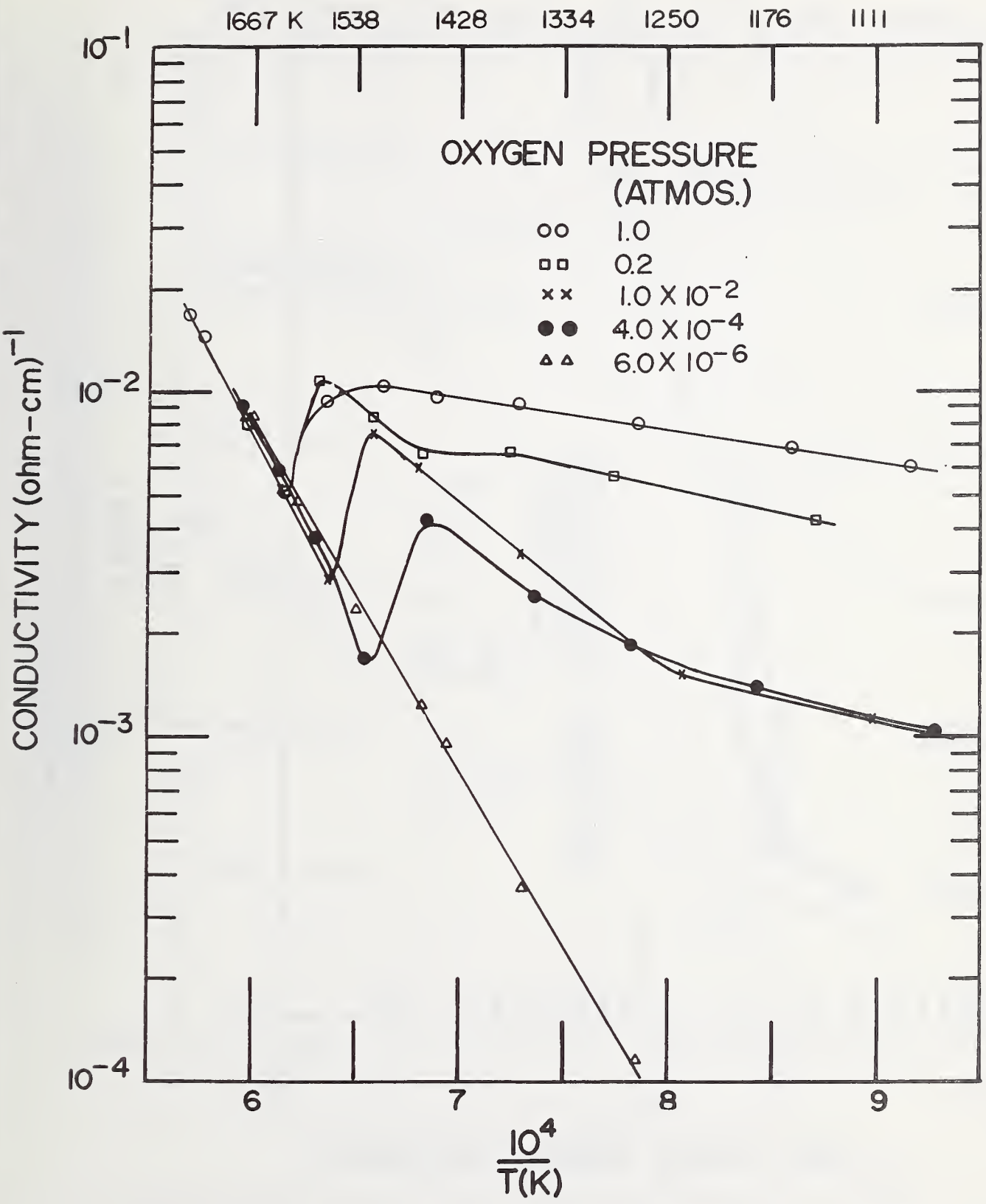

Figure 18. Conductivity as a function of reciprocal temperature for slag (sample MHD-12)

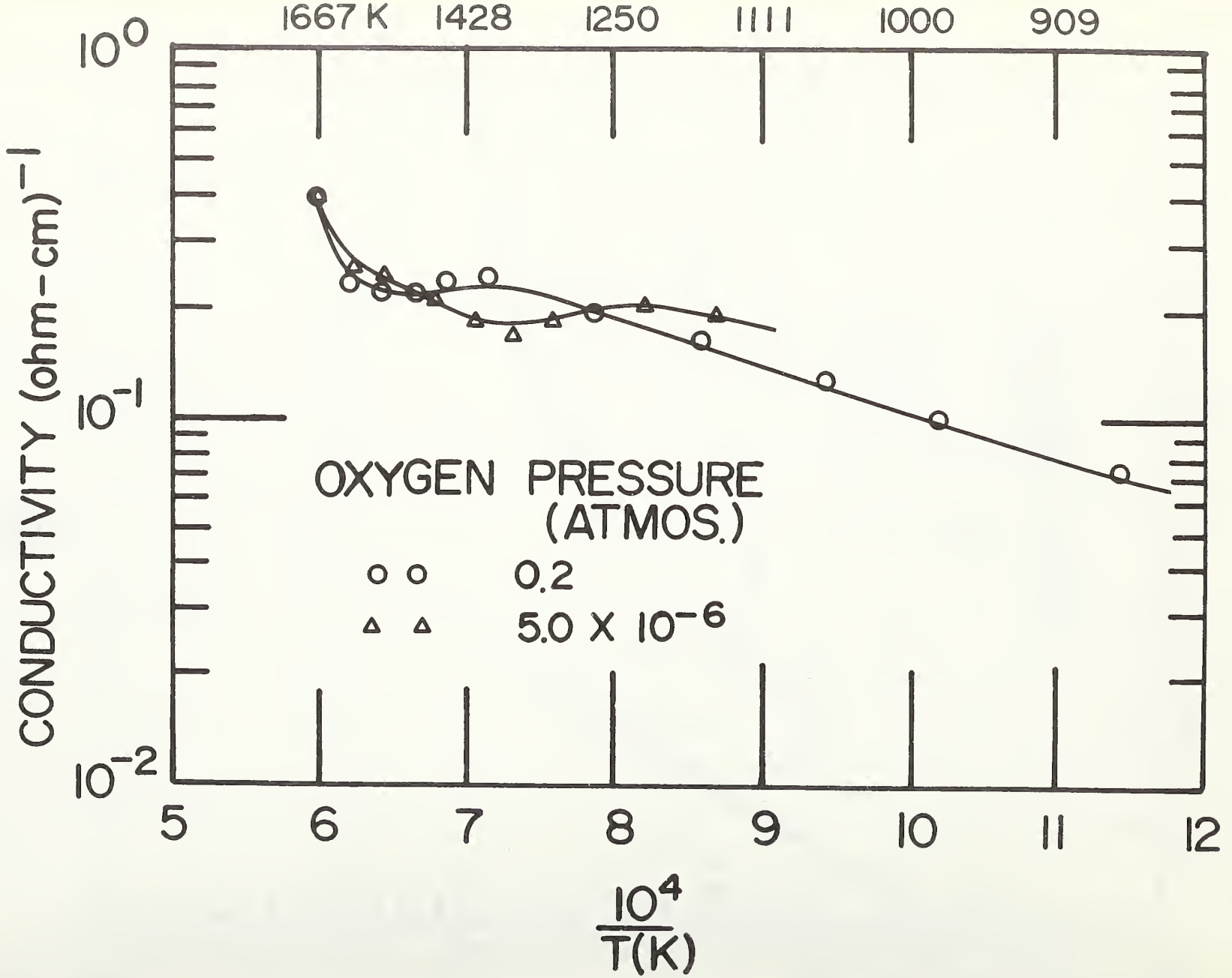

Figure 19. Conductivity as a function of reciprocal temperature for synthetic slag (sample K 216)

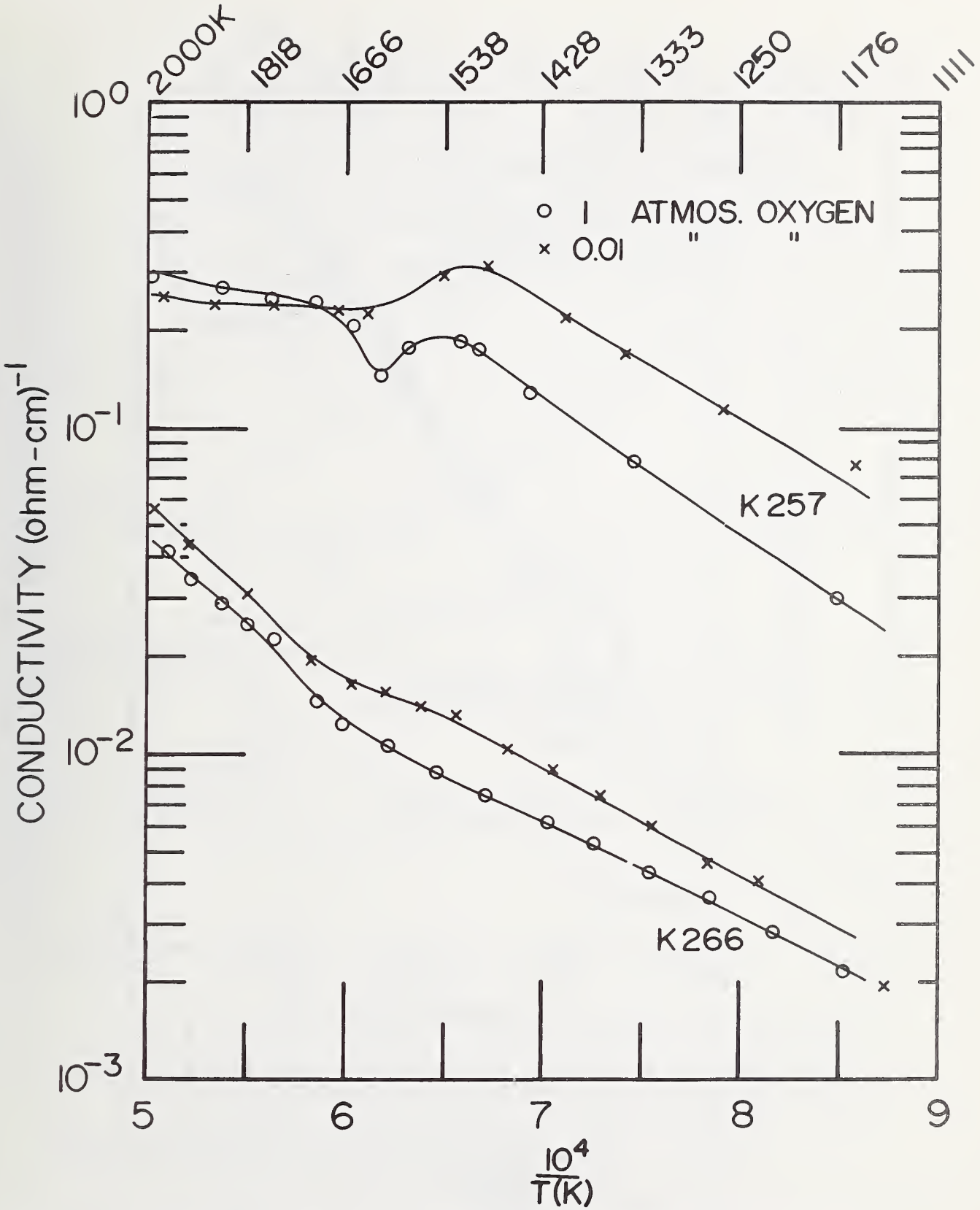

Figure 20. Electrical conductivity of base oxide slag sample (K 257) and of slag-seed mixture (base oxide with 20% K_2SO_4; sample K 266) at two oxygen pressures.

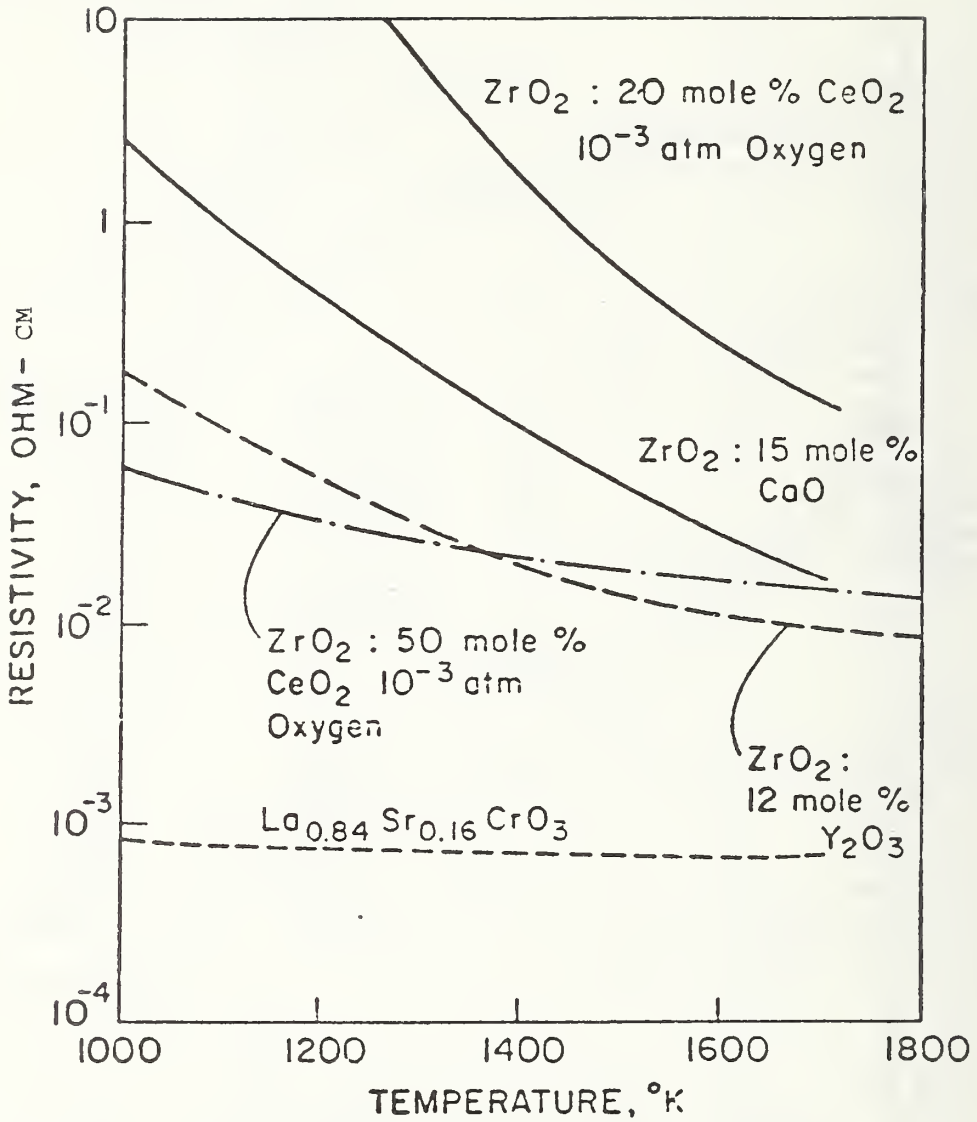

Figure 21. Resistivity as a function of temperature for the ceramics of most interest as electrode materials. (from ref. [37]).

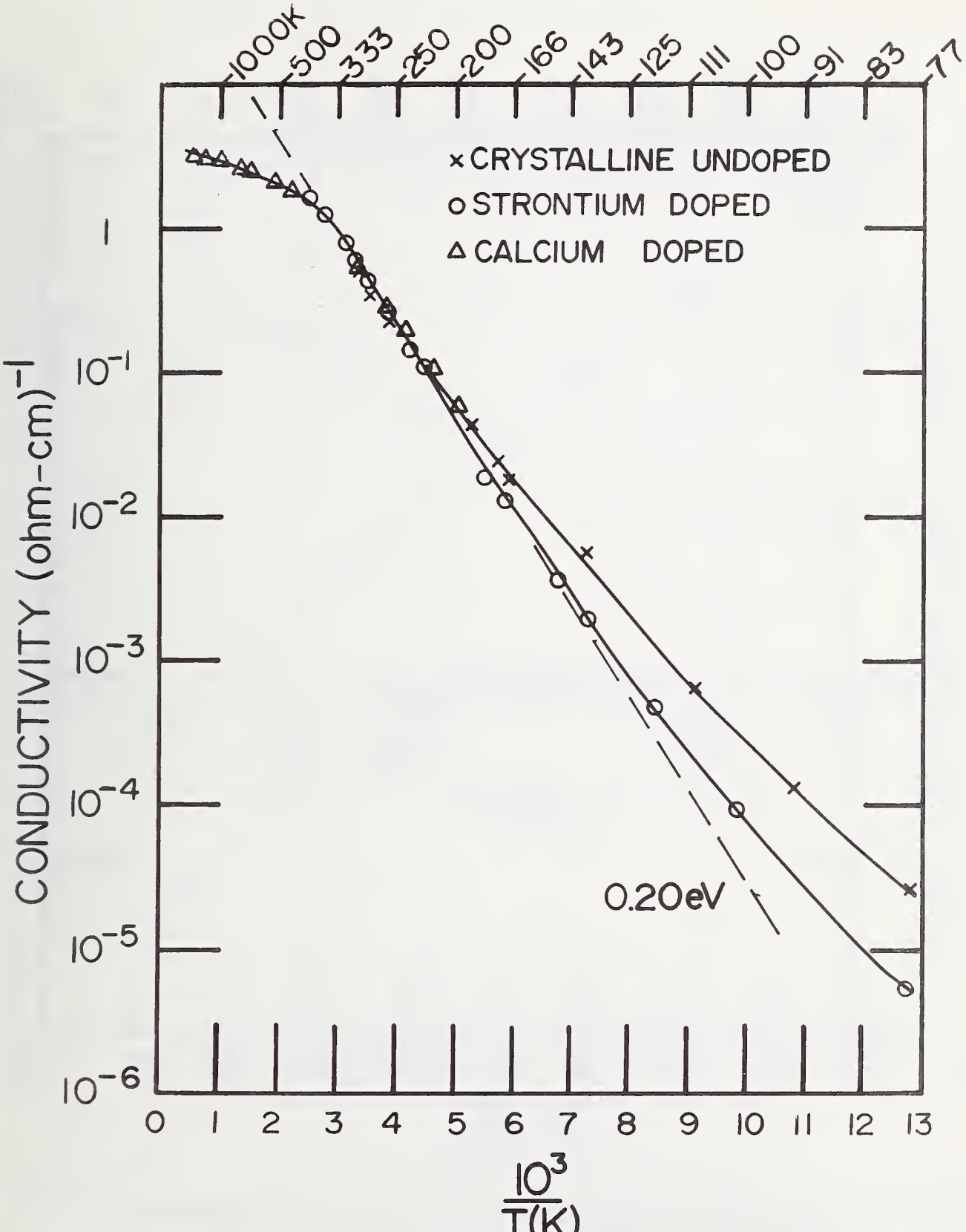

Figure 22. Conductivity versus 1/T of crystalline doped $LaCrO_3$, $La_{0.9}Sr_{0.1}CrO_3$ and $La_{1-x}Ca_xCrO_3$ (0.1>x>0.01). Note donor exhaustion and donor reserve regions.

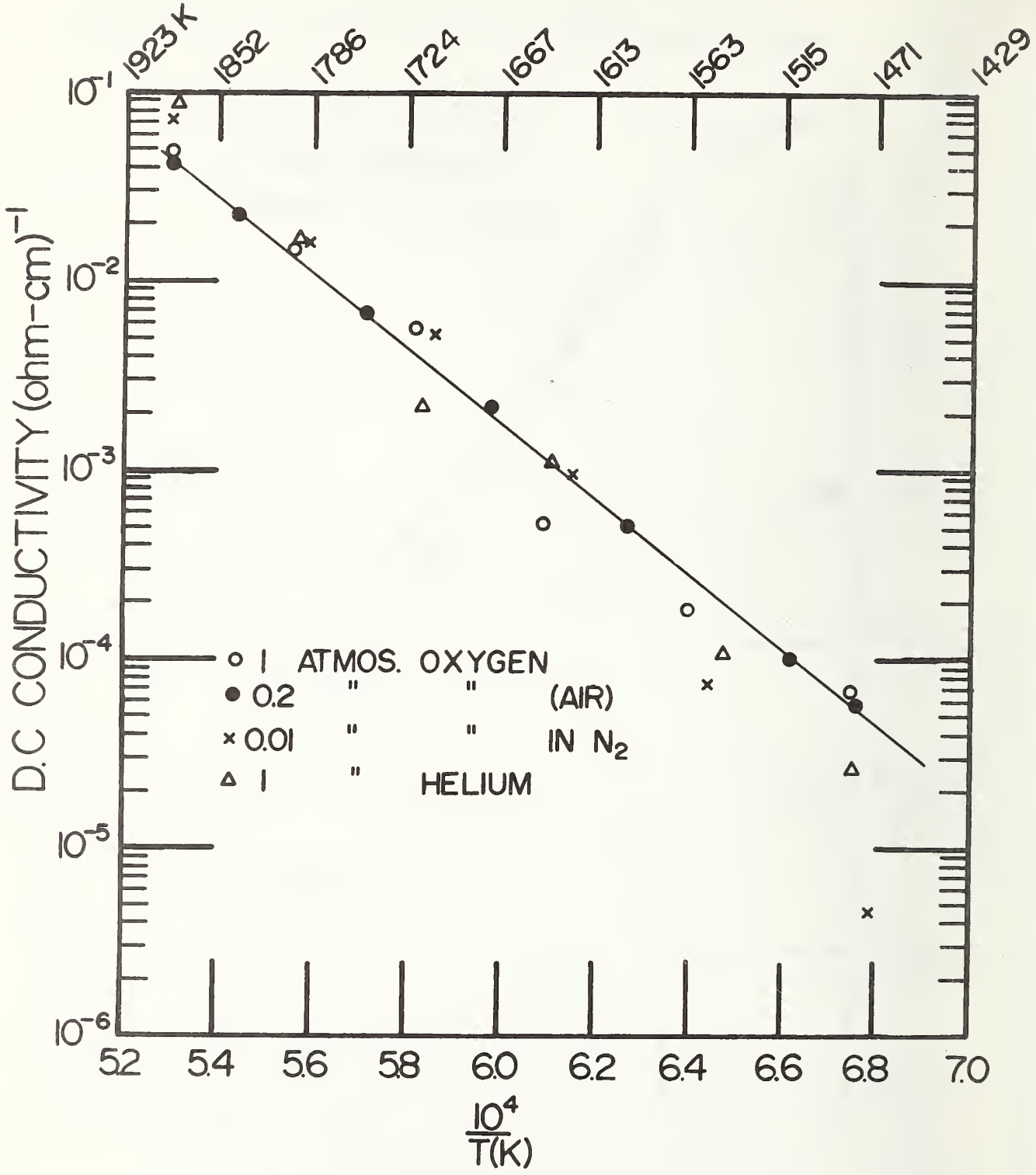

Figure 23. D.C. conductivity of $SrZrO_3$-14 CeO_2 (mol %) at different oxygen pressures and in helium.

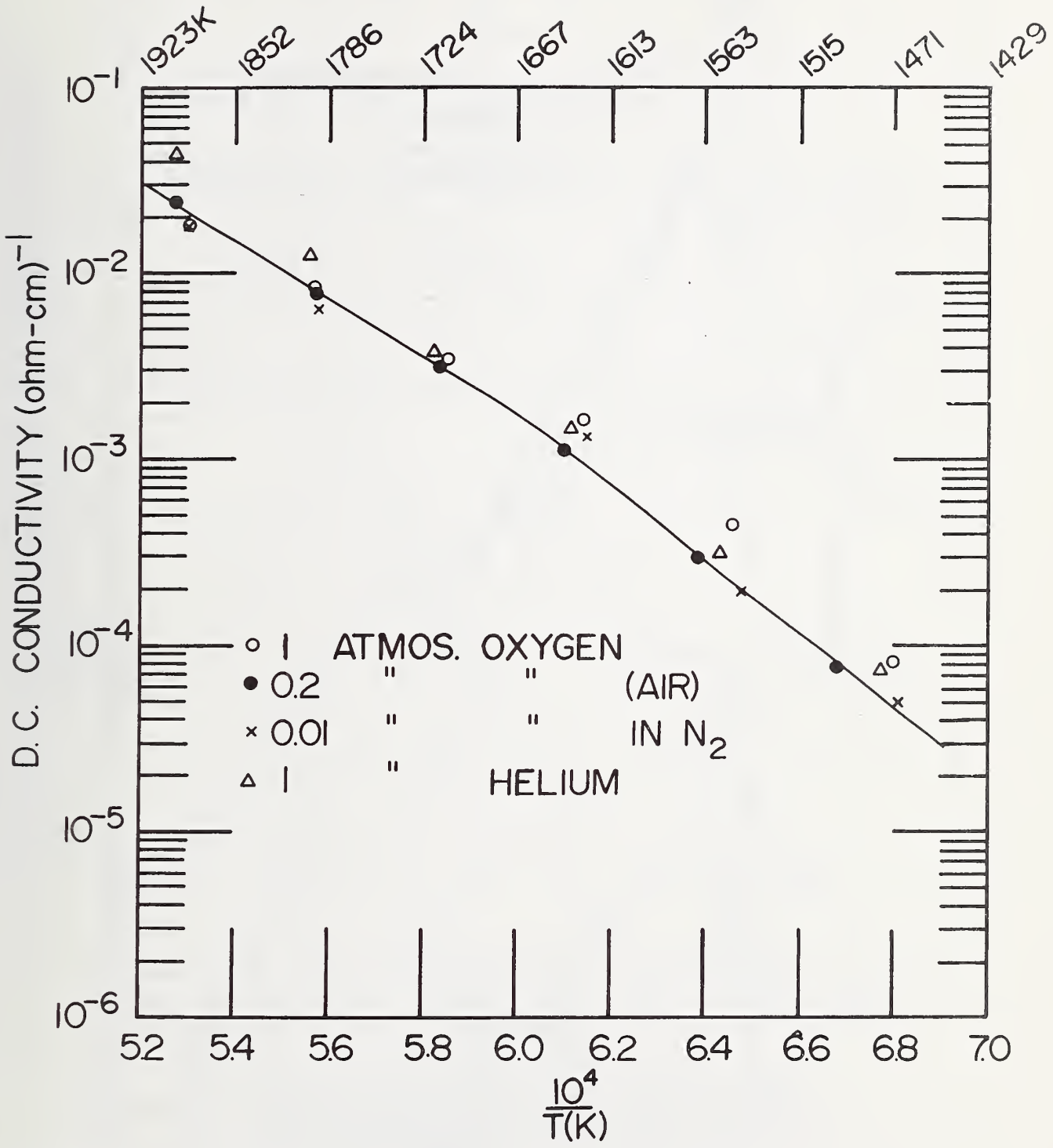

Figure 24. D.C. conductivity of $SrZrO_3$-6 $SrTiO_3$-1.5 Ta_2O_5 (mol %) at different oxygen pressures and in helium.

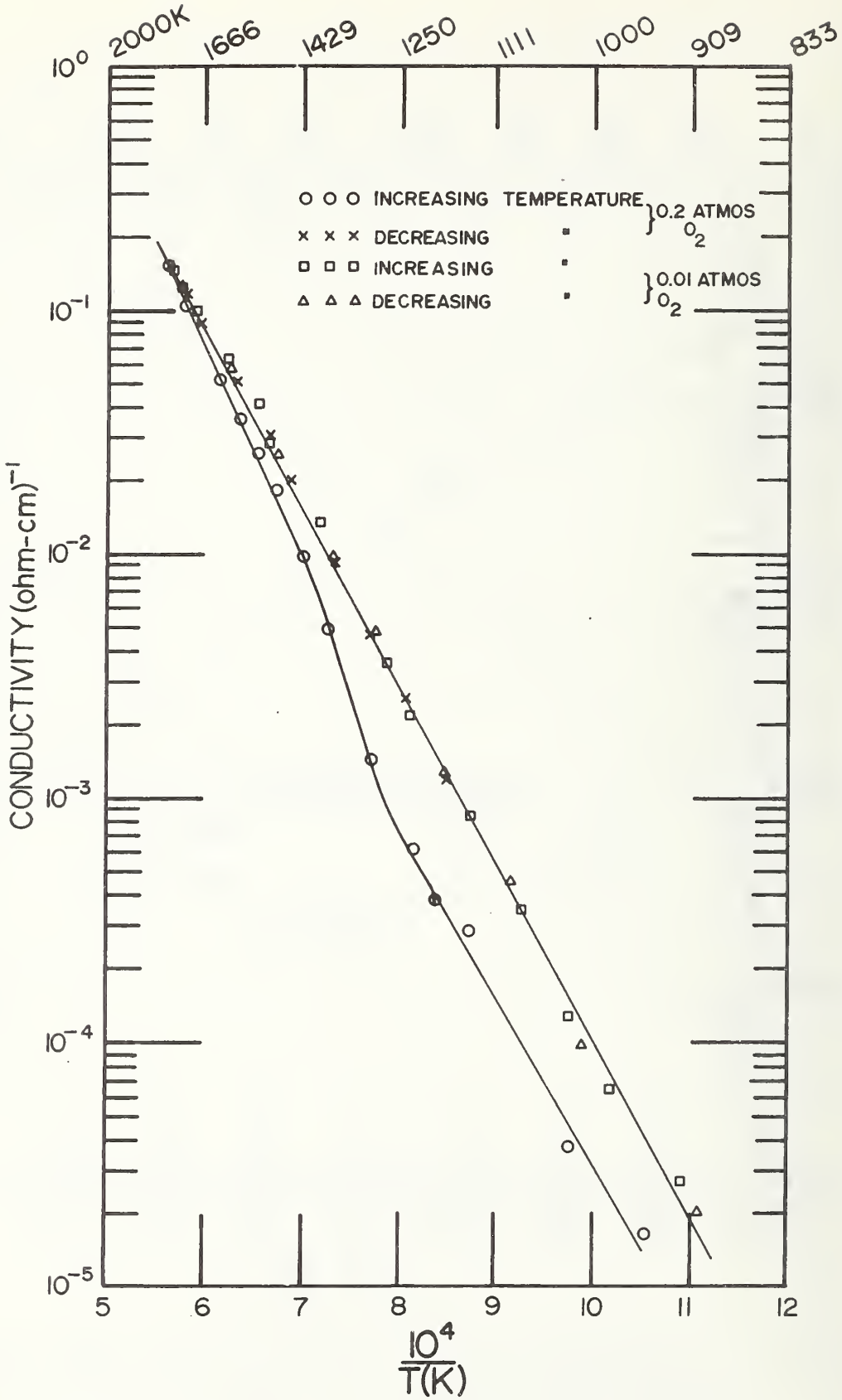

Figure 25. Conductivity of channel coating (ZrO_2 + MgO) to 1750 K at 0.2 atm. and 0.01 atm. oxygen.

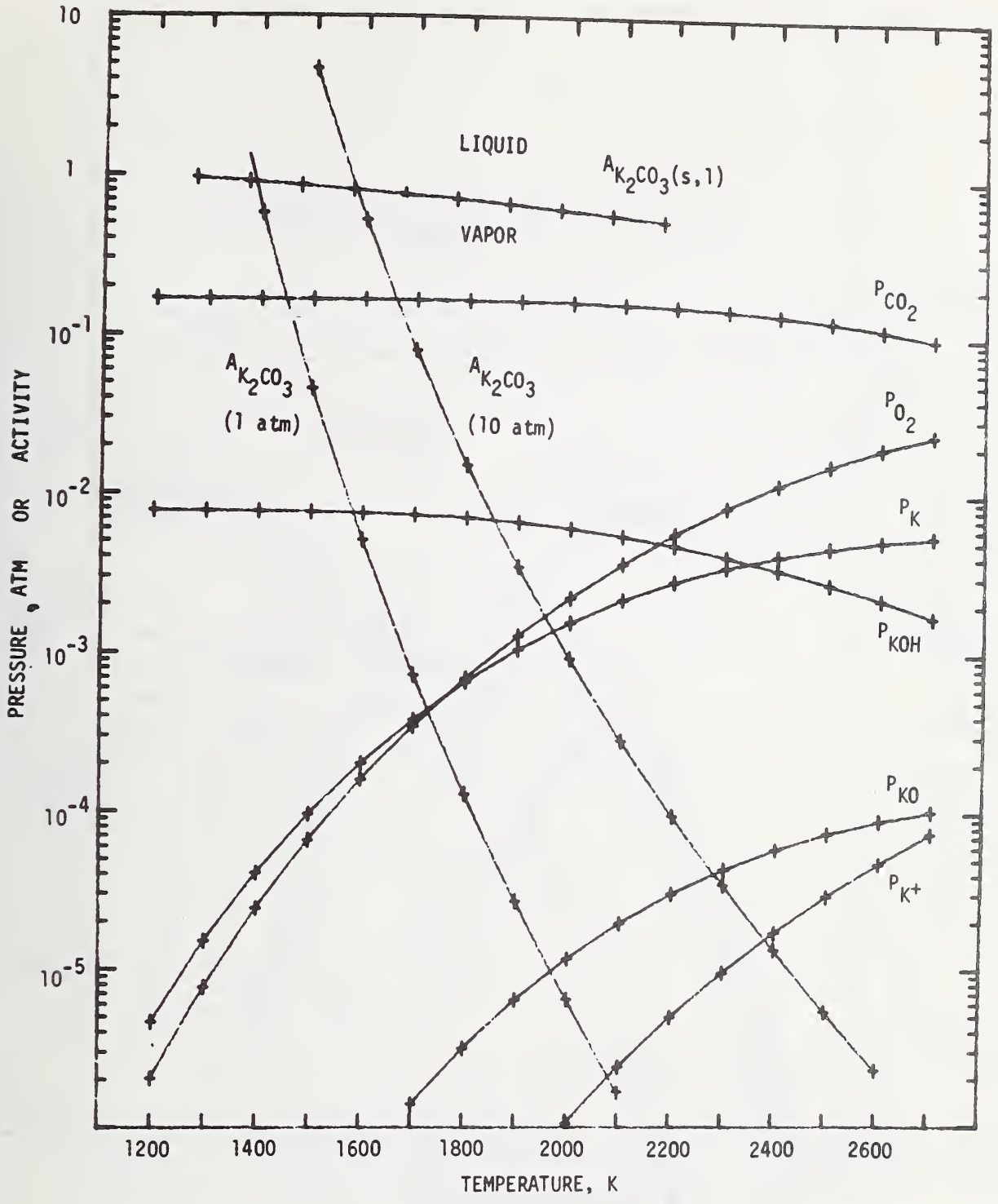

Fig. 26: Calculated Partial Pressures of Gases and Activities of K_2CO_3 at 1 atm for the Combustion of $CH_{0.7}$ Seeded with 1 wt % K as K_2CO_3.

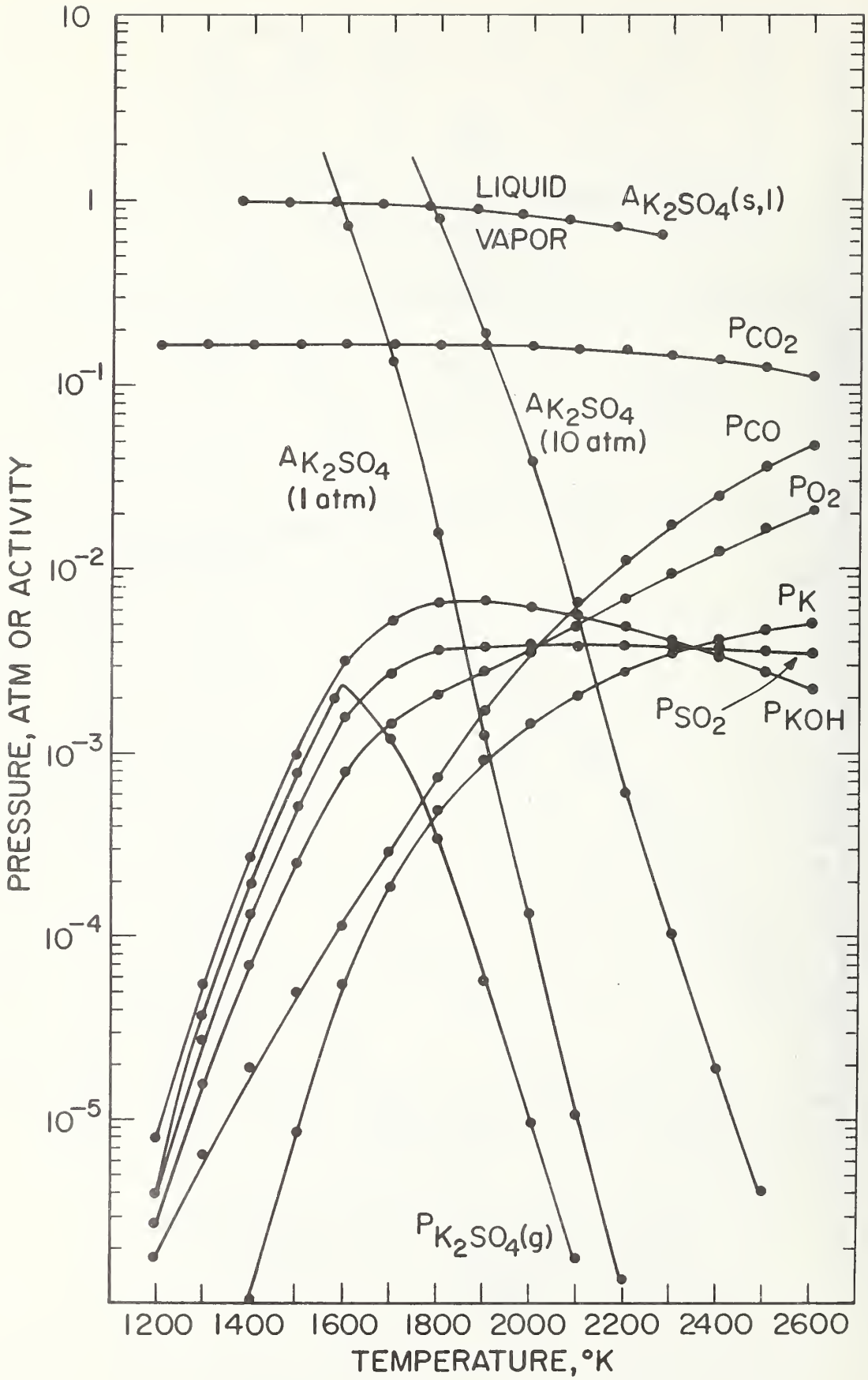

Fig. 27: Calculated Partial Pressures of Gases and Activities of K_2SO_4 at 1 atm for the Combustion of $CH_{0.7}$ Seeded with 1 wt % K as K_2SO_4.

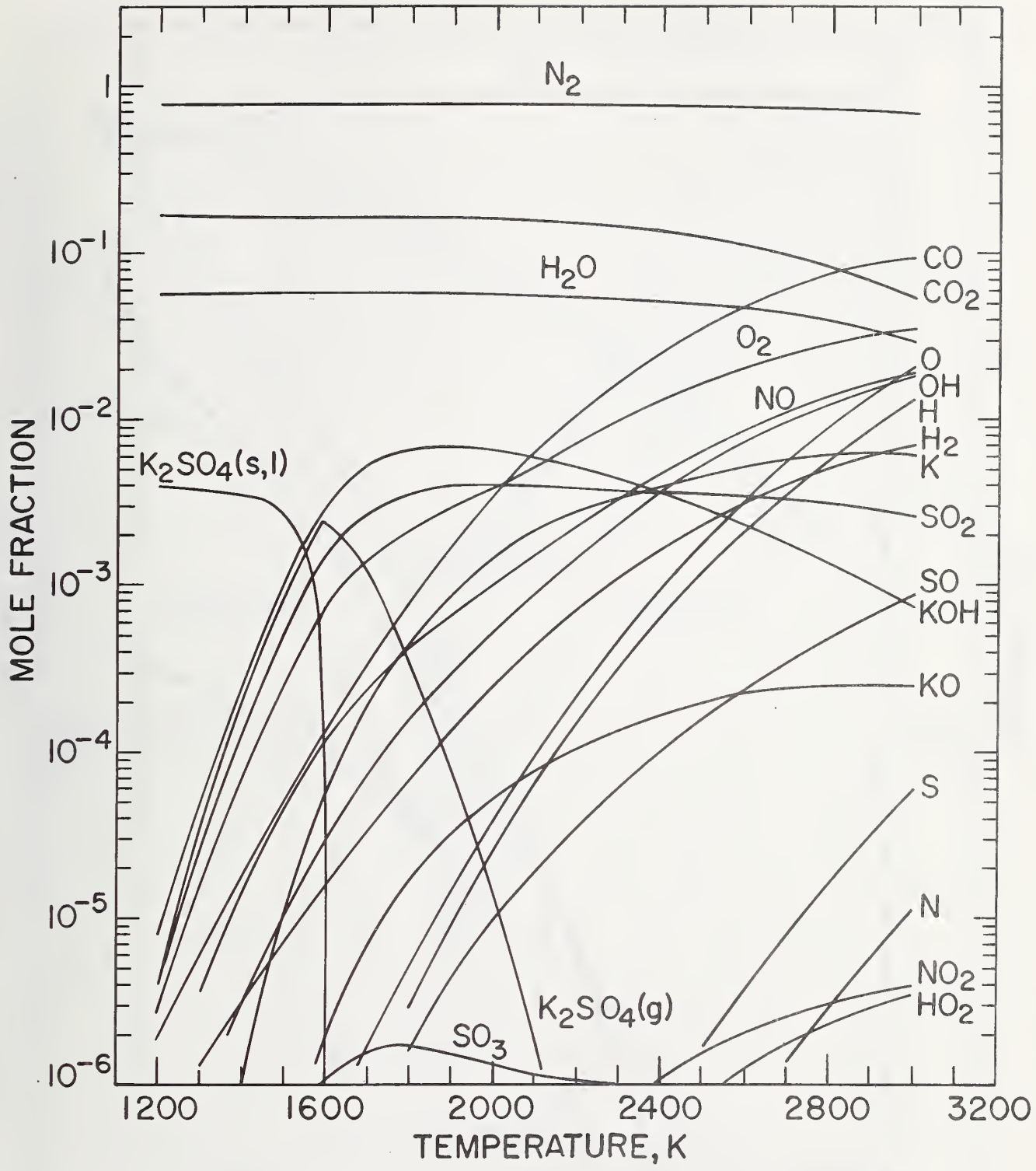

Fig. 28: Stoichiometric Combustion of $CH_{0.7}$ with 80/20 mole % N_2/O_2 Seeded with 1 wt %K as K_2SO_4 at 1 atm Total Pressure.

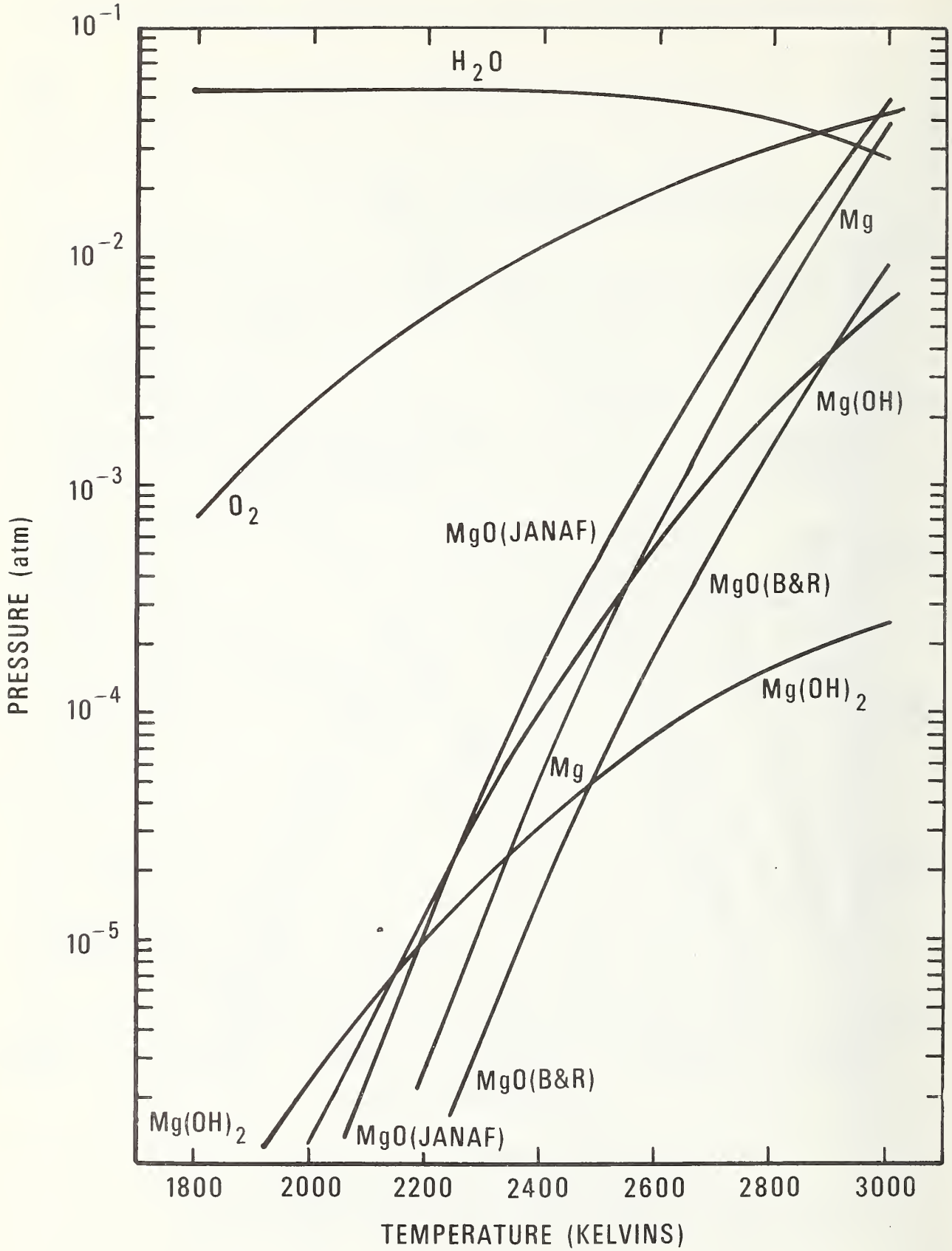

Fig. 29: Saturation Pressures of Magnesium Bearing Species in an MHD Environment at a Total Pressure of 1 atm. (Solid MgO Present).

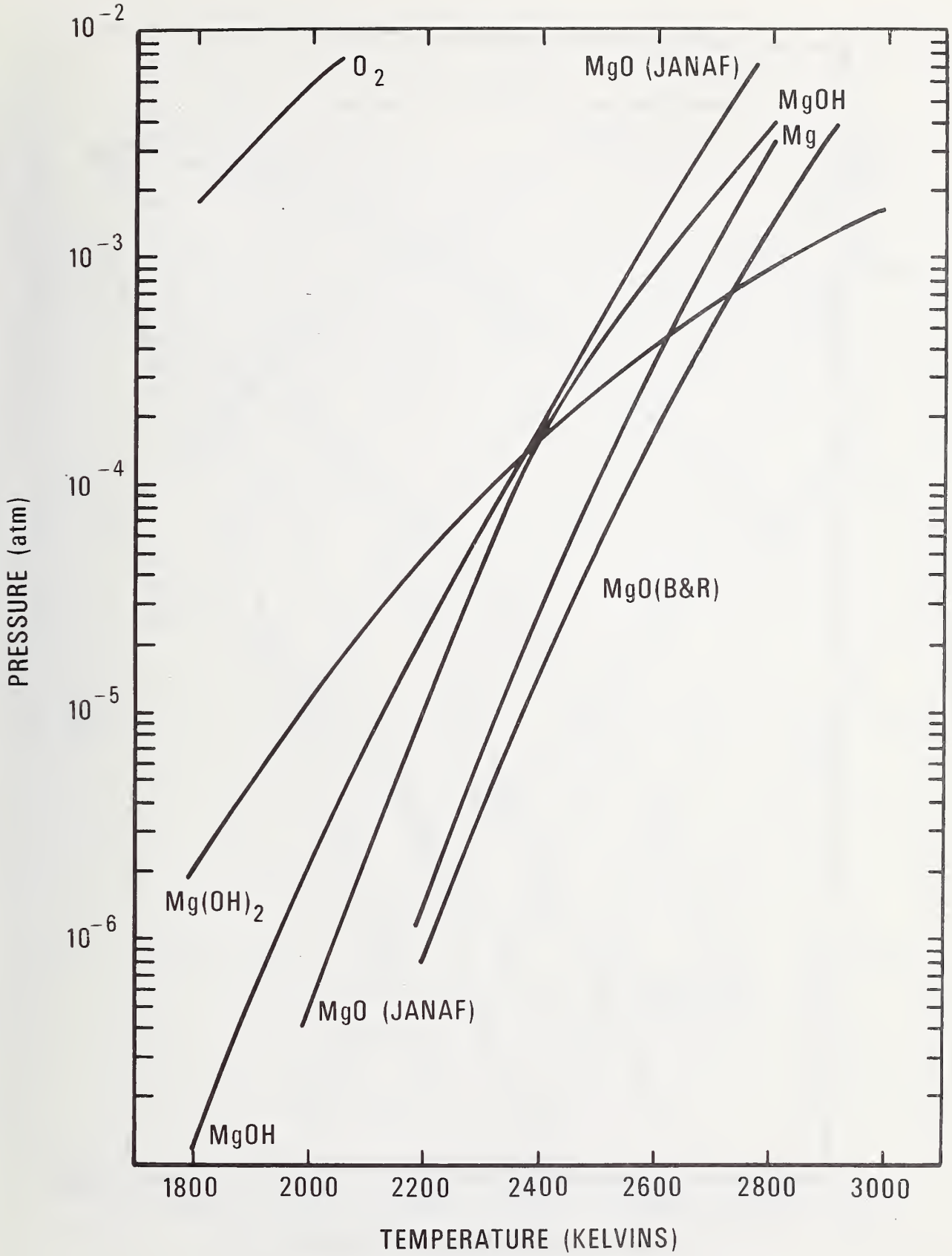

Fig. 30: Saturation Pressures of Magnesium Bearing Species in an MHD Environment at a Total Pressure of 5 atm. (Solid MgO Present).

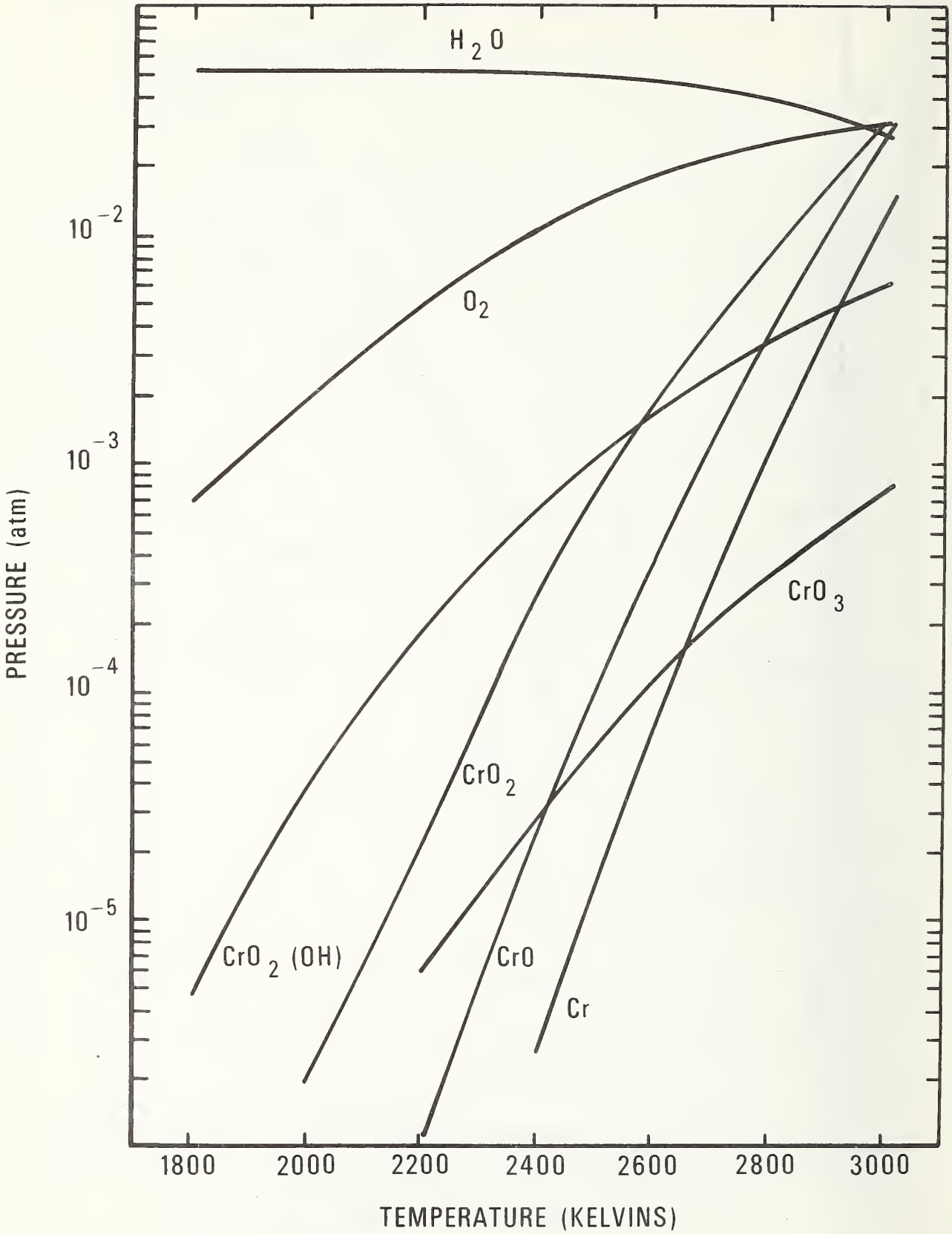

Fig. 31: Saturation Pressures of Chromium Bearing Species in an MHD Environment at a Total Pressure of 1 atm. (Solid Cr_2O_3 Present).

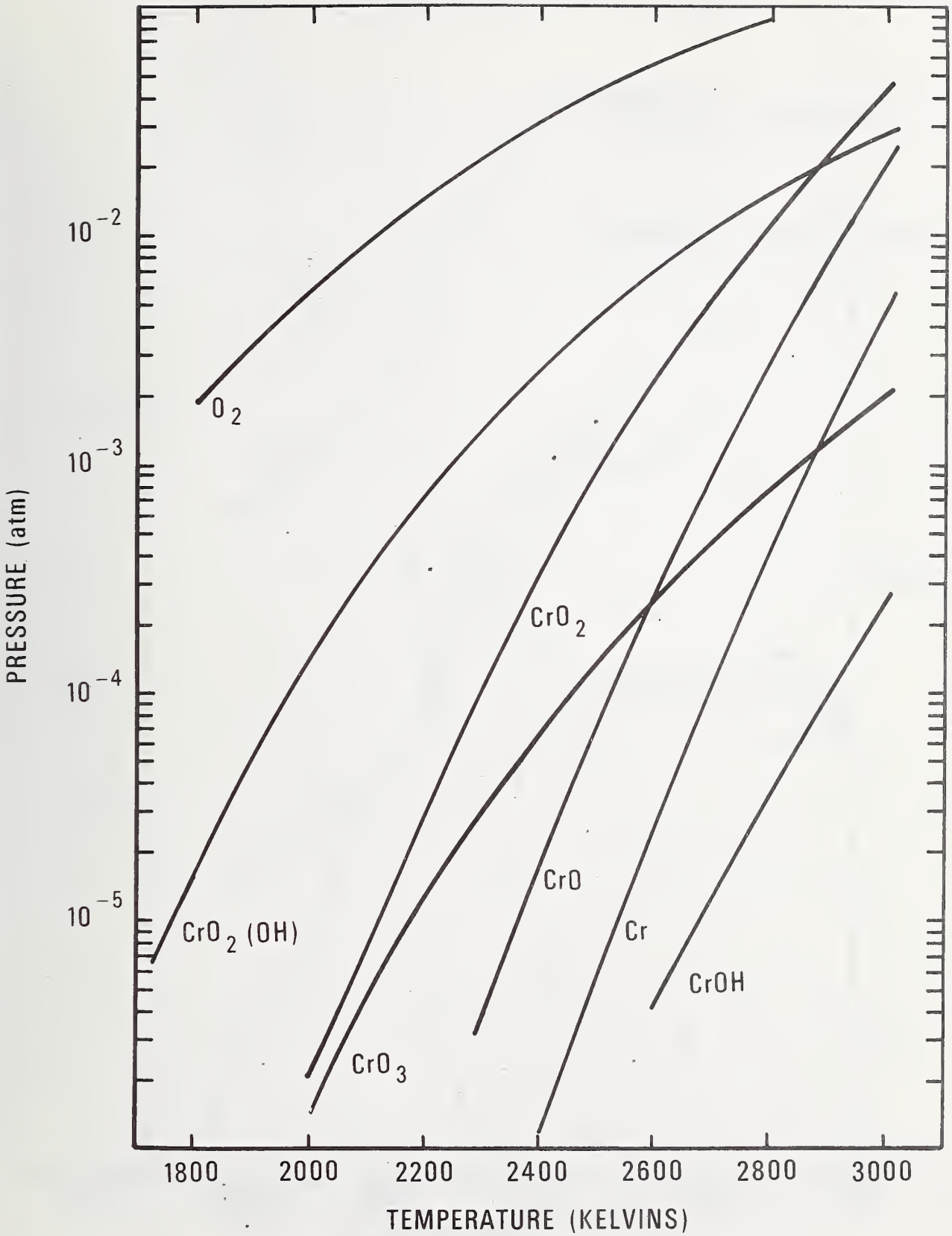

Fig. 32: Saturation Pressures of Chromium Bearing Species in an MHD Environment at a Total Pressure of 5 atm. (Solid Cr_2O_3 Present).

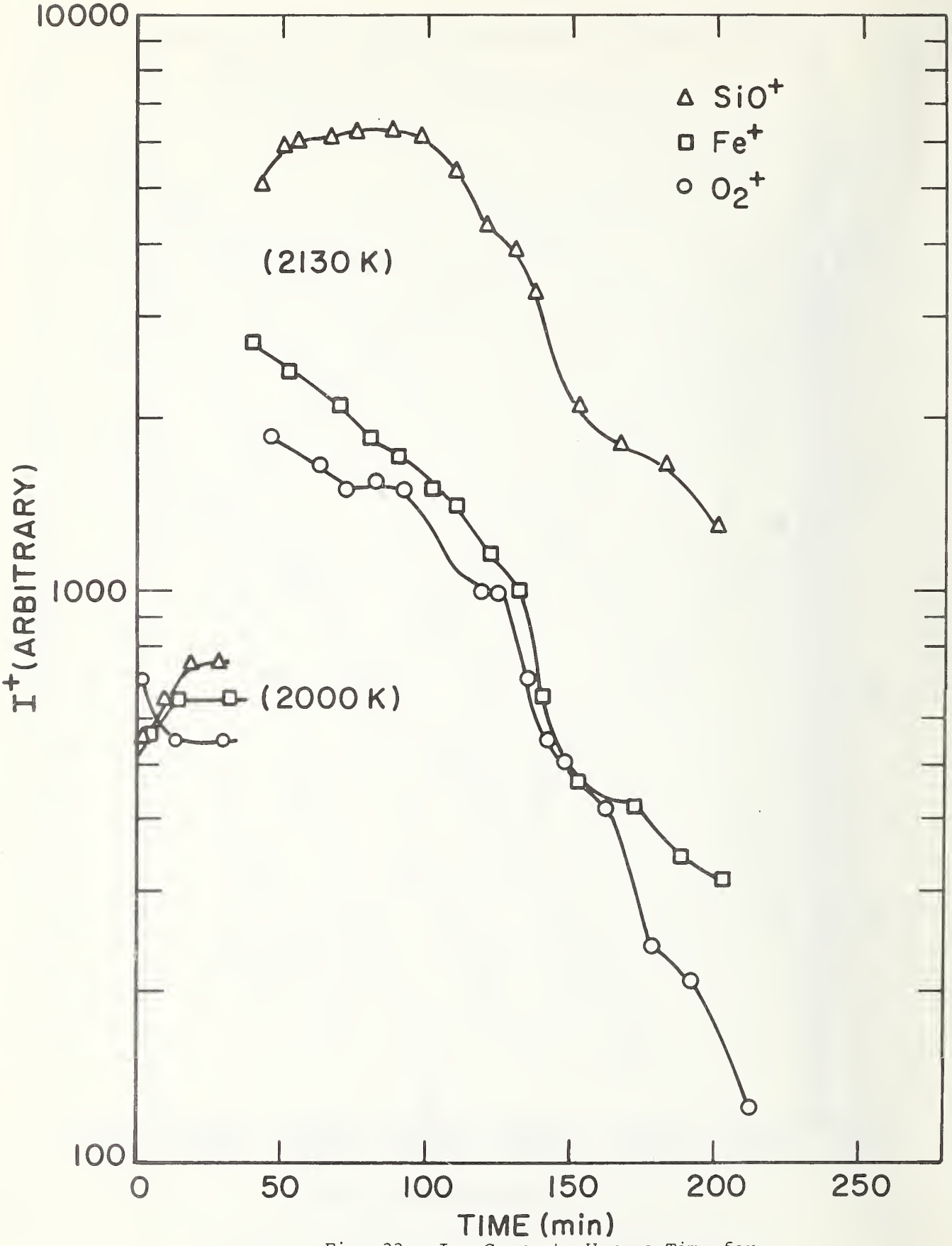

Fig. 33: Ion Currents Versus Time for Isothermal Evaporation of Slag at 2000 and 2130 K.

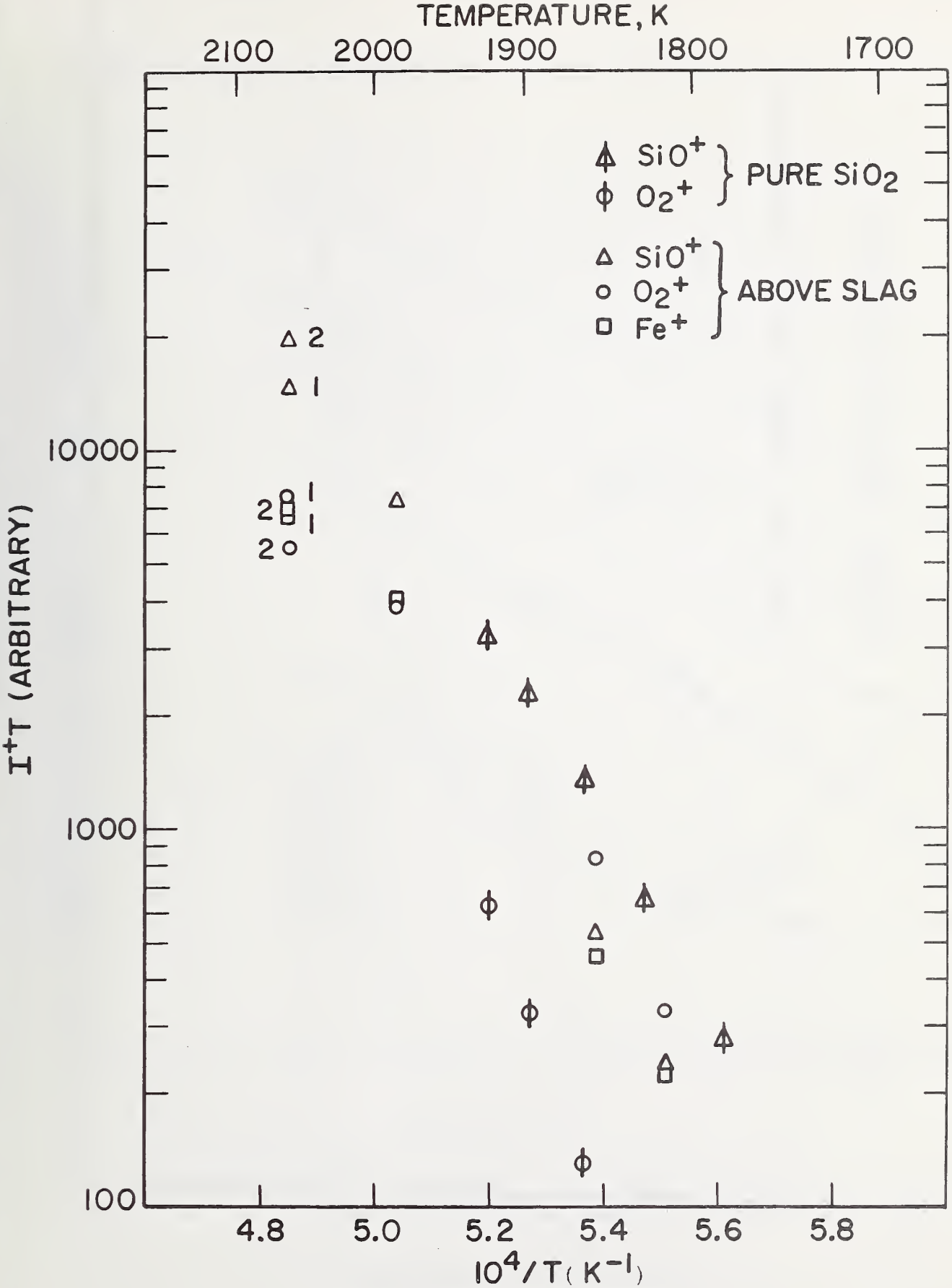

Fig. 34: I^+T Versus $10^4/T$ for Evaporation of Slag and Pure SiO_2.

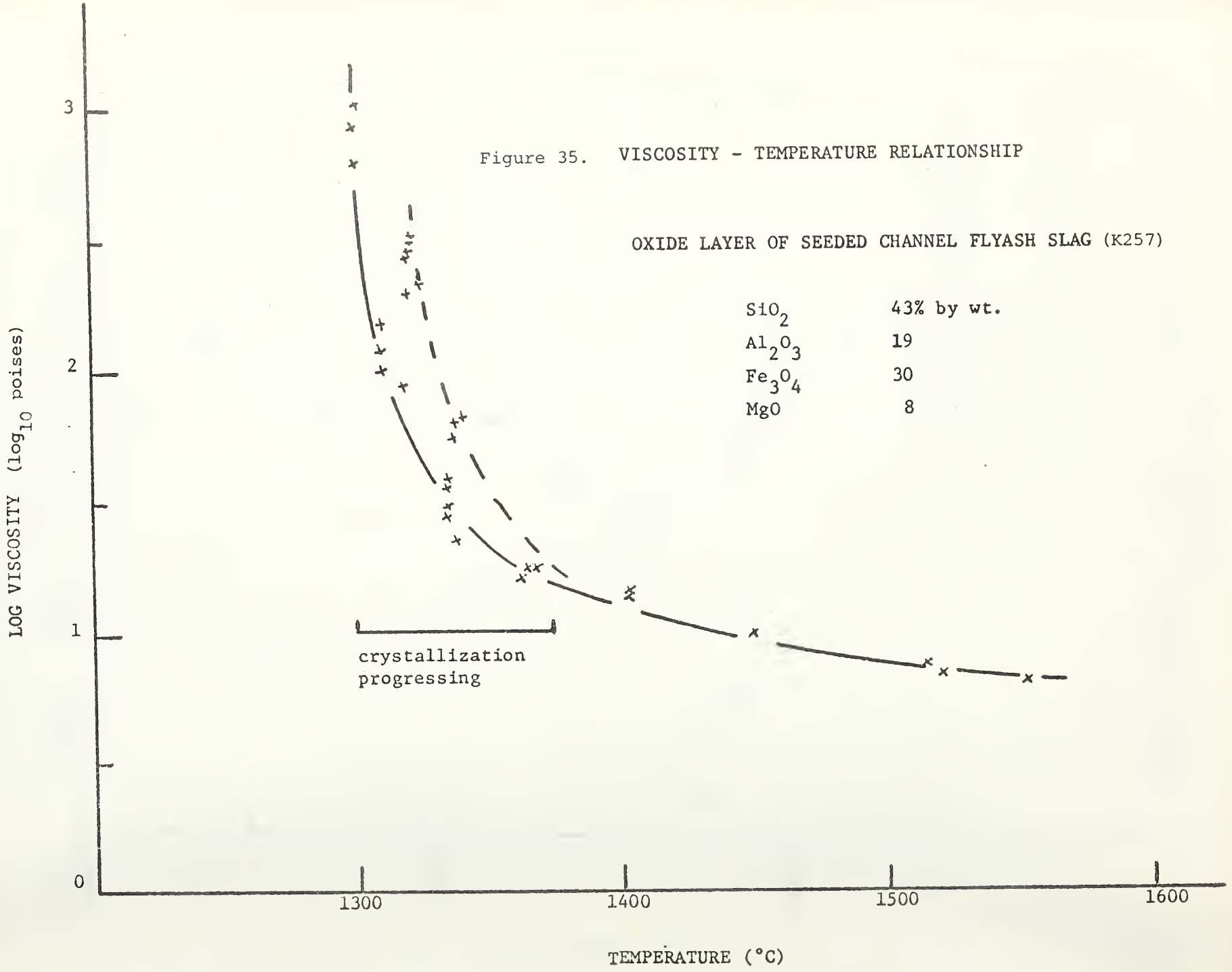
Figure 35. VISCOSITY - TEMPERATURE RELATIONSHIP
OXIDE LAYER OF SEEDED CHANNEL FLYASH SLAG (K257)
SiO2 43% by wt.
Al2O3 19
Fe3O4 30
MgO 8
crystallization progressing
LOG VISCOSITY (log10 poises)
3
2
1
0
1300
1400
1500
1600
TEMPERATURE (°C)

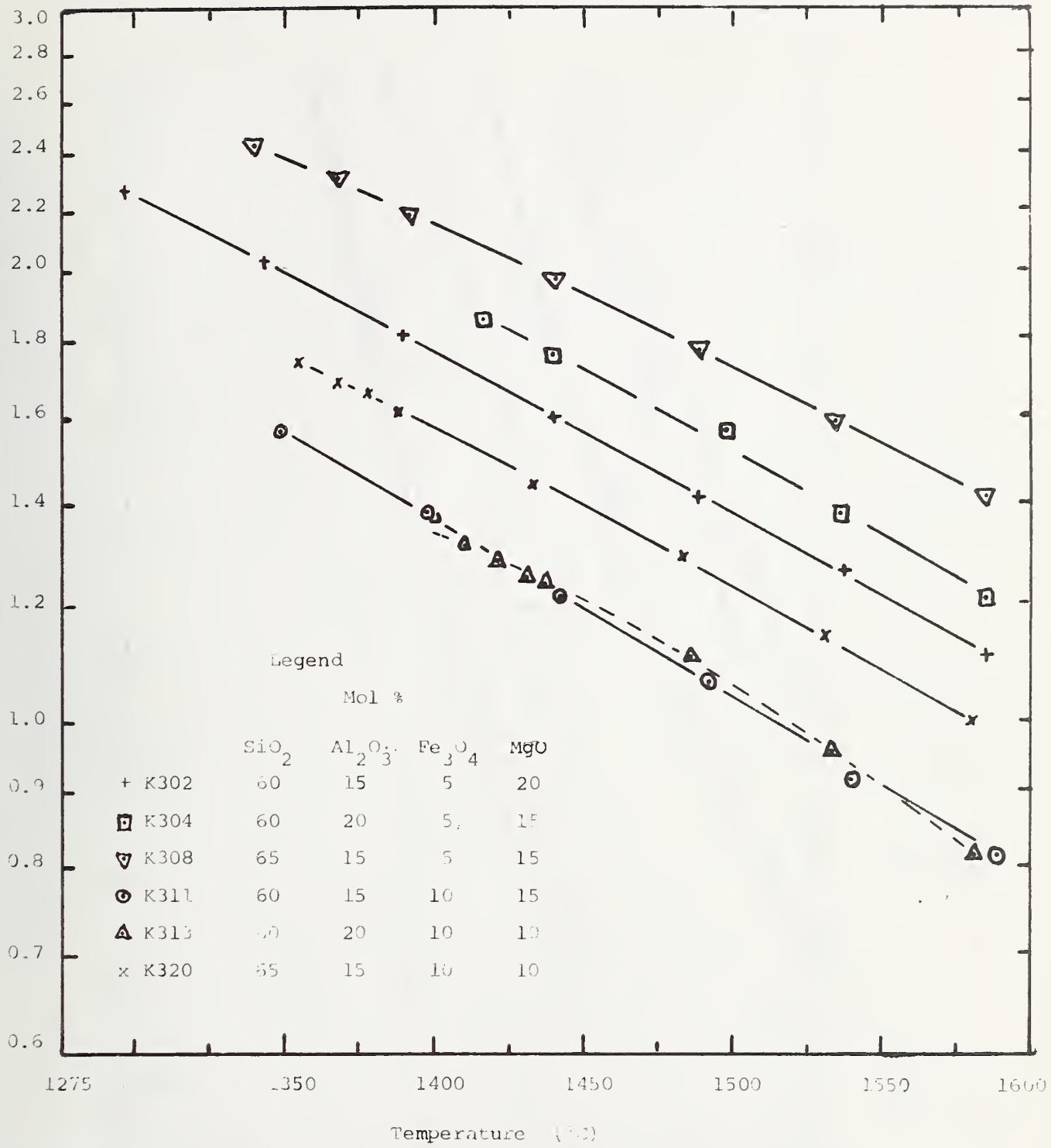

Figure 36. Viscosity Temperature Relationships for Some Model Coal Slags

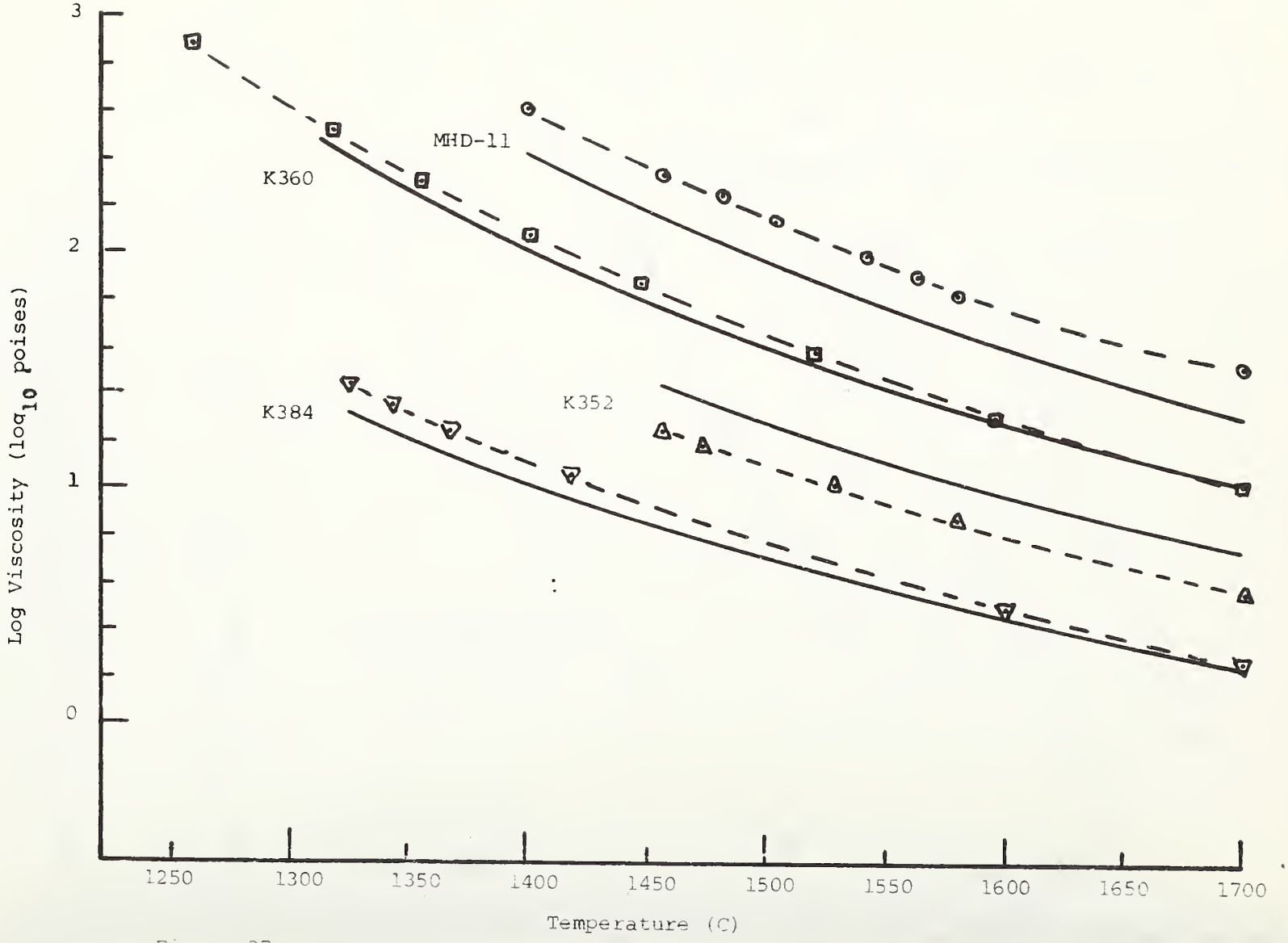

Figure 37. VISCOSITY-TEMPERATURE RELATIONSHIPS OF COAL SLAGS
Data points at 1600 C and below are measured values. Data points at 1700 C are Fulcher extrapolations of measured data. Solid lines are Watt-Fereday calculated curves

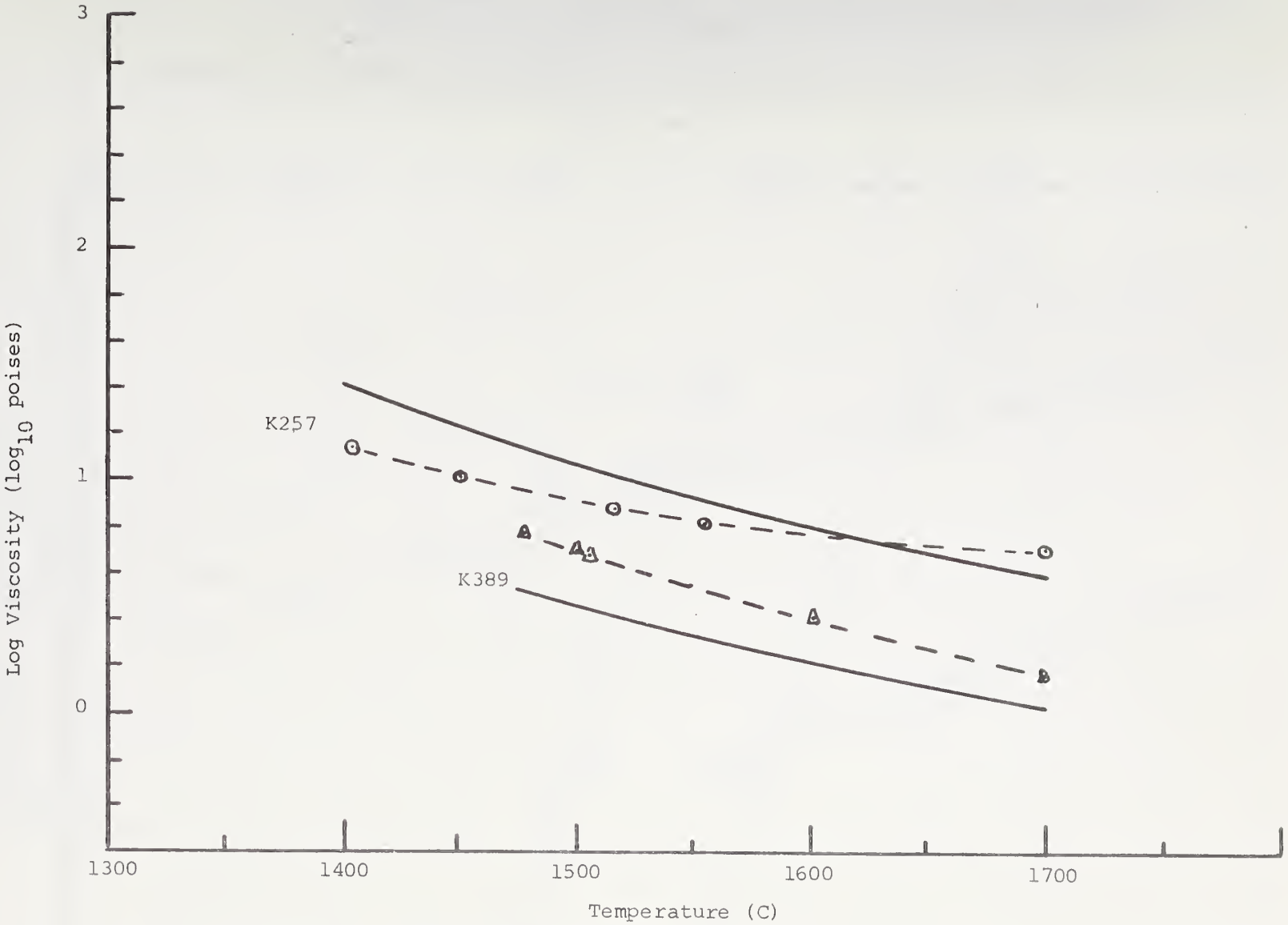

Figure 38. VISCOSITY-TEMPERATURE RELATIONSHIPS OF COAL SLAGS
Data points at 1600 C and below are measured values. Data points at 1700 C are Fulcher extrapolations of measured data. Solid lines are Watt-Fereday calculated curves.

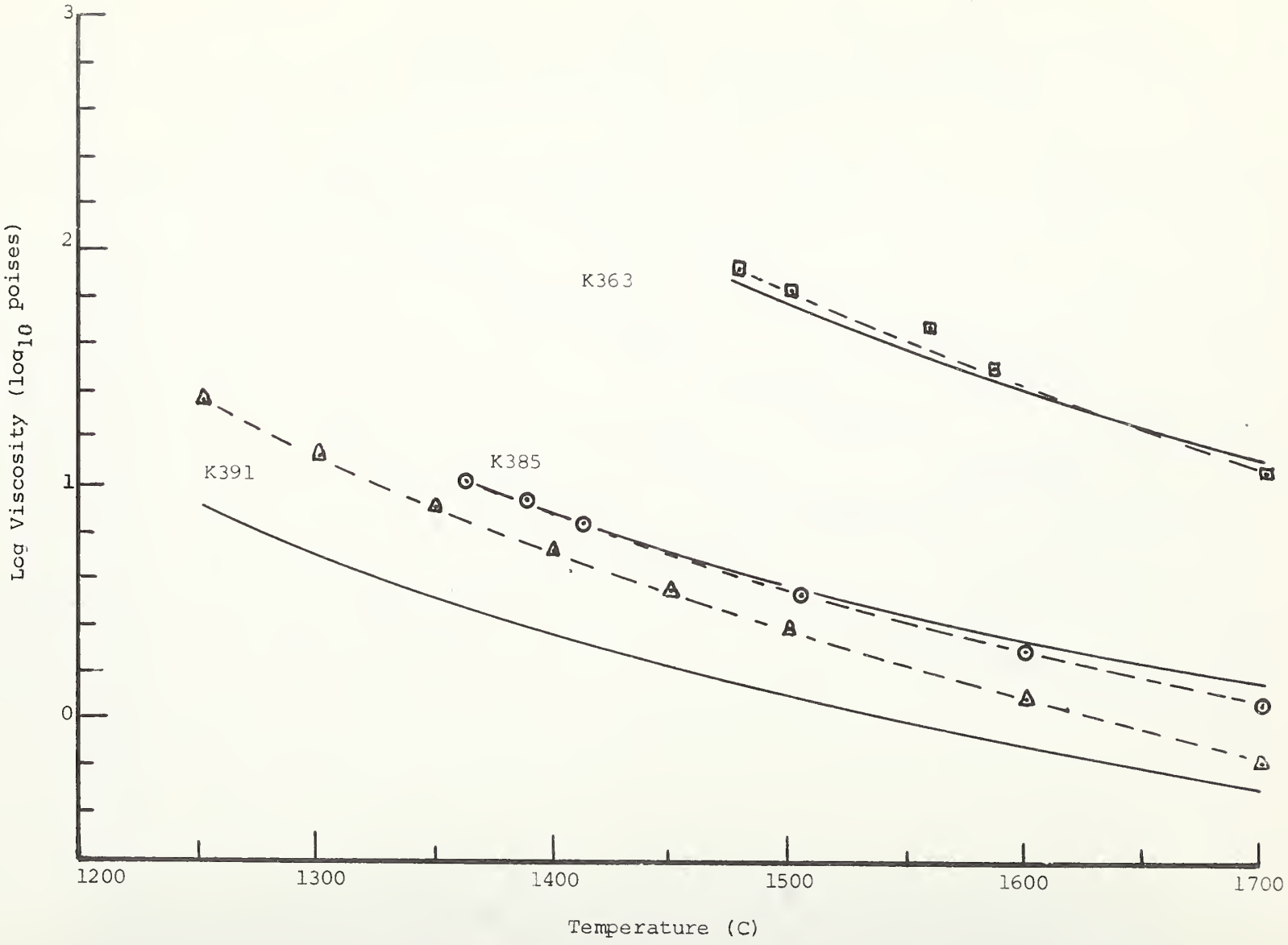

Figure 39. VISCOSITY-TEMPERATURE RELATIONSHIPS OF COAL SLAGS

Data points at 1600 C and below are measured values. Data points at 1700 C are Fulcher extrapolations of measured data. Solid lines are Watt-Fereday calculated curves.

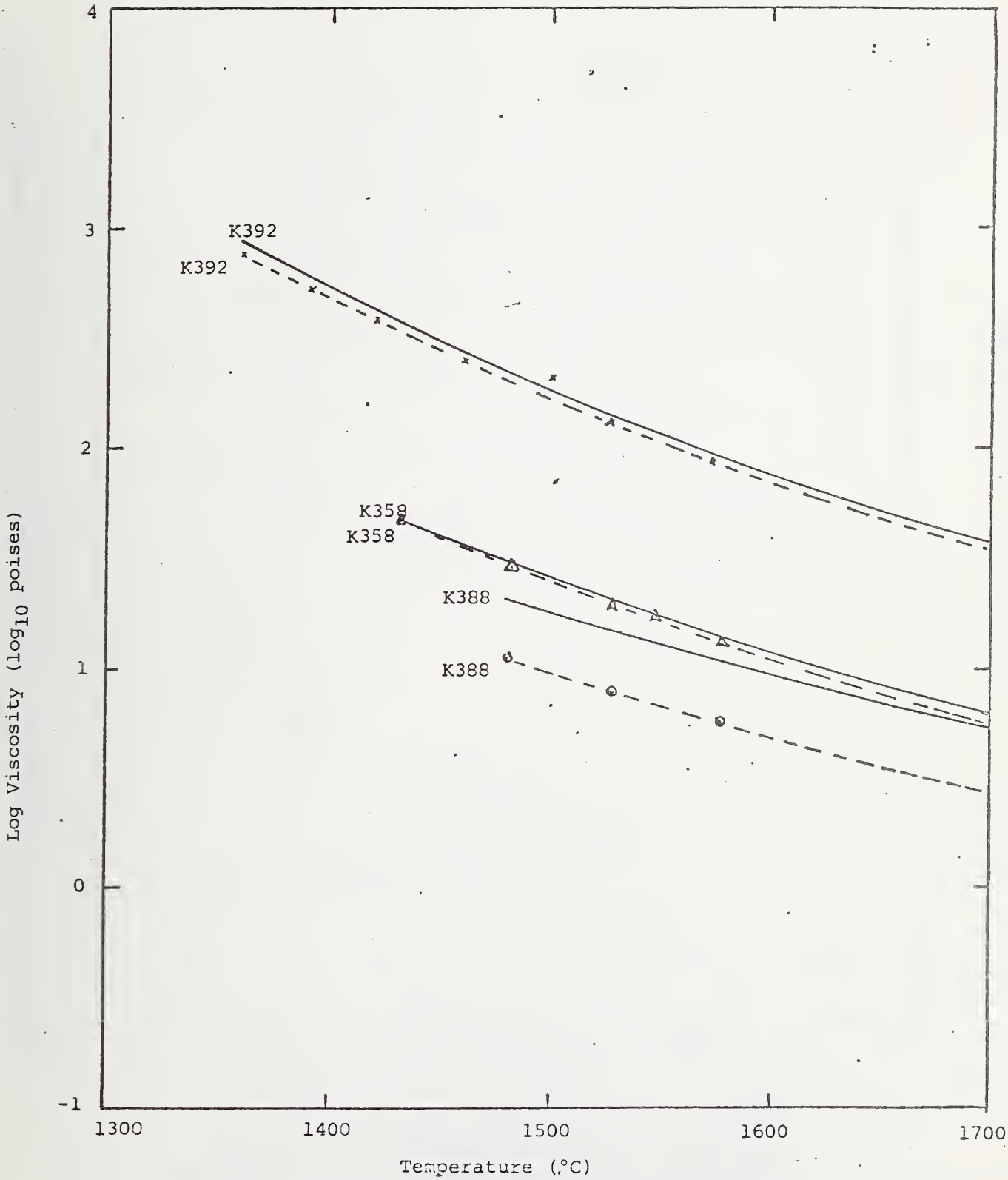

Figure 40. VISCOSITY-TEMPERATURE RELATIONSHIPS OF COAL SLAGS
Data points are measured values. Solid lines are Watt-Fereday calculated curves.

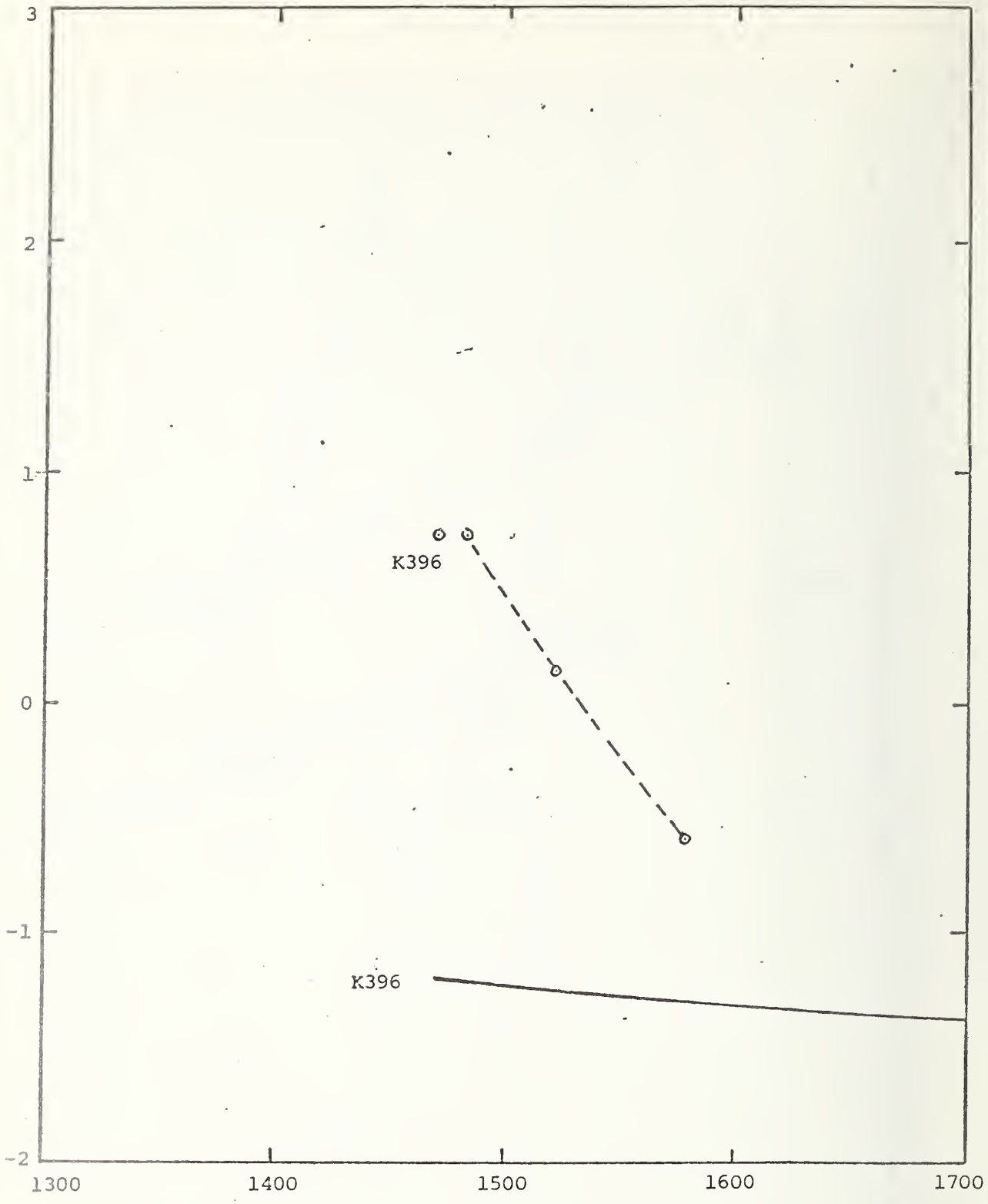

Figure 41. VISCOSITY-TEMPERATURE RELATIONSHIPS OF COAL SLAGS
Data points are measured values. Solid lines are Watt-Fereday calculated curves.

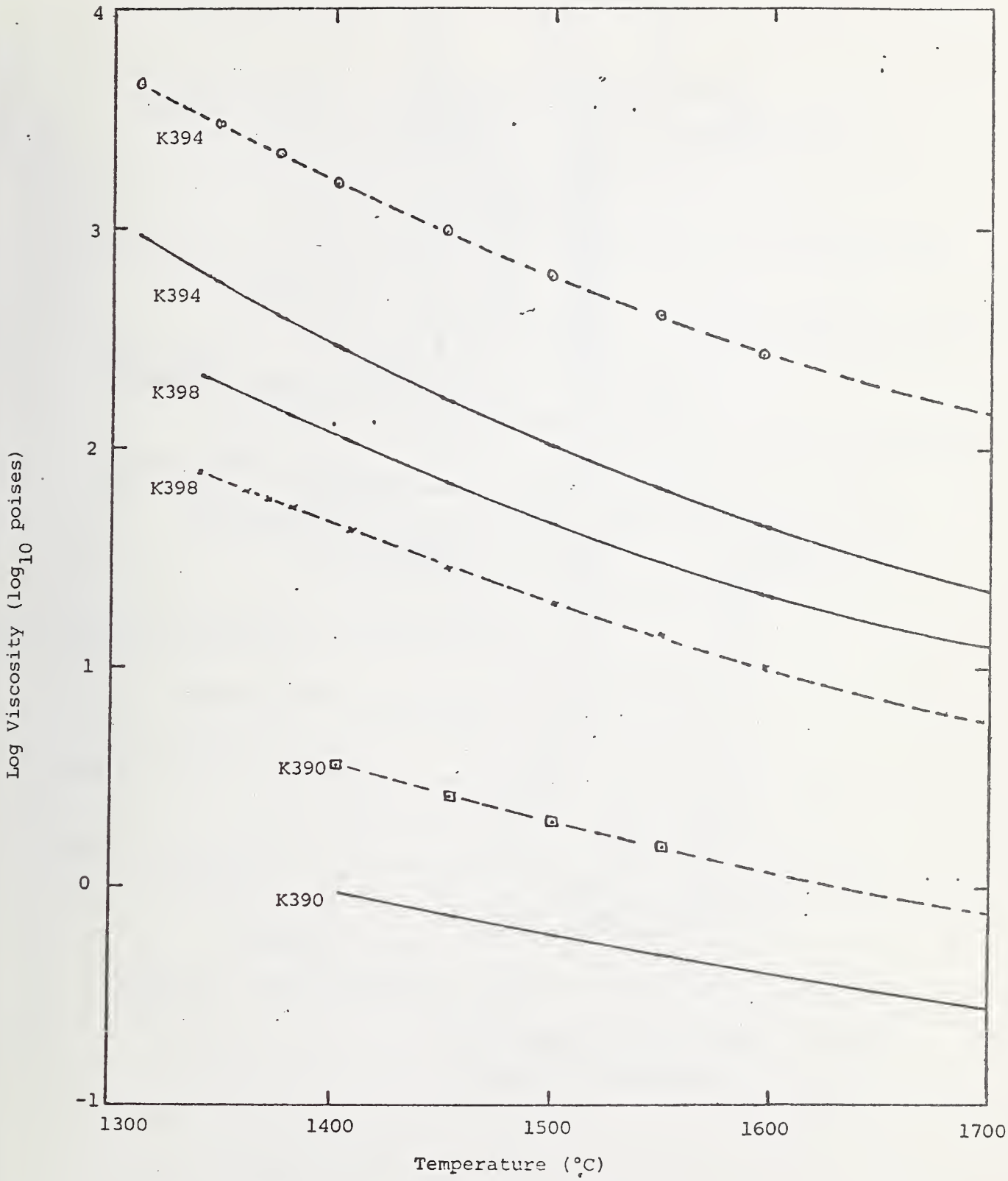

Figure 42. VISCOSITY-TEMPERATURE RELATIONSHIPS OF COAL SLAGS
Data points are measured values. Solid lines are Watt-Fereday calculated curves.

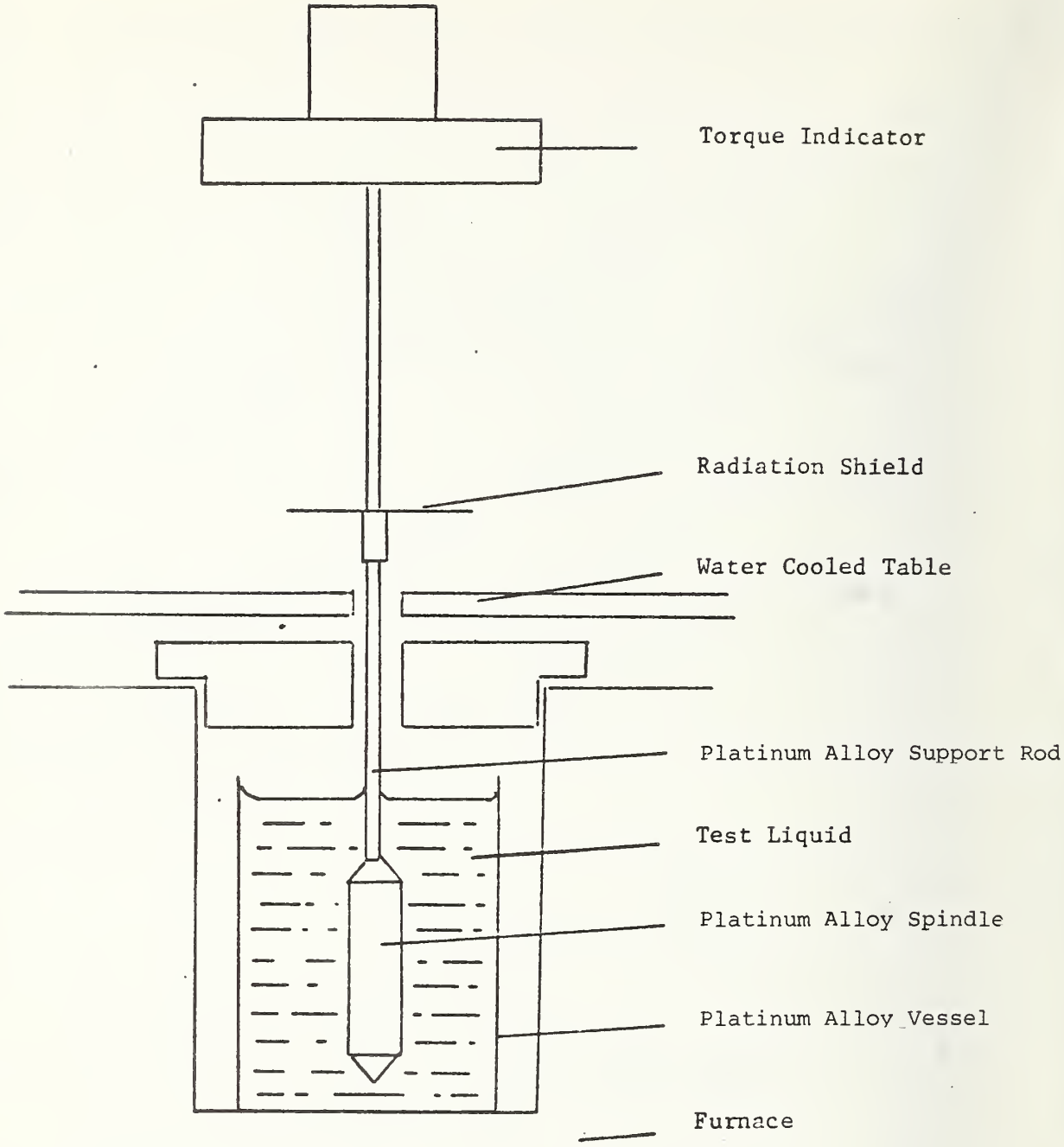

Figure 43. High Temperature Adaptation of Brookfield Viscometer

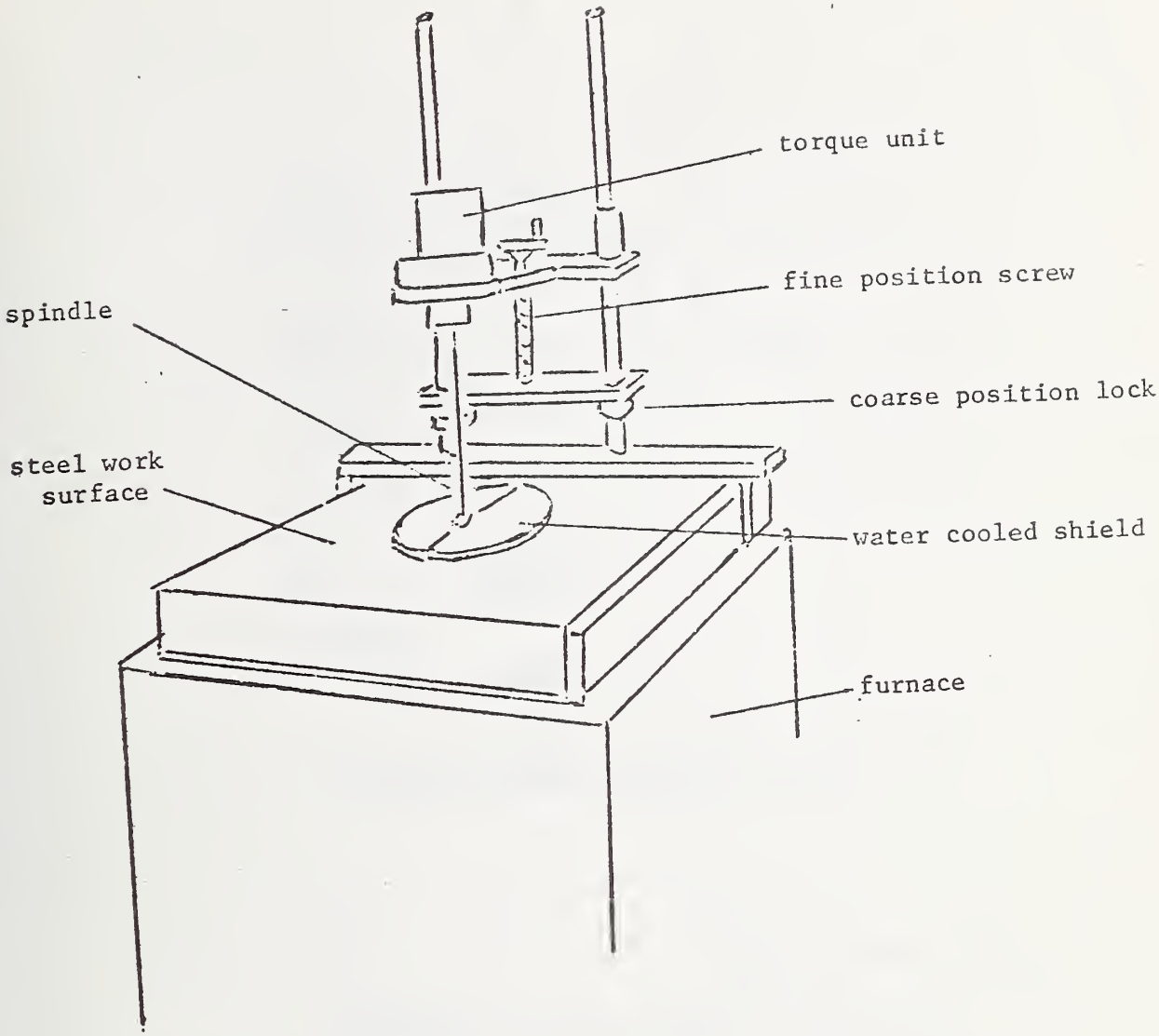

Figure 44. High Temperature Viscometer and Furnace

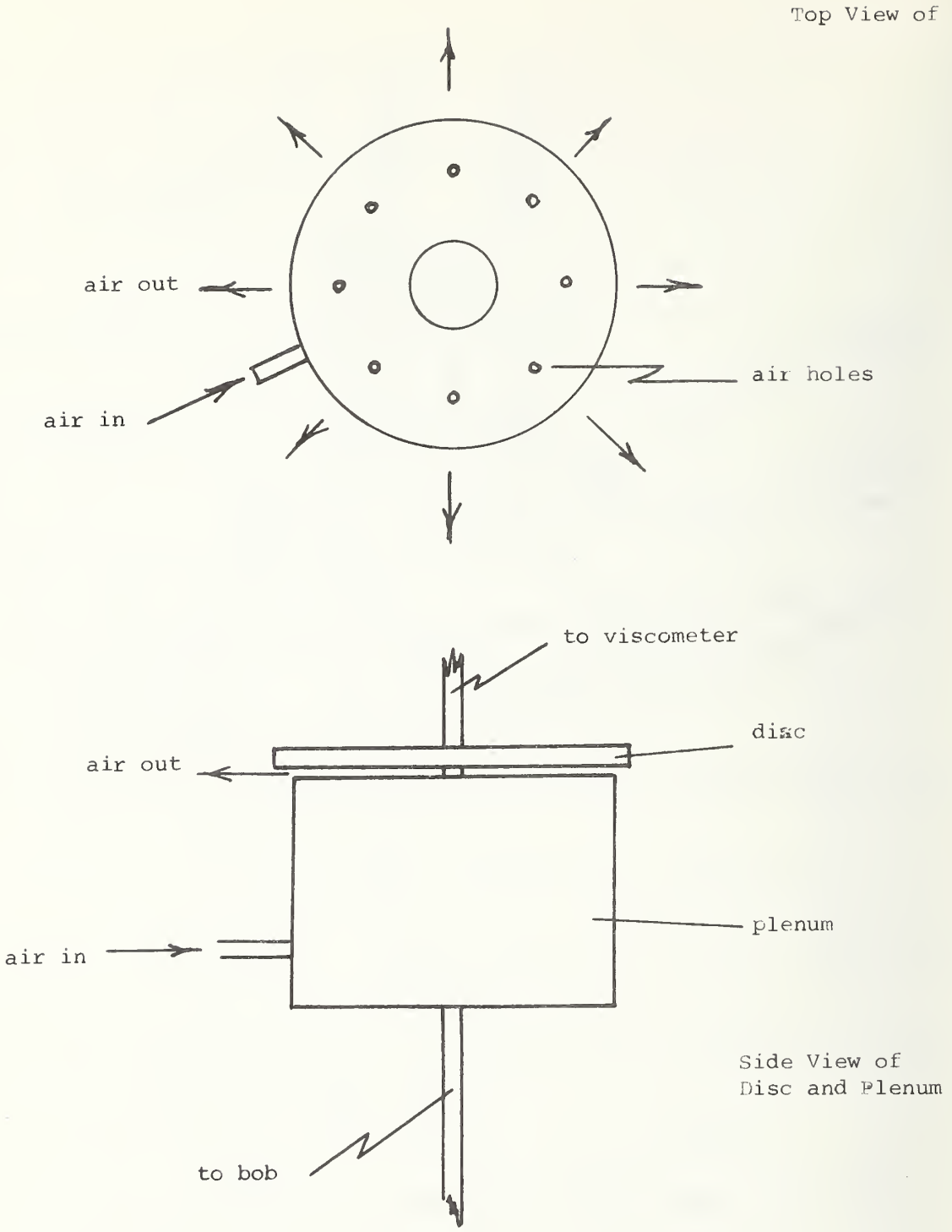

Figure 45. Schematic Diagram of Air-Bearing for Supporting Viscometer Spindle

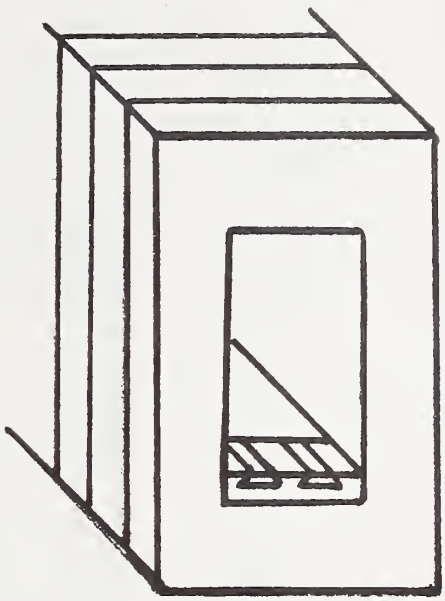

Figure 46. Position of test samples in channel

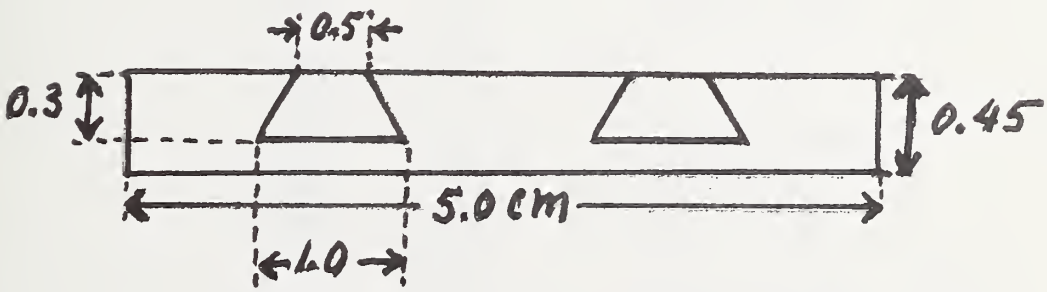

Figure 47. Sample holder with test samples

Table 1. Nominal Slag Chemical Compositions

	UTSI channel slag	Bu Mines (probe deposit)
	wt. %	wt. %
SiO_2	49	43
Al_2O_3	27	19
Fe_3O_4	19*	30**
RO (CaO & MgO)	5	8
	100	100

* Fe^{2+}/Fe^{3+} = 2:1

** Fe^{2+}/Fe^{3+} = 4:1

Table 2. Experimental Data for Compositions in the K_2SO_4-$LaCrO_3$ System in Air

Composition		Heat Treatment[a]		X-ray Diffraction Analyses[b]
K_2SO_4	$LaCrO_3$	Temp.	Time	
mole%	mole%	°C	hr	
95	5	900	21	K_2SO_4 + $LaCrO_3$
		1000	18	" "
		1000	66	" "
		1060	21	" "
		1100	24	K_2SO_4 + $LaCrO_3$ + x[d]
		1200	66	La_2O_3 + $LaCrO_3$ + K_2SO_4
		1300	22	La_2O_3 + $LaCrO_3$
		1500[c]	2	K_2SO_4 + La_2O_3
		1700[c]	4	La_2O_3 + K_2SO_4
90	10	900	21	K_2SO_4 + $LaCrO_3$
		1000	18	" "
		1100	24	K_2SO_4 + $LaCrO_3$ + x[d]
		1200	66	$LaCrO_3$ + K_2SO_4 + La_2O_3
		1300	18	La_2O_3 + $LaCrO_3$
		1500[c]	2	K_2SO_4 + La_2O_3
		1700[c]	4	La_2O_3 + K_2SO_4
75	25	900	21	K_2SO_4 + $LaCrO_3$
		1000	18	" "
		1100	24	$LaCrO_3$ + K_2SO_4
		1200	66	$LaCrO_3$ + K_2SO_4 + La_2O_3
		1300	17	$LaCrO_3$ + La_2O_3
		1400	18	" "
		1700	4	" "
50	50	900	21	$LaCrO_3$ + K_2SO_4
		950	20	" "
		1000	18	" "
		1050	120	" "
		1100	24	" "
		1200	66	$LaCrO_3$ + K_2SO_4 + La_2O_3
		1300	22	$LaCrO_3$ + La_2O_3
		1400	18	" "
		1500	3	" "
		1700[c]	4	" "

25	75	900	21	$LaCrO_3$ + K_2SO_4
		1000	18	" "
		1100	24	" "
		1200	66	$LaCrO_3$ + K_2SO_4 + La_2O_3
		1300	22	$LaCrO_3$ + La_2O_3
		1400	18	" "
		1500[c]	2	$LaCrO_3$ + La_2O_3 + K_2SO_4
		1700	3	$LaCrO_3$ + La_2O_3
10	90	900	21	$LaCrO_3$ + K_2SO_4
		1000	18	" "
		1100	24	" "
		1200	66	$LaCrO_3$ + La_2O_3
		1300	18	" "
		1500	67	" "

[a] All specimens were heat treated at 800°C a minimum 18 hrs unless otherwise indicated.

[b] The phases identified are given in order of the relative amount present at room temperature.

[c] Specimen had no previous heat treatment.

[d] Unidentified phase.

Table 3. Experimental Data for Compositions in the K_2CO_3-$LaCrO_3$ System in Air

Composition		Heat Treatment		X-ray Diffraction Analyses[a]
K_2CO_3	$LaCrO_3$	Temp.	Time	
mole%	mole%	°C	hr	
75	25	700	23	La_2O_3 + K_2CO_3 + K_2CrO_4
		800	21	K_2CO_3 + La_2O_3 + K_2CrO_4 + x[b]
		900	20	K_2CrO_4 + K_2CO_3 + La_2O_3 + x[b]
		900	22	" " " "
		1000	22	K_2CrO_4 + y[b] + La_2O_3
		1100	23	La_2O_3 + K_2CrO_4 + Pt + y[b]
		1200	42	La_2O_3 + Pt + K_2CrO_4 + $LaCrO_3$
		1300	67	$LaCrO_3$ + Pt + La_2O_3
		1400	18	" " "
		1500	3	" " "
		1700	2	" " "
50	50	700	20	K_2CrO_4 + La_2O_3 + x[b]
		700	23	" " " "
		800	21	La_2O_3 + K_2CrO_4
		900	20	" "
		1000	22	" "
		1100	23	" "
		1200	42	La_2O_3 + $LaCrO_3$ + K_2CrO_4
		1300	92	La_2O_3 + $LaCrO_3$
		1400	20	La_2O_3 + $LaCrO_3$ + y[b]
		1500	3	La_2O_3 + $LaCrO_3$
		1700	2	" "
25	75	700	23	$LaCrO_3$ + La_2CrO_6 + K_2CrO_4
		800	21	" " "
		900	20	$LaCrO_3$ + K_2CrO_4 + x[b] + y[b]
		1000	22	$LaCrO_3$ + x[b] + K_2CrO_4
		1100	23	$LaCrO_3$ + La_2O_3 + K_2CrO_4
		1200	42	" " "
		1300	67	" " "
		1400	20	$LaCrO_3$ + La_2O_3
		1500	3	" "
		1700	4	" "

[a] The phases identified are given in order of the relative amount present at room temperature.

[b] Unidentified phases

Table 4

Compositions of a real coal slag (MHD-11) and some synthetic slags which are used for comparison of measured with calculated viscosities.

Melt	SiO_2	Al_2O_3	Fe_3O_4	CaO	MgO	K_2O	Na_2O
MHD-11*	55	25	12	2	4	2	
K257**	43	19	30	0	8		
K352	45	20	15	15	5		
K360	50	25	12	8	5		
K363	50	30	10	6	4		
K384	40	20	15	17	8		
K385	40	15	20	17	8		
K386	70	24	3	2	1		
K387	60	32	4	2	2		
K389	30	30	20	14	6		
K391	40	10	5	30	15		
K358	45	30	10	10	5		
K388	40	30	25	3	2		
K390	30	15	15	30	10		
K392	60	20	17	2	1		
K394	63	13.5	10.8	1.8	.9		10
K396	20	10	20	30	20		
K398	50	20	27	2	1		

* Nominal composition of a real Bu Mines combustor coal slag.

** Synthetic melt representing oxide portion of two-phase Bu. Mines seeded, channel flyash (MHD-12F).

Table 5

Chemical Analyses of Some Simulated Seeded Coal Slags
(weight %)

Melt	SiO_2	Al_2O_3	Fe_3O_4	MgO	K_2O	SO_3
K264U	0.03	0.03	0.051	0.43	54.00	45.90
K264L	34.06	16.03	22.04	5.30	18.80	1.39
K265U	0.01	0.02	0.041	0.36	54.00	45.70
K265L	32.39	13.98	21.94	10.68	18.20	2.47
K266	37.83	16.20	24.46	7.49	12.38	0.00

Notes:

1. Before melting, K264 contained 20% oxides and 80% K_2SO_4. K265 contained 50% oxides and 50% K_2SO_4. K266 contained 80% oxides and 20% K_2SO_4.
2. Melt designation U means upper layer after separation; L means lower layer after separation.
3. Melts were soaked at 1500° C without stirring to allow equilibrium to be reached.

BIBLIOGRAPHIC DATA SHEET	1. Report No. NBSIR 74-543	2.	3. Recipient's Accession No.

4. Title and Subtitle

HIGH TEMPERATURE MHD MATERIALS

5. Report Date

August 1974

6. Performing Organization Code

7. Author(s) S.J. Schneider, W. Capps, H.P.R. Frederikse, W.R. Hosler, D.A. Kauffman, E.M. Levin, C.L. McDaniel, T. Negas and E.R. Plante

8. Performing Organization Rept. No.

9. Performing Organization Name and Address

National Bureau of Standards
Washington, D.C. 20234

10. Project/Task/Work Unit No.

11. Contract/Grant No.

OCR 14-32-0001-1230

12. Sponsoring Agency Name and Address

Department of the Interior
Office of Coal Research
2100 M Street, N.W.
Washington, D.C. 20240

13. Type of Report & Period Covered Interim Report
July 1972 - June 1974

14. Sponsoring Agency Code

15. Supplementary Notes

Project Manager: Dr. William Jackson

16. Abstracts

Under the auspices of the Office of Coal Research the National Bureau of Standards has underway a program of materials research appropriate to magnetohydrodynamics (MHD). The overall objective of the work is to provide materials property information necessary for the design, construction, and operation of an open cycle, coal fired MHD electric generation plant. The program consists of several interrelated investigations in the areas of phase equilibria, electrical properties, vaporization, viscosity and materials testing. Initial work has centered on the behavior of coal slag but also encompasses the physical and chemical characteristics of other MHD process contaminants (alkali seed) and important electrode and insulator materials. The report summarizes the important technical results obtained during the period July 1, 1972 - June 30, 1974 under the combined NBS-OCR program.

17. Key Words and Document Analysis. 17a. Descriptors

Coal slag; electrical conductivity (MHD); electrodes; insulators; MHD; MHD materials; MHD materials testing; phase equilibria (MHD); vaporization (MHD); viscosity (MHD)

17b. Identifiers/Open-Ended Terms

17c. COSATI Field/Group

18. Distribution Statement	19. Security Class (This Report)	21. No. of Pages
Unclassified, Unlimited	UNCLASSIFIED	128
	20. Security Class (This Page) UNCLASSIFIED	22. Price


AMERICAN REVOLUTION BICENTENNIAL
1776-1976